Editor's Note

Contributions Dedicated to the 160th Anniversary of Louis Pasteur's Discovery

The creative power of Louis Pasteur (1822–1895) has affected the entire science. As noticed by him, his discoveries stemmed from the combination of chemical (synthesis), physical (polarimetry, crystallography), and biological (enzymes) methods. Thus his exploratory approach pioneered the development of modern stereochemistry, microbiology, immunology as well as the interdisciplinary fields.

In 1848, Pasteur discovered the fundamental phenomenon of chirality and went on to develop three methods for resolution of racemates. One of them, the enzymatic resolution, led to a deeper understanding of microbiological processes, while his concept of vaccination made it possible to subdue epidemic infections. His works provided the basis for modern pharmaceutical industry, i.e., production of chiral drugs, including use of chemzyms and public health care such as application of synthetic vaccines.

The series of papers in this and the following few issues of *Chirality*, published on the occasion of the 160th anniversary of Pasteur's discovery, covers the recent development of his ideas and the consequences in the various fields. We hope that these contributions will provide an overview of the current status and promote a further understanding of this important field.

Professor Remir G. Kostyanovsky
Guest Editor
N. N. Semenov Institute of Chemical Physics
Russian Academy of Sciences, Moscow

Professor Nina Berova
Editor
Department of Chemistry
Columbia University, New York

DOI: 10.1002/chir.20646
Published online 24 July 2008 in Wiley InterScience
(www.interscience.wiley.com).

CHIRALITY 20:1072–1084 (2008)

Review Article

When Did Louis Pasteur Present His Memoir on the Discovery of Molecular Chirality to the *Académie Des Sciences*? Analysis of a Discrepancy

JOSEPH GAL*

Division of Clinical Pharmacology and Toxicology, University of Colorado School of Medicine, Denver, Colorado

Dedicated to the 160th Anniversary of Louis Pasteur's Discovery

ABSTRACT Louis Pasteur presented his historic memoir on the discovery of molecular chirality to the *Académie des sciences* in Paris on May 22nd, 1848. The literature, however, nearly completely ignores this date, widely claiming instead May 15th, 1848, which first surfaced in 1922 in Pasteur's collected works edited by his grandson Louis Pasteur Vallery-Radot. On May 21st, 1848, i.e., one day before Pasteur's presentation in Paris, his mother died in Arbois, eastern France. Informed at an unknown point in time that she was "very ill," Pasteur left for Arbois only after his presentation. Biographies of Pasteur by his son-in-law René Vallery-Radot or the grandson, and Pasteur's collected correspondence edited by the grandson are incomprehensibly laconic or silent about the historic presentation. While no definite conclusions are possible, the evidence strongly suggests a deliberate alteration of the record by the biographer relatives, presumably for fear of adverse public judgment of Pasteur for a real or perceived insensitivity to a grave family medical emergency. Such fear would have been in accord with their hagiographic portrayal of Pasteur, and the findings raise questions concerning the extent of their zeal in protecting his "demigod" image. Universal recognition of the true date of Pasteur's announcement of molecular chirality is long overdue. *Chirality 20:1072–1084, 2008.*

KEY WORDS: discovery of molecular chirality; enantiomorphism; falsification of history; hagiography; stereochemistry; history of chemistry; Pasteur; biography

INTRODUCTION

Louis Pasteur (1822–1895), a chemist by training, discovered molecular chirality in 1848, and thereby made a fundamentally important contribution to chemistry and several other fields, e.g., crystallography, biochemistry, pharmacology, clinical therapeutics, etc. He presented his revolutionary discovery to the *Académie des sciences* (Academy of Sciences, *Académie* henceforth) in Paris in May of the same year, but the correct date of his presentation has been nearly completely ignored and instead an incorrect date has widely persisted in the literature to the present day. In this report the circumstances, causes and implications of the emergence and widespread acceptance of the wrong date are analyzed.

THE DISCOVERY OF MOLECULAR CHIRALITY

Background

Optical rotation was discovered by the French physicist François Arago (1786–1853) when he found, in 1811, that crystalline quartz slices rotated the plane of "plane-polarized" (i.e., circularly polarized) light.[1] Subsequently, Jean-Baptiste Biot (1774–1862) found,[1] beginning in 1815, that some substances rotate polarized light in the noncrystalline state, e.g., in the liquid or gas phase or in solution, and by the mid-1840s a variety of compounds, all natural products (e.g., tartaric acid, oil of turpentine, camphor, quinine, morphine, brucine, various sugars, albumin, etc.), were known to rotate polarized light in the noncrystalline state.[2] Biot understood that optical rotation by substances in the noncrystalline state required that some aspect of the structure of the molecules themselves was responsible for the rotation, and he referred[3] to such compounds as "substances moléculairement actives" (molecularly active substances; translations are by the present author unless otherwise indicated), but an explanation of the phenomenon was not available. It was Louis Pasteur who made the connection between optical rotation and molecular structure when he discovered *molecular chirality.*[4]

*Correspondence to: Joseph Gal, Division of Clinical Pharmacology C 237, University of Colorado Health Sciences Center, 4200 East 9th Avenue, Denver, CO 80262. E-mail: joe.gal@uchsc.edu

Received for publication 1 October 2007; Accepted 29 November 2007
DOI: 10.1002/chir.20532
Published online 17 March 2008 in Wiley InterScience (www.interscience.wiley.com).

Pasteur Discovers Molecular Chirality

Pasteur obtained his doctorate from the University of Paris in August 1847 with two theses, one in chemistry[5] and another in physics.[6] At the time of his discovery of molecular chirality, in the spring of 1848, he was an assistant to Antoine-Jêrome Balard (1802–1876), a professor of chemistry at the *École normale supérieure*, a prestigious university-level institution in Paris.[7] In a letter to his friend Charles Chappuis dated January 20th, 1848, Pasteur mentioned that he had undertaken new studies and hoped to present the results to the *Académie* sometime later that year.[8] These were the studies of the tartrate crystals that led to the discovery of molecular chirality.[9]

Pasteur's key finding was that the sodium ammonium salt of *paratartaric acid* (racemic tartaric acid or (±)-tartaric acid by today's nomenclature) crystallized under the conditions of his experiments as a conglomerate, i.e., as a mechanical mixture of two crystal types. One of the crystal types contained one of the enantiomers, while the other enclosed only molecules of the other enantiomer. He was led to this finding by his recognition—based on careful observation that identified opposing hemihedral facets on the two crystal types—that the two crystal types were chiral and *enantiomorphous*, meaning that they resembled each other as the right and left hands, i.e., as a "handed" object and its nonsuperposable mirror image. Pasteur manually separated the two types of crystals and showed that in solution the two tartrate salts (dissolved separately) had equal optical rotation in absolute value (within experimental error) but opposite in direction, and the same was true for the crystal hemihedrism and optical rotation in solution of the corresponding tartaric acids liberated from the salts.[10] As Kauffman and Myers pointed out, the experiments required considerable laboratory skills and powers of observation.[11]

Pasteur's key experiments were carried out in the spring[12] of 1848, and he read his memoir on the discovery at a session of the *Académie* in May, 1848. The memoir was published in the proceedings of the *Académie*, the *Comptes rendus des séances de l'Académie des sciences* (*Comptes rendus* hereafter) with the following title: "Memoir on the relation that may exist between crystal form and chemical composition and on the cause of rotatory polarization."[4]

Pasteur understood that the cause of optical rotation in the noncrystalline state was the *inherent chirality* of the *molecules* of *dextro-* and *levo*-tartaric acids, and he expressed this crucial point in his historic memoir to the *Académie* in the following manner: "Is it not evident by now that the property of certain molecules of rotating the plane of polarization has as its cause, or at least is linked in a most intimate manner to, the dissymmetry of these molecules?"[4] By *dissymmetry*, Pasteur meant *chirality*.[13]

Pasteur's discovery was received by the Parisian scientific establishment with a great deal of interest. For example, Biot insisted on verifying the discovery by having Pasteur repeat the experiment in his presence and using reagents provided by Biot,[14] and in October, 1848, a commission appointed by the *Académie* and consisting of distinguished scientists—including Biot and the celebrated chemist Jean-Baptiste Dumas (1800–1884)—produced a highly favorable report on Pasteur's chirality work.[15] Pasteur had indeed caught the attention of the scientific establishment, and was appointed *professeur suppléant* (substituting or acting professor) in chemistry at the University of Strasbourg in late 1848, followed a few years later by appointment as *professeur titulaire* (tenured professor).[16]

Pasteur's discovery, i.e., that some molecules are chiral, was the first clear experimental indication of the importance of the three-dimensional nature of molecules, and is rightly considered the beginning of stereochemistry.[17] His discovery of molecular chirality is all the more remarkable, as it was made at a time when little was known about chemical structure and atomic bonding. For example, the quadrivalency of carbon was first proposed[18] only in 1858, and the earliest speculations on the tetrahedral nature of saturated carbon only appeared in the 1860s.[19] Despite this highly limited state of understanding of molecular structure at the time, Pasteur strongly suspected that molecular chirality would be shown to have important implications for chemistry and biology,[20,21] and his intuition in this regard has been amply confirmed. He even proposed that a tetrahedral or a helical arrangement of the atoms within the molecules could be the source of molecular chirality.[22] As we know today, he was correct with both suggestions. By the early part of the 20th century, Pasteur's discovery of molecular chirality was recognized as fundamentally important for the development of stereochemistry.[23]

DISCREPANCY IN THE DATE OF PASTEUR'S PRESENTATION TO THE *ACADÉMIE*

Pasteur's memoir to the *Académie* on the discovery of molecular chirality published in the *Comptes rendus*[4] was reprinted in Volume 1 of *Œuvres de Pasteur* (Pasteur's collected works, *Œuvres* hereafter) published in 1922, i.e., 74 yr after Pasteur's presentation and 27 yr after his death.[24] The *Œuvres* were collected and edited by Pasteur's grandson, Louis Pasteur Vallery-Radot (1886–1970, LPVR henceforth, see Fig. 1), who devoted a great deal of effort to the preservation and dissemination of the record of Pasteur's life and scientific work. An editorial footnote accompanying the reprinted memoir in the *Œuvres* gives the correct reference (source, year, volume, and pages) to the original memoir in the *Comptes rendus*, and indicates that the presentation of the memoir took place at the May 15th, 1848, session of the *Académie*[25] (see Fig. 2). However, an examination of the volume of the *Comptes rendus* containing Pasteur's memoir[4] reveals unequivocally that Pasteur in fact presented the memoir during the session of Monday, May 22nd, 1848, i.e., 1 wk later than the date given in the *Œuvres*. [25]

Determination of the date of the session of any presentation before the *Académie* is trivially simple. The presentations and other material from each session of the *Académie* were collected in an individual issue (called *Compte rendu des séances de l'Académie des science*, *Compte rendu*,

Fig. 1. Louis Pasteur Vallery-Radot. (Reprinted from the page on Louis Pasteur Vallery-Radot on the official website of the Académie Française (http://academie-francaise.fr/immortels/index.html).

in the singular, henceforth), and the issues were collected in the various volumes of the journal (*Comptes rendus*, in the plural), each issue appearing as an individual subdivision in a given volume. The first page of each issue clearly indicates the date of the session. Thus, we see in Figure 3(a) "SÉANCE DU LUNDI 22 MAI 1848," i.e, "Session of Monday, May 22nd, 1848." In addition, at the bottom of the page we see "C. R., 1848, 1er *Semestre*, (T. XXVI, N^o 21)". "C. R." stands for *Comptes rendus*, "1er *Semestre*" for 1st semester, "T. XXVI" for Volume XXVI (T. = *tome*, i.e., volume), "N^o 21" is the issue number, i.e., the number of the individual *Compte rendu* within the volume. The image in Figure 3(a) is the first page of the issue for the session at which Pasteur presented his memoir (the page number was not printed on the first page of the issues; for the page shown in Figure 3(a) the page number is 529). Therefore, the date can be readily determined for any presentation by simply turning to the first page of the issue in which the presentation appears. Pasteur's memoir began on page 535 (Fig. 3b), and turning back to page 529 in the same issue we find (Fig. 3a) the date of the presentation, "22 Mai 1848." Moreover, there are two other pieces of information in the memoir that formally link it to the date of the session (May 22nd) and rule out May 15th as the session of the presentation. Thus, each issue (i.e., each *Compte rendu*) is identified with an issue number ("N^o") which was given at the bottom of the first page of the issue, together with the other information listed above. As mentioned earlier and seen on Figure 3(a), the issue number for the May 22nd, 1848, session at which Pasteur presented his memoir was 21, shown as "N^o 21" at the bottom of the first page of the issue. The issue number also appeared, sporadically, on a few additional pages of every issue. Thus, "N^o 21" did appear (together with the year, volume, etc.) on page 537 of Pasteur's memoir (Fig. 3c). For comparison, Figure 3(d) shows the first page of the issue for the May 15th, 1848, session, i.e., that of the wrong date. The issue number, "N^o 20," appears at the bottom. Secondly, and obviously, the page numbers of Pasteur's memoir (535–538) also rule out the May 15th session, inasmuch as the last page of the *Compte rendu* for that session is 528. All of the above, then, readily, unequivocally, and clearly links Pasteur's memoir with the May 22nd, 1848, session of the *Académie*. All in all, therefore, it is clear that Pasteur's memoir was presented during the May 22nd session and not on May 15th as claimed in the *Œuvres*.

The first appearance of the erroneous date, May 15th, seems to have been in Volume 1 of the *Œuvres* in 1922,[25] and a search of the literature failed to identify an earlier instance. However, since its first appearance the incorrect date has spread widely, at the expense of the correct date, which is nearly completely absent from the literature. In fact, efforts to locate references to the correct date identified only two independent sources: Jacques Nicolle's 1953 volume on Pasteur contains the correct date[26] (in several subsequent works on Pasteur Nicolle repeated the correct date), and Mislow has it in a recent article.[27] The correct

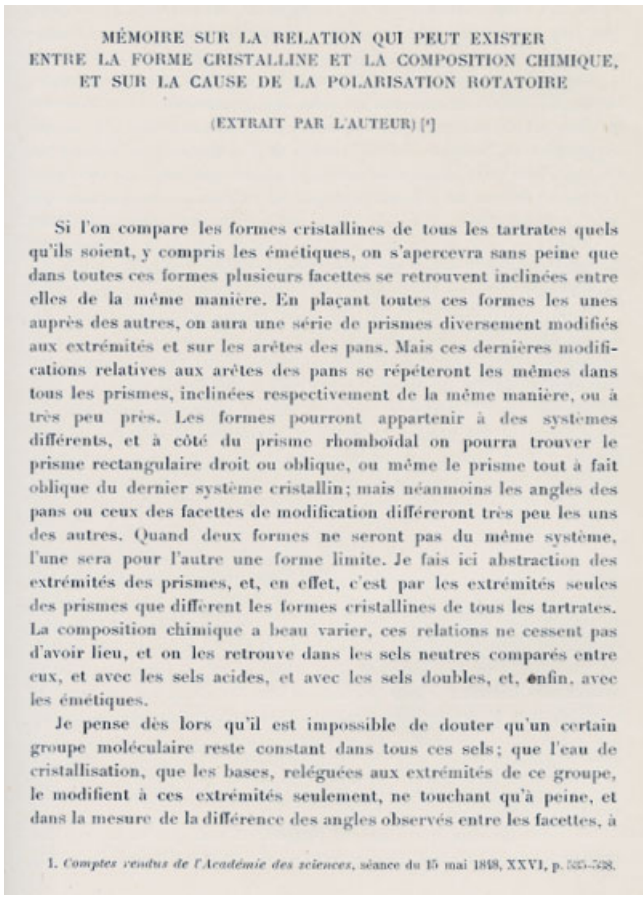

MÉMOIRE SUR LA RELATION QUI PEUT EXISTER ENTRE LA FORME CRISTALLINE ET LA COMPOSITION CHIMIQUE, ET SUR LA CAUSE DE LA POLARISATION ROTATOIRE

(EXTRAIT PAR L'AUTEUR) [1]

Si l'on compare les formes cristallines de tous les tartrates quels qu'ils soient, y compris les émétiques, on s'apercevra sans peine que dans toutes ces formes plusieurs facettes se retrouvent inclinées entre elles de la même manière. En plaçant toutes ces formes les unes auprès des autres, on aura une série de prismes diversement modifiés aux extrémités et sur les arêtes des pans. Mais ces dernières modifications relatives aux arêtes des pans se répéteront les mêmes dans tous les prismes, inclinées respectivement de la même manière, ou à très peu près. Les formes pourront appartenir à des systèmes différents, et à côté du prisme rhomboïdal on pourra trouver le prisme rectangulaire droit ou oblique, ou même le prisme tout à fait oblique du dernier système cristallin; mais néanmoins les angles des pans ou ceux des facettes de modification différeront très peu les uns des autres. Quand deux formes ne seront pas du même système, l'une sera pour l'autre une forme limite. Je fais ici abstraction des extrémités des prismes, et, en effet, c'est par les extrémités seules des prismes que diffèrent les formes cristallines de tous les tartrates. La composition chimique a beau varier, ces relations ne cessent pas d'avoir lieu, et on les retrouve dans les sels neutres comparés entre eux, et avec les sels acides, et avec les sels doubles, et, enfin, avec les émétiques.

Je pense dès lors qu'il est impossible de douter qu'un certain groupe moléculaire reste constant dans tous ces sels; que l'eau de cristallisation, que les bases, reléguées aux extrémités de ce groupe, le modifient à ces extrémités seulement, ne touchant qu'à peine, et dans la mesure de la différence des angles observés entre les facettes, à

1. *Comptes rendus de l'Académie des sciences*, séance du 15 mai 1848, XXVI, p. 535-538.

Fig. 2. First page of Pasteur's memoir on the discovery of molecular chirality in Volume 1 of the *Œuvres* (p 61). Note "séance du 15 Mai 1848" (i.e., session of May 15th, 1848) in the footnote. [Color figure can be viewed in the online issue, which is available at www.interscience.wiley.com.]

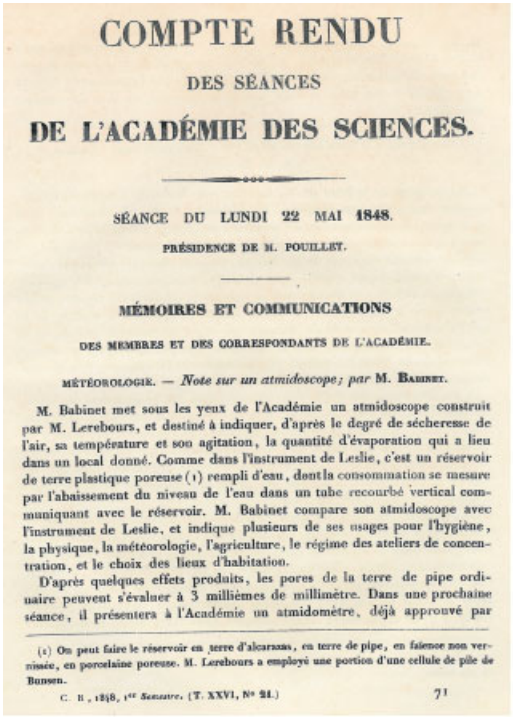

COMPTE RENDU

DES SÉANCES

DE L'ACADÉMIE DES SCIENCES.

SÉANCE DU LUNDI 22 MAI 1848.

PRÉSIDENCE DE M. POUILLET.

MÉMOIRES ET COMMUNICATIONS

DES MEMBRES ET DES CORRESPONDANTS DE L'ACADÉMIE.

MÉTÉOROLOGIE. — *Note sur un atmidoscope; par* M. BABINET.

M. Babinet met sous les yeux de l'Académie un atmidoscope construit par M. Lerebours, et destiné à indiquer, d'après le degré de sécheresse de l'air, sa température et son agitation, la quantité d'évaporation qui a lieu dans un local donné. Comme dans l'instrument de Leslie, c'est un réservoir de terre plastique poreuse (1) rempli d'eau, dont la consommation se mesure par l'abaissement du niveau de l'eau dans un tube recourbé vertical communiquant avec le réservoir. M. Babinet compare son atmidoscope avec l'instrument de Leslie, et indique plusieurs de ses usages pour l'hygiène, la physique, la météorologie, l'agriculture, le régime des ateliers de concentration, et le choix des lieux d'habitation.

D'après quelques effets produits, les pores de la terre de pipe ordinaire peuvent s'évaluer à 3 millièmes de millimètre. Dans une prochaine séance, il présentera à l'Académie un atmidomètre, déjà approuvé par

(1) On peut faire le réservoir en terre d'alcarazas, en terre de pipe, en faïence non vernissée, en porcelaine poreuse. M. Lerebours a employé une portion d'une cellule de pile de Bunsen.

C. R., 1848, 1er Semestre. (T. XXVI, N° 21.) 71

(a)

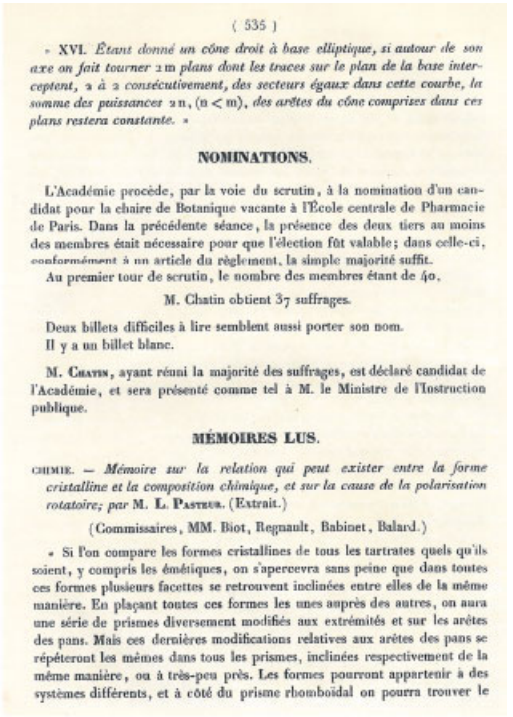

(535)

« XVI. *Étant donné un cône droit à base elliptique, si autour de son axe on fait tourner* 2m *plans dont les traces sur le plan de la base interceptent,* 2 *à* 2 *consécutivement, des secteurs égaux dans cette courbe, la somme des puissances* 2n, (n < m), *des arêtes du cône comprises dans ces plans restera constante.* »

NOMINATIONS.

L'Académie procède, par la voie du scrutin, à la nomination d'un candidat pour la chaire de Botanique vacante à l'École centrale de Pharmacie de Paris. Dans la précédente séance, la présence des deux tiers au moins des membres était nécessaire pour que l'élection fût valable; dans celle-ci, conformément à un article du règlement, la simple majorité suffit.

Au premier tour de scrutin, le nombre des membres étant de 40,

M. Chatin obtient 37 suffrages.

Deux billets difficiles à lire semblent aussi porter son nom.

Il y a un billet blanc.

M. CHATIN, ayant réuni la majorité des suffrages, est déclaré candidat de l'Académie, et sera présenté comme tel à M. le Ministre de l'Instruction publique.

MÉMOIRES LUS.

CHIMIE. — *Mémoire sur la relation qui peut exister entre la forme cristalline et la composition chimique, et sur la cause de la polarisation rotatoire; par* M. L. PASTEUR. (Extrait.)

(Commissaires, MM. Biot, Regnault, Babinet, Balard.)

« Si l'on compare les formes cristallines de tous les tartrates quels qu'ils soient, y compris les émétiques, on s'apercevra sans peine que dans toutes ces formes plusieurs facettes se retrouvent inclinées entre elles de la même manière. En plaçant toutes ces formes les unes auprès des autres, on aura une série de prismes diversement modifiés aux extrémités et sur les arêtes des pans. Mais ces dernières modifications relatives aux arêtes des pans se répéteront les mêmes dans tous les prismes, inclinées respectivement de la même manière, ou à très-peu près. Les formes pourront appartenir à des systèmes différents, et à côté du prisme rhomboïdal on pourra trouver le

(b)

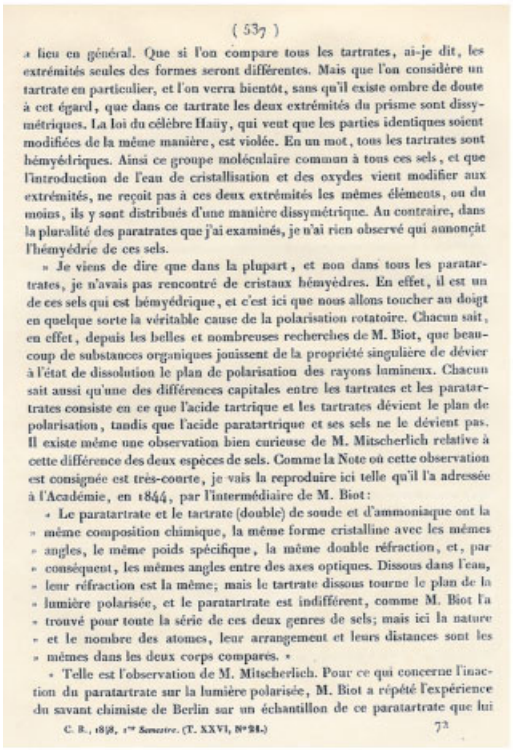

(537)

» lieu en général. Que si l'on compare tous les tartrates, ai-je dit, les extrémités seules des formes seront différentes. Mais que l'on considère un tartrate en particulier, et l'on verra bientôt, sans qu'il existe ombre de doute à cet égard, que dans ce tartrate les deux extrémités du prisme sont dissymétriques. La loi du célèbre Haüy, qui veut que les parties identiques soient modifiées de la même manière, est violée. En un mot, tous les tartrates sont hémyédriques. Ainsi ce groupe moléculaire commun à tous ces sels, et que l'introduction de l'eau de cristallisation et des oxydes vient modifier aux extrémités, ne reçoit pas à ces deux extrémités les mêmes éléments, ou du moins, ils y sont distribués d'une manière dissymétrique. Au contraire, dans la pluralité des paratrates que j'ai examinés, je n'ai rien observé qui annonçât l'hémyédrie de ces sels.

» Je viens de dire que dans la plupart, et non dans tous les paratartrates, je n'avais pas rencontré de cristaux hémyèdres. En effet, il est un de ces sels qui est hémyédrique, et c'est ici que nous allons toucher au doigt en quelque sorte la véritable cause de la polarisation rotatoire. Chacun sait, en effet, depuis les belles et nombreuses recherches de M. Biot, que beaucoup de substances organiques jouissent de la propriété singulière de dévier à l'état de dissolution le plan de polarisation des rayons lumineux. Chacun sait aussi qu'une des différences capitales entre les tartrates et les paratartrates consiste en ce que l'acide tartrique et les tartrates dévient le plan de polarisation, tandis que l'acide paratartrique et ses sels ne le dévient pas. Il existe même une observation bien curieuse de M. Mitscherlich relative à cette différence des deux espèces de sels. Comme la Note où cette observation est consignée est très-courte, je vais la reproduire ici telle qu'il l'a adressée à l'Académie, en 1844, par l'intermédiaire de M. Biot :

« Le paratartrate et le tartrate (double) de soude et d'ammoniaque ont la » même composition chimique, la même forme cristalline avec les mêmes » angles, le même poids spécifique, la même double réfraction, et, par » conséquent, les mêmes angles entre des axes optiques. Dissous dans l'eau, » leur réfraction est la même; mais le tartrate dissous tourne le plan de la » lumière polarisée, et le paratartrate est indifférent, comme M. Biot l'a » trouvé pour toute la série de ces deux genres de sels; mais ici la nature » et le nombre des atomes, leur arrangement et leurs distances sont les » mêmes dans les deux corps compares. »

» Telle est l'observation de M. Mitscherlich. Pour ce qui concerne l'inaction du paratartrate sur la lumière polarisée, M. Biot a répété l'expérience du savant chimiste de Berlin sur un échantillon de ce paratartrate que lui

C. R., 1848, 1er Semestre. (T. XXVI, N° 21.) 72

(c)

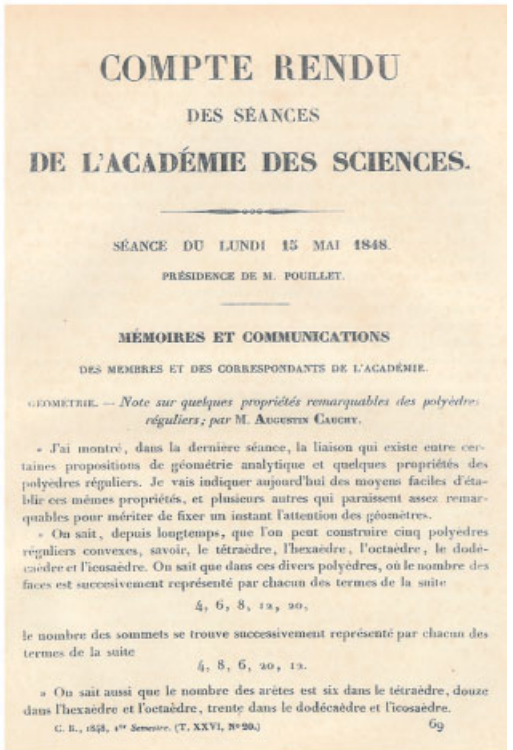

COMPTE RENDU

DES SÉANCES

DE L'ACADÉMIE DES SCIENCES.

SÉANCE DU LUNDI 15 MAI 1848.

PRÉSIDENCE DE M. POUILLET.

MÉMOIRES ET COMMUNICATIONS

DES MEMBRES ET DES CORRESPONDANTS DE L'ACADÉMIE.

GÉOMÉTRIE. — *Note sur quelques propriétés remarquables des polyèdres réguliers; par* M. AUGUSTIN CAUCHY.

« J'ai montré, dans la dernière séance, la liaison qui existe entre certaines propositions de géométrie analytique et quelques propriétés des polyèdres réguliers. Je vais indiquer aujourd'hui des moyens faciles d'établir ces mêmes propriétés, et plusieurs autres qui paraissent assez remarquables pour mériter de fixer un instant l'attention des géomètres.

» On sait, depuis longtemps, que l'on peut construire cinq polyèdres réguliers convexes, savoir, le tétraèdre, l'hexaèdre, l'octaèdre, le dodécaèdre et l'icosaèdre. On sait que dans ces divers polyèdres, où le nombre des faces est successivement représenté par chacun des termes de la suite

4, 6, 8, 12, 20,

le nombre des sommets se trouve successivement représenté par chacun des termes de la suite

4, 8, 6, 20, 12.

» On sait aussi que le nombre des arêtes est six dans le tétraèdre, douze dans l'hexaèdre et l'octaèdre, trente dans le dodécaèdre et l'icosaèdre.

C. R., 1848, 1er Semestre. (T. XXVI, N° 20.) 69

(d)

Fig. 3. (**a**) The first page of the *Compte rendu* for the session of May 22nd, 1848, of the *Académie.* (**b**) The first page of Pasteur's memoir on the discovery of molecular chirality, from the *Compte rendu* of (a). (**c**) Page 537 from Pasteur's memoir showing the issue number, 21, in the footnote. (**d**) The first page of the *Compte rendu* of the session of May 15th, 1848, of the *Académie.* Note the issue number, 20, in the footnote. [Color figure can be viewed in the online issue, which is available at www.interscience.wiley.com.]

date also appears in the *Encyclopedia Britannica*, but the article was authored by Nicolle.[28] Finally, McManus[29] and Buckingham[30] also provide the correct date in their recent respective volumes but both cite Nicolle as their source.

The scarcity of the correct date in the public record is in sharp contrast to the abundance of May 15th, 1848, the incorrect date, in the literature. Since its first appearance in the *Œuvres* in 1922, it has appeared regularly in a variety of publications (many of them important analyses of Pasteur's life or work), e.g., Lowry's milestone volume[31] on optical rotation and chirality which appeared more than 70 yr ago, 13 yr after Volume 1 of the *Œuvres*; an in-depth critique (which appeared 20 yr ago) by Geison and Secord of Pasteur's own account of his discovery of molecular chirality[32]; a detailed review and seminal analysis of Pasteur's discovery by Mauskopf from 1976[33]; the 1994 biography[34] of Pasteur by Maurice Vallery Radot (MVR); Debré's 1994 biography of Pasteur (Debré is also mistaken in claiming that Pasteur's memoir was presented by Balard)[35]; Geison's 1995 volume[36] on Pasteur's ethics in science; an article by Kauffman et al.,[37] and other publications.[38–40] In addition, several websites give May 15th, 1848, as the date of the presentation, including, surprisingly, the website of the Pasteur Institute in Paris.[41]

Admittedly, it has not been possible in this survey to examine every publication or document in the massive literature on Pasteur, but the relative proportions found clearly indicate the scarcity of the correct date in comparison to the abundance of the erroneous date.

Fig. 4. Pasteur's mother, Jeanne-Étiennette Pasteur; pastel by Louis Pasteur, 1836. (Reprinted from "IMAGES DE LA VIE ET DE LŒUVRE DE PASTEUR," by L. Pasteur Vallery-Radot, Flammarion, 1956).

THE EVENTS OF THE EPISODE: WHAT DO WE KNOW?

As discussed earlier, Pasteur read his memoir to the *Académie* in Paris on Monday, May 22nd, 1848. His parents lived in the small town of Arbois, in the *département* (administrative district) of Jura, in the Franche-Comté region of eastern France. On Sunday, May 21st, 1848—i.e., one day before Pasteur presented his memoir to the *Académie* in Paris—his mother, Jeanne Étiennette Pasteur (née Roqui, 1793–1848, see Fig. 4), died in Arbois.[42–44] In view of the one-day separation between the death of Pasteur's mother in Arbois and his presentation at the *Académie* in Paris, the mysterious appearance of the incorrect date for the presentation inevitably attracts the attention.

On May 27th Pasteur wrote to Dumas from Arbois: "I have just returned to my family, called by a *letter informing me that my mother was very ill*. By the time I arrived she had died." [my emphasis]. This letter appears[45] in the *Correspondance de Pasteur* (Pasteur's published correspondence, *Correspondance* hereafter), which was also collected and edited by Pasteur's grandson. On the same day, May 27th, 1848, Pasteur also wrote[46] to Paul-François Dubois, director of the École normale: "By the time I arrived my mother had died. She succumbed in a few hours to an attack of apoplexy." On the following day, May 28th, Pasteur, still in Arbois, wrote to Chappuis in a similar vein, indicating that his mother had died within a few hours.[47] In these letters no date or time is given for the mother's death, nor are the dates of Pasteur's departure from Paris and arrival in Arbois provided.

MVR, grand-nephew of Pasteur's son-in-law René Vallery-Radot (1853–1933, RVR henceforth, see Fig. 5), writes in his 1994 biography of Pasteur that his mother died suddenly while preparing to attend mass on Sunday, May 21st, 1848, but he does not identify the source of this information nor does he provide any additional details on the events.[48]

We do not know when Pasteur received the letter alerting him to his mother's *illness*, and no information appears to have been published on the method by which the letter was transported from Arbois to him in Paris. Pasteur used the word *lettre* (i.e., letter) to refer to the communication which informed him of his mother's illness.[45] According to the *Musée de la Poste* (the museum of the French postal services in Paris), it was only in 1851 that electric telegraph service became available to the public in France[49] (in 1853, Pasteur marveled at the newly available telegraph system and used it to send a message—he used the term *dépêche télégraphique,* i.e., telegram—to Biot).[50]

As for letters sent via the postal service, according to the *Musée de la poste* a letter sent from Arbois in 1848 would have taken at least 3 days to reach Paris (personal communication obtained at the museum in May 2006). Thus, a letter mailed from Arbois by post a few hours

Fig. 5. René Vallery-Radot. (Reprinted from "IMAGES DE LA VIE ET DE LŒUVRE DE PASTEUR," by L. Pasteur Vallery-Radot, Flammarion, 1956).

before the death of Pasteur's mother on May 21st would have reached him well after his presentation at the *Académie* on the 22nd.

It is also possible, however, that the letter was carried from Arbois to Pasteur in Paris by a courier. In 1848 there was no rail link to Arbois (see Fig. 6), and even today, there is no railway service to Arbois. The map in Figure 6 shows the service as it existed in 1850, and it is not certain that every railway line on the map was also functioning in 1848; thus, the map is a best-case scenario of the service that may have been available 2 yr earlier. The nearest train stops to Arbois with service to Paris were in Tonnerre and Nevers (see Fig. 6). Thus, a courier would have had to take a *diligence* (stagecoach) from Arbois at least to one of these towns and then take a train from there to Paris. In 1848 (the year of the events in question) it took "une journée," i.e., at the minimum the daylight hours of a day, to travel by train from Paris to Le Havre,[51] a distance roughly equal to the train trajectory from Nevers to Paris. As for the time it would have taken a stagecoach to travel from Arbois to Nevers or Tonnerre (if indeed there was such a service), it is difficult to estimate it, but it is instructive that Pasteur's father indicated in 1845 that it took 3 h to travel from Arbois to Dijon (a town considerably closer to Arbois than are Tonnerre and Nevers, see Fig. 6).[52] Since there was no train service between Arbois and Dijon at the time, Pasteur's father was presumably referring to travel by stagecoach or to a combination of stagecoach to Chalon and from there by train to Dijon (see Fig. 6). Taking into account the likely limitations of stagecoach and train schedules, connections, delays, etc., it does not appear at all certain that a courier leaving Arbois Sunday morning, at the earliest, would have been able to reach Pasteur with the letter before the presentation at the *Académie* in Paris the following day. It is also instructive in this regard that in 1844 Pasteur complained[53] to Chappuis that it had taken him 3 days to travel from Paris to Arbois. While Pasteur indicated that on that occasion the service was particularly slow, and it took place 4 yr earlier than the events in question, the three-day trip nevertheless gives an indication of the time-scale of travel between Paris and Arbois in the mid-1840s. Thus, overall, delivery of the letter to Pasteur in Paris before the presentation appears to have been unlikely, but, technically, without more definitive information, it cannot be ruled out with certainty.

Two points need to be emphasized here. (1) If it is true that Pasteur's mother fell ill on Sunday, the 21st of May and died within a few hours, and if he did receive the letter informing him of her illness *before* the presentation at the *Académie* on the 22nd and had immediately departed for Arbois, he would not have arrived in time to see his mother alive. (2) Given the short time frame between his mother's death on the 21st and his presentation at the *Académie* on the 22nd, if Pasteur did leave for Arbois before his presentation, he could not have returned to Paris in time to appear before the *Académie* on the 22nd. It is therefore an inescapable conclusion that Pasteur must have left for Arbois *after* his presentation at the *Académie* on May 22nd, even if he received the letter before his presentation. This conclusion is in accord with his statement in the above-cited[45] letter of May 27th from Arbois that "I have just returned to my family ...."

TREATMENT OF THE EPISODE IN THE LITERATURE ON PASTEUR

The Works of René Vallery-Radot

Pasteur's first biographer was his son-in law, RVR (LPVR's father). His first biography[54] of Pasteur appeared (anonymously) in 1883, while Pasteur was still alive, and is known to have been produced under Pasteur's control.[55,56] The biography focused on Pasteur's scientific work, with few personal details of his adult life mentioned. Pasteur's presentation of his discovery of molecular chirality to the *Académie* is not mentioned in this biography, while many other of Pasteur's presentations to the *Académie* are mentioned by date and discussed. A few examples: his presentation in 1857 of lactic fermentation[57]; the presentation of April 30th, 1877, on anthrax[58]; the presentation of February 28th, 1881, on the anthrax vaccine,[59] etc. It is simply incomprehensible that Pasteur's presentation of his first major discovery, molecular chirality, before the *Académie* was not even mentioned in RVR's scientific biography of Pasteur. This was the discovery that catapulted the

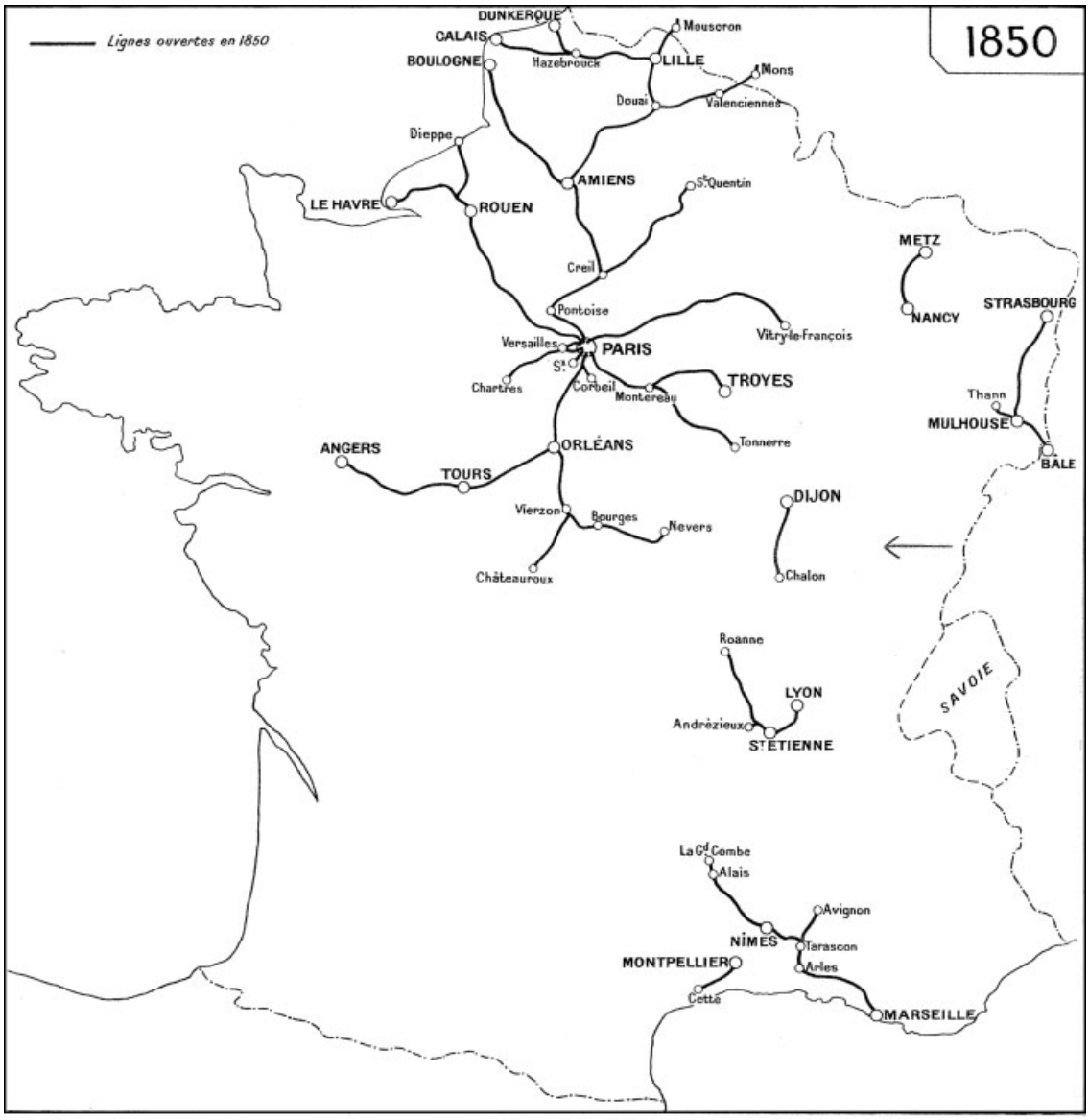

Fig. 1. — Le Réseau ferré français en 1850.

Fig. 6. Map of the railway network in France in 1850. Arbois is located at the tip of the arrow, added by the present author. (Reprinted from "GÉOGRAPHIE DES CHEMINS DE FER FRANÇAIS", by Henri Lartilleux, Chaix, 1962).

unknown 25-yr-old new doctor of science from obscurity to the forefront of French science, brought him recognition and admiration from the French scientific establishment,[15] and launched his stellar career.

Pasteur died in 1895, and in 1900 RVR published *La Vie de Pasteur* (The Life of Pasteur), a celebrated biography which went through numerous subsequent editions. In this work RVR mentions[60] the death of Pasteur's mother but does not give a date, and quotes from Pasteur's May 28th letter[47] to Chappuis (see above). Moreover, while RVR outlines the main events of the discovery of molecular chirality, Pasteur's presentation of the discovery to the *Académie* is not mentioned.[61] This treatment by RVR of two major events in Pasteur's life in the detailed and then-definitive biography of Pasteur is, again, difficult to comprehend. The absence of a reference to the presentation of molecular chirality to the *Académie* is particularly unexpected, since the great importance of the discovery was well-known to RVR in 1900, more than 50 yr after it was made, and the omission from *La Vie de Pasteur* of its announcement by Pasteur to the *Académie* is all the more puzzling, since as in the earlier biography by RVR (see above), the author mentions by date and discusses many other of Pasteur's presentations to the *Académie*. A few examples: the presentation of March 20th, 1848,[62] which took place 2 mo before that on molecular chirality and dealt with a study of dimorphism, an investigation whose significance can only be described, at best, as minor when compared with the discovery of molecular chirality; the presentation of September 30th, 1850[63]; the presentation

of May 30th, 1881, on rabies[64]; etc. To summarize, the presentation by Pasteur of the discovery of molecular chirality to the *Académie* is conspicuously and inexplicably absent from RVR's biographies of Pasteur. Moreover, no information is provided by RVR on the circumstances of the death of Pasteur's mother or on Pasteur's trip to Arbois in conjunction with her death.

The Works of LPVR

The Œuvres. The editorial inclusion of the incorrect date, May 15, 1848, in the *Œuvres* for Pasteur's presentation to the *Académie*[25] is puzzling because the date of the session for any presentation appearing in the *Comptes rendus* is immediately obvious upon examining the article in the particular volume it appears in, as discussed earlier. LPVR was a distinguished professor of medicine, a noted medical researcher, accomplished writer, and member of the *Académie de Médecine* (Academy of Medicine) and the prestigious *Académie française* (French Academy [of letters]).[65,66] It is difficult indeed to understand that he could have failed to extract the correct date from the *Comptes rendus*. The *Œuvres* were published during the period of 1922–1939. The final volume, 7, dated 1939, contains a detailed chronological table of Pasteur's work, an extensive index, and other material. In the chronological table, Pasteur's presentation to the *Académie* of the discovery of molecular chirality is still shown[67] to have taken place on May 15th 1848. Thus, after its first appearance in Volume 1 in 1922, the error was repeated 17 yr later in Volume 7.

It is also relevant here that Jacques Nicolle's 1953 volume on Pasteur gives the correct date of Pasteur's presentation,[26] as mentioned above. Jacques Nicolle (1901–1971)[68] was a French physicist, director of the Laboratory of Biochemistry of Isomers of the *École pratique des hautes études*, Paris. His father, Maurice Nicolle[69] (1862–1932), was a collaborator of Pasteur, and his uncle, Charles Nicolle (1866–1936), also a disciple of Pasteur, was a Nobel laureate (1928) bacteriologist.[70] In his autobiography (published in 1966), LPVR describes his admiration for and close friendship with Charles Nicolle,[71] and also indicates that he knew Maurice Nicolle.[72] In light of the above and considering LPVR's exhaustive work on Pasteur, it would be difficult to believe that LPVR was not aware of Jacques Nicolle's publications on Pasteur, and the true date of the presentation therein. LPVR does not mention Jacques Nicolle (who was his contemporary) in his autobiography.

The Correspondance. Aside from the above-cited letters by Pasteur from Arbois concerning his mother's death no other information on her illness or death or on his return to Arbois in connection with these events is found in the letters included in the *Correspondance*. The letter Pasteur refers to which informed him of his mother's illness does not appear in the *Correspondance*.

It is also troubling that in the *Correspondance* we find no letter by or to Pasteur about his momentous announcement to the *Académie* of the discovery of molecular chirality. This lack is most puzzling in view of the presence in the *Correspondance* of many letters referring to other presentations by Pasteur to the *Académie*. For example, in a letter[73] to Chappuis dated May 5, 1848, Pasteur expressed satisfaction over the favorable reception ("très bien accueilli") of the memoir on dimorphism (see above) which he had read to the *Académie* ca. 2 mo before the presentation of the memoir on molecular chirality. Another example is that of the presentation of January 3rd, 1853,[74] etc.

Other works by LPVR. In addition to the *Œuvres* and the *Correspondance*, LPVR produced several other volumes about Pasteur, including a short biography in which he gives the date of the death of Pasteur's mother and writes that "she died suddenly." He then adds that "Pasteur's grief was hardly lessened by the satisfaction with which he had, *a few days before*, presented at the Academy of Sciences" his memoir on molecular dissymmetry[75] [my emphasis]. Thus, here too, LPVR places the presentation *before* the death of Pasteur's mother on May 21st; however, here he gives no date for the presentation.

In addition to placing the presentation before May 21st, LPVR treats Pasteur's historic announcement very differently from his handling of other presentations by Pasteur to the *Académie*, several of which are given by date in the biography.[76–78] Moreover, on October 26, 1868, shortly after Pasteur suffered a stroke, Dumas read a note by Pasteur to the *Académie*, and this too is mentioned[79] by date in the biography by LPVR. The contrast is striking and it is, again, difficult to comprehend why Pasteur's historic announcement to the *Académie* of his first major discovery is almost entirely ignored by LPVR.

LPVR died in 1970, and a search of the literature failed to identify a correction by him of the erroneous date.

Works by Other Authors

Since his death more than a century ago, Pasteur's life and work has been the subject of numerous other publications. In recent years, several authors have studied extensive portions of the considerable documentary record of Pasteur's life and work. Geison, for example, examined a large number of archival sources and documents (published and unpublished) in France and elsewhere for his volume, and the French writers Debré and MVR also drew on large portions of the documentary record in the preparation of their biographies. Nevertheless, all three authors cite the wrong date for Pasteur's presentation to the *Académie*.[34–36]

For the purposes of this article, in addition to the sources cited earlier, many other publications[80–94] on Pasteur were examined but none of these mention a specific date for the presentation in May 1848. Moreover, no discussion of the discrepancy in the date of the presentation or any correction of the erroneous date has been found in the literature. However, in one of their articles, Kauffman and Myers state[95] that Pasteur's presentation took place on May 15th, 1848, and the memoir published a week later, i.e., on the 22nd. There is, however, no basis for their claim: the *Comptes rendus* clearly and unequivocally indicates the session in which a memoir was presented, as discussed above. To further illustrate, on the 12th of August,

1858, Pasteur wrote[96] to the members of the Commission on the Experimental Physiology Prize of the *Académie*: "I had the honor to present to the *Académie* during its session of March 29th, 1858, some results of a study of the fermentation of tartaric acid and its isomers." The issue of the *Comptes rendus* for the session of March 29th, 1858, in fact contains Pasteur's memoir on the fermentation of tartaric acid.[97] In summary, then, the claim by Kauffman and Myers that Pasteur presented his memoir on May 15th, 1848, and that the memoir was then published a week later, on May 22nd, 1848, is contradicted by the evidence.

The Events in the Literature: Conclusions

As we have seen above, overall, the literature is of little help in our attempt to determine the details and implications of the relevant events of May 1848. Little information is available on the circumstances of the death of Pasteur's mother, and most publications that give a date for Pasteur's presentation cite the wrong date. Moreover, the conflict in the dates is not discussed in the literature. Of considerable significance is the unmistakably terse treatment of the events of the episode in the works of RVR and LPVR. It is indeed difficult to comprehend that Pasteur's prestigious appearance, at age 25, before the *Académie* to present his first major discovery should be nearly completely ignored by his biographer relatives in their works, which otherwise can only be described as hagiographic portrayals of the public scientist and the private man.

THE HAGIOGRAPHY

Pasteur worked on chirality for ca. 10 yr,[98] and by the late 1850s had moved on to microbiology, followed later by his celebrated work on infectious diseases. As is well-known, his work in these fields was revolutionary and of great benefit to human health and the practice of medicine, veterinary medicine, agriculture, etc. His discoveries reveal a scientist with superior scientific intuition, an exceptional observer, and an outstanding experimentalist.

However, these qualities and achievements of Pasteur do not suffice in the reconstruction of the totality of the individual. Pasteur was, to be sure, one of the most accomplished scientists the world has known, but he was also a complex individual with both admirable qualities and human failings.[99–102] Moreover, it is now recognized that a great deal of the published writings on Pasteur's life and work engaged in hagiography and often presented a less-than-accurate image of the scientist and the man, an image closer to a demigod than to a human being with complexities and imperfections.[99,102–105]

The hagiographic distortion of Pasteur began in his own lifetime, with his first biography, by RVR,[54] and continued soon after his death with RVR's *La Vie de Pasteur*. Moreover, *La Vie de Pasteur* considerably influenced[103] a great deal of the subsequent works on Pasteur. In this regard, a reading of LPVR's biography[106] of Pasteur clearly shows that LPVR relied heavily on his father's *La Vie de Pasteur*, and continued the hagiographic portrayal of Pasteur. The hagiographic image of Pasteur has persisted in the literature for much of the 20th century, and its deconstruction began only relatively recently, but a more accurate depiction of Pasteur and his place in 19th century science, culture, society, and politics remains to be published.[102]

THE ESSENTIAL QUESTIONS

Overall, then, we are left with a striking paucity of facts concerning this important episode in Pasteur's life. The available information is limited to a puzzling, terse, and incomplete recounting of the events in the biographies by RVR and LPVR, the absence of the presentation at the *Académie* in the *Correspondance*, and a bizarre incorrect date in the *Œuvres*. In light of the pervasive hagiographic approach to Pasteur by his biographer relatives, this state of affairs prompts the following questions: was the true date of the presentation deliberately altered in the *Œuvres* and did the two family biographers manipulate and hide the facts surrounding the events in their works on Pasteur? That is, was Pasteur's famous presentation in Paris one day after his mother's death in Arbois viewed by LPVR and RVR as potentially intolerably damaging to their faultless image of the national hero, regardless of the precise reasons for his absence from Arbois at the time of her death? According to this hypothesis, it is also logical to assume that in addition to altering the date of Pasteur's presentation, minimizing the discussion of the events would have seemed necessary to RVR and LPVR to avoid potentially causing the emergence of some inconvenient details. This, then, would explain the laconic or silent treatment of Pasteur's first great discovery and his mother's death by the two biographers.

Another question of interest is whether Pasteur—if he received the letter alerting him to his mother's illness *before* the presentation at the *Académie*—decided to delay his departure to Arbois until after the presentation. Such a decision would presumably have been influenced by several factors, e.g., the exact contents of the letter, the precise time of its receipt, and by train and stagecoach schedules, etc. As we have seen, it is not very likely that Pasteur received notification of his mother's illness before his appearance at the *Académie,* but technically it cannot be ruled out. As we have also seen, however, given the limited amount of time available and the travel conditions in the 1840s, in any case, Pasteur could not have arrived in time to see his mother alive. Furthermore, it is also clear that he left for Arbois only after his presentation at the *Académie.*

The silence about Pasteur's presentation of May, 1848, in the 1883 biography by RVR is also relevant in this context, inasmuch as it is clear that the biography was written under close supervision by Pasteur (see earlier), raising the question of Pasteur's role in the affair.

In considering these matters, we must also bear in mind Pasteur's renowned unrelenting work habits,[107,108] ambition,[109] and pursuit of glory,[110] which are known to have interfered, at times drastically, with his family life. A portion of a letter Pasteur's wife Marie (née Laurent, 1826–1910, see Fig. 7) wrote to her daughter Marie-Louise and son-in-law RVR on her (Marie's) 35th wedding anniversary

Fig. 7. Marie Pasteur, 8 yr after marrying Pasteur. (Reprinted from "IMAGES DE LA VIE ET DE LŒUVRE DE PASTEUR," by L. Pasteur Vallery-Radot, Flammarion, 1956).

is illustrative in this context: "Your father, always very busy, speaks little to me, sleeps little, and gets up at dawn; in a word, he continues the life I started with him 35 yr ago today."[111]

Also relevant in this context is the death of Cécile, one of the Pasteurs' four daughters. In May, 1866, at age 12, she is stricken with typhoid fever in Chambéry. Pasteur is in Alès, engaged in studies on diseases of silkworms, studies which he had been asked to undertake by Dumas, and which were eventually credited with saving the French silk industry. Despite the alarming news about Cécile, Pasteur remains in Alès. His wife Marie writes him pressing letters urging him to join her at Cécile's bedside, and he finally leaves for Chambéry. He finds his daughter feeling somewhat better and remains with her only 3 days, returning thereafter to Alès, apparently not trusting his collaborators' work in his absence. Cécile dies on May 23rd without having seen her father again.[112] Jeanne, another of Pasteur's daughters, died at age 9 in Arbois 7 yr earlier, in September, 1859, also of typhoid fever; Pasteur arrived from Paris too late to see her alive.[113] Debré, a biographer of Pasteur highly sympathetic to his subject, writes that after the death of his father in 1865 Pasteur often sought to justify himself in reaction to his own feelings of remorse about putting his passion for science ahead of love for his family.[114]

Given all of the above, then, it does not appear unreasonable to suggest that RVR and LPVR may have been apprehensive of a potentially negative judgment that would be created by Pasteur's absence from Arbois on the day of his mother's death, when that absence is coupled with his appearance before the *Académie* in Paris on the following day. Does this mean that they did falsify the record? We can only conjecture, but the evidence, in its totality, is strongly suggestive of an affirmative answer to the question.

CONCLUSIONS

RVR's and LPVR's hagiographic treatment of Pasteur's life and work is a matter of public record, and an inexplicably terse or silent treatment of the events of May, 1848, is also unmistakable in their works on Pasteur. Nonetheless, definite answers to the questions raised above cannot be given in the absence of additional, specific, information. Yet the available evidence strongly suggests an alteration and manipulation of the record, presumably for fear of an adverse public judgment of Pasteur for a real or perceived insensitivity at a time of a grave family medical emergency. Such concerns for Pasteur's reputation would have been expected from RVR and LPVR, who were the early creators and fervent protectors of the hagiographic image of Pasteur as a "demigod." Thus, the findings of this article raise new questions concerning the state of mind of Pasteur's closest biographers and the extent and limit of their zeal in protecting the exalted image they constructed of him.

Why has the discrepancy in the date of Pasteur's historic presentation escaped attention until now? A part of the answer is undoubtedly the paucity of information on the facts of the case. In addition, one wonders whether a century of hagiography on Pasteur has dampened interest in potentially unfavorable information about the "lay saint." As for the continuing recurrence of the erroneous date in the literature today, the explanation may lie in the considerably greater worldwide availability of the *Œuvres* than the 1848 issues of the *Comptes rendus* (personal communication from Clark Driese of Denison Memorial Library, University of Colorado Health Sciences Center).

In chronicling the history of science, it is obviously essential to be accurate about the chronology. Some, however, may think that a ("small") 1-wk error perpetuated in the literature concerning the date of the announcement of one of the most important discoveries in science matters little. This author (probably as many others) believes, on the other hand, that accuracy in science, including in accounts of its history, is of paramount importance. If we cannot get a simple date right, how much confidence can we have in getting the concepts right? Moreover, researching the origins and causes of errors in historical accounts and correcting them is essential not only for historical accuracy, but also because such investigations can produce additional insights into the history of science, scientists, and their chroniclers. In this case, for example, tracking down the conflict in the dates has revealed that Pasteur's closest biographers most likely falsified the date and dis-

torted their accounts of his work to protect his hagiographic image. Surely, these findings are significant and helpful for an understanding of the biographers' state of mind, their great zeal to protect his image, and for interpreting their writings.

Finally, a last observation: regardless of the reasons for the original appearance of May 15th in the *Œuvres* and irrespective of the explanation for the continuing acceptance of the wrong date in the literature, there is no doubt that by now—160 yr after the historic presentation and 86 yr after the emergence of the erroneous date—universal recognition of May 22nd, 1848, as the correct date of Pasteur's announcement of his discovery of molecular chirality is long overdue.

ACKNOWLEDGMENTS

The author is indebted to Catherine Reiter, Dr. Lilian Hoffecker, Lisa Traditi, and Clark Driese of Denison Memorial Library, University of Colorado Health Sciences Center, for valuable assistance. The author is also deeply grateful to Agnès Fontaine of the *Association des Anciens Élèves de l'École normale supérieure* in Paris for providing a copy of Chappuis' obituary of Pasteur. Information on the French railroad network in 1850 kindly provided by Marie-Noëlle Polino of the *Association de l'Histoire des chemins de fer en France, AHICF*, i.e., French Railway Historical Society, Dominique Perchet of *CILAC: la base de données du patrimoine industriel*, and Professor Goulven Guilcher of the University of Paris is acknowledged with gratitude. Helpful comments from the anonymous reviewers are also greatly appreciated.

LITERATURE CITED

1. Eliel EL, Wilen S. Stereochemistry of organic compounds. New York: Wiley; 1994. p 2.
2. Biot J-B. Instructions pratiques sur l'observation et la mesure des propriétés optiques appelées rotatoires. Paris: Bachelier; 1845.
3. Biot J-B. Instructions pratiques sur l'observation et la mesure des propriétés optiques appelées rotatoires. Paris: Bachelier; 1845. p 3.
4. Pasteur L. Mémoire sur la relation qui peut exister entre la forme crystalline et la composition chimique, et sur la cause de la polarisation rotatoire. C R Séances Acad Sci 1848;26:535–538.
5. Pasteur L. Thèse de chimie. Recherches sur la capacité de saturation de l'acide arsénieux. Étude des arsénites de potasse, de soude et d'ammoniaque. In: Pasteur Vallery-Radot L, editor. Œuvres de Pasteur, Vol. 1. Paris: Masson et C^{ie}; 1922. p 1–18.
6. Pasteur L. Thèse de physique. 1. Étude des phénomènes relatifs à la polarisation rotatoire des liquides. 2. Application de la polarisation rotatoire des liquides à la solution de diverses questions de chimie. In: Pasteur Vallery-Radot L, editor. Œuvres de Pasteur, Vol. 1. Paris: Masson et C^{ie}; 1922. p 19–30.
7. Geison GL. Pasteur, Louis. In: Gillispie CC, editor. Dictionary of Scientific Biography, Vol. X. New York: Charles Scribner's Sons; 1974. p 356–357.
8. Pasteur L. In: Pasteur Vallery-Radot L, editor. Correspondance de Pasteur I. Lettres de jeunesse. L'étape de la crystallographie. 1840–1857. Paris: Flammarion; 1940. p 162–163.
9. Pasteur Vallery-Radot L. In: Pasteur Vallery-Radot L, editor. Correspondance de Pasteur I. Lettres de jeunesse. L'étape de la crystallographie. 1840–1857. Paris: Flammarion; 1940. p 163.
10. Pasteur L. Recherches sur la dissymétrie moléculaire des produits organiques naturels. In: Pasteur Vallery-Radot L, editor. Œuvres de Pasteur, Vol. 1. Paris: Masson et C^{ie}; 1922. p 320–327.
11. Kaufmann GB, Myers D. The resolution of racemic acid. A classic stereochemical experiment for the undergraduate laboratory. J Chem Ed 1975;52:777–781.
12. Geison GL. The Private Science of Louis Pasteur. Princeton: Princeton University Press; 1995. p 53.
13. Nicolle J. Structure Moléculaire et Propriétés Biologiques. Cas Particulier des Isomères Optiques. Paris: Flammarion; 1973. p 12.
14. Vallery-Radot R. La vie de Pasteur. Paris: Librairie Hachette et C^{ie}; 1900. p 46–47.
15. Regnault HV, Balard J-A, Dumas J-B, Biot J-B. I. Rapport sur un mémoire présenté à l'Académie par M. L. Pasteur, avec ce titre: Recherches sur les relations qui peuvent exister entre la forme crystalline, la composition chimique et le sens du pouvoir rotatoire. In: Pasteur Vallery-Radot L, editor. Œuvres de Pasteur, Vol. 1. Paris: Masson et C^{ie}; 1922. p 415–423.
16. Geison GL. Pasteur, Louis. In: Gillispie CC, editor. Dictionary of Scientific Biography, Vol. X. New York: Charles Scribner's Sons; 1974. p 360.
17. Eliel EL, Wilen S. Stereochemistry of Organic Compounds. New York: Wiley; 1994. p 6.
18. Brock WH. The Norton History of Chemistry. New York: WW Norton; 1992. p 245–256.
19. Brock WH. The Norton History of Chemistry. New York: WW Norton; 1992. p 259.
20. Pasteur L. Recherches sur la dissymétrie moléculaire des produits organiques naturels. Première leçon. In: Pasteur Vallery-Radot L, editor. Œuvres de Pasteur, Vol. 1. Paris: Masson et C^{ie}; 1922. p 315–328.
21. Pasteur L. Recherches sur la dissymétrie moléculaire des produits organiques naturels. Deuxième leçon. In: Pasteur Vallery-Radot L, editor. Œuvres de Pasteur, Vol 1. Paris: Masson et C^{ie}; 1922. p 329–344.
22. Pasteur L. Recherches sur la dissymétrie moléculaire des produits organiques naturels. In: Pasteur Vallery-Radot L, editor. Œuvres de Pasteur, Vol. 1. Paris: Masson et C^{ie}; 1922. p 327.
23. Walden P. Salts, Acids, and Bases: Electrolytes: Stereochemistry. New York: McGraw-Hill Book; 1929. p 346–347.
24. Pasteur L. Mémoire sur la relation qui peut exister entre la forme crystalline et la composition chimique, et sur la cause de la polarisation rotatoire. In: Pasteur Vallery-Radot L, editor. Œuvres de Pasteur, Vol. 1. Paris: Masson et C^{ie}; 1922. p 61–64.
25. Pasteur L. Mémoire sur la relation qui peut exister entre la forme crystalline et la composition chimique, et sur la cause de la polarisation rotatoire. In: Pasteur Vallery-Radot L, editor. Œuvres de Pasteur, Vol. 1. Paris: Masson et C^{ie}; 1922. p 61.
26. Nicolle J. Louis Pasteur: Un maître de l'enquête scientifique. Paris: La Colombe; 1953. p 25–26.
27. Mislow K. Introduction—Retournons à Pasteur! In: Lough WJ, Wainer IW, editors. Chirality in Natural and Applied Science. Oxford: Blackwell Science; 2002. p iii.
28. "Pasteur, Louis." Encyclopædia Britannica. 2007. Encyclopædia Britannica Online. Available at: http://www.britannica.com/eb/article-12563. Accessed on September 24, 2007.
29. McManus C. Right Hand, Left Hand: The Origins of Asymmetry in Brains, Bodies, Atoms, and Cultures. London: Weidenfeld and Nicholson; 2002. p 7, 363.
30. Buckingham J. Chasing the Molecule. Phoenix Mill: Sutton Publishing; 2004. p 201, 234.
31. Lowry TM. Optical Rotatory Power. London: Longmans, Green and Co.; 1935. p 28.
32. Geison GL, Secord JA. Pasteur and the process of discovery: The case of optical isomerism. Isis 1988;79:32–33.
33. Mauskopf SH. Crystals and compounds: Molecular structure and composition in nineteenth-century French science. Trans Am Philos Soc 1976;66:78.
34. Vallery-Radot M. Pasteur. Paris: Perrin; 1994. p 418.
35. Debré P. Louis Pasteur. Paris: Flammarion; 1994. p 63, 530.
36. Geison GL. The Private Science of Louis Pasteur. Princeton: Princeton University Press; 1995. p 85.
37. Kauffman GB, Bernal I, Schütt H-W. Overlooked opportunities in stereochemistry. IV. Eilhard Mitscherlich's near discovery of con-

glomerate crystallization: On the sesquicentennial of Pasteur's resolution of sodium ammonium racemate. Enantiomer 1999;4:33.
38. Jacques J. La dissymétrie moléculaire. In: Balibar F, Prévost M-L, editors. Pasteur—Cahier d'un savant. Paris: CNRS Éditions; Cadeilhan: Zulma; 1995. p 54.
39. Kostyanovsky RM. Louis Pasteur did it for us especially. Mendeleev Communications (Electronic Version) 2003; Issue 3:2.
40. Vallery-Radot M. Pasteur: Dessins et Pastels. Paris: Éditons Hervas; 1987. p 133.
41. http://www2.pasteur.fr/infosci/biblio/ressources/histoire/pasteur.php.
42. Vallery-Radot M. Pasteur. Paris: Perrin; 1994. p 29, 418.
43. Bellague M, Gallois J-M. Généalogie des familles Pasteur. Salins les-Bain: E. Bellague-Gallois; 1999. p Jean. 74.
44. Debré P. Louis Pasteur. Paris: Flammarion; 1994. p 530.
45. Pasteur L. À J.-B. Dumas. In: Pasteur Vallery-Radot L, editor. Correspondance de Pasteur I. Lettres de jeunesse. L'étape de la crystallographie. 1840–1857. Paris: Flammarion; 1940. p 172.
46. Pasteur L. À M. Dubois, conseiller de l'Université, Directeur de l'École normale supérieure. In: Pasteur Vallery-Radot L, editor. Correspondance de Pasteur I. Lettres de jeunesse. L'étape de la crystallographie. 1840–1857. Paris: Flammarion; 1940. p 173.
47. Pasteur L. À Chappuis. In: Pasteur Vallery-Radot L, editor. Correspondance de Pasteur I. Lettres de jeunesse. L'étape de la crystallographie. 1840–1857. Paris: Flammarion; 1940. p 174.
48. Vallery-Radot M. Pasteur. Paris: Perrin; 1994. p 29.
49. http://www.museedelaposte.fr/Collections/Salle_4/index.htm.
50. Pasteur L. À son père. In: Pasteur Vallery-Radot L, editor. Correspondance de Pasteur I. Lettres de jeunesse. L'étape de la crystallographie. 1840–1857. Paris: Flammarion; 1940. p 313–315.
51. Caron F. Histoire des Chemins de Fer en France—Tome premier 1740–1883. Paris: Fayard: 1997; p 366–367.
52. Pasteur J-J. À son fils. In: Pasteur Vallery-Radot L, editor. Correspondance de Pasteur I. Lettres de jeunesse. L'étape de la crystallographie. 1840–1857. Paris: Flammarion; 1940. p 127.
53. Pasteur L. À Chappuis. In: Pasteur Vallery-Radot L, editor. Correspondance de Pasteur I. Lettres de jeunesse. L'étape de la crystallographie. 1840–1857. Paris: Flammarion; 1940. p 113.
54. Anonymous. M. Pasteur—Histoire d'un Savant par un Ignorant. Paris: J. Hetzel et C^{ie}; 1883.
55. Vallery-Radot M. Pasteur. Paris: Perrin; 1994. p 18.
56. Anonymous. M. Pasteur—Histoire d'un Savant par un Ignorant. Paris: J. Hetzel et C^{ie}; 1883. p 273.
57. Anonymous. M. Pasteur—Histoire d'un Savant par un Ignorant. Paris: J. Hetzel et C^{ie}; 1883. p 57.
58. Anonymous. M. Pasteur—Histoire d'un Savant par un Ignorant. Paris: J. Hetzel et C^{ie}; 1883. p 247.
59. Anonymous. M. Pasteur—Histoire d'un Savant par un Ignorant. Paris: J. Hetzel et C^{ie}; 1883. p 309.
60. Vallery-Radot R. La vie de Pasteur. Paris: Librairie Hachette et C^{ie}; 1900. p 45.
61. Vallery-Radot R. La vie de Pasteur. Paris: Librairie Hachette et C^{ie}; 1900. p 43–48.
62. Vallery-Radot R. La vie de Pasteur. Paris: Librairie Hachette et C^{ie}; 1900. p 41.
63. Vallery-Radot R. La vie de Pasteur. Paris: Librairie Hachette et C^{ie}; 1900. p 62.
64. Vallery-Radot R. La vie de Pasteur. Paris: Librairie Hachette et C^{ie}; 1900. p 562.
65. Wolff E. Éloge de Pasteur Vallery-Radot "Un vrai non conformiste". Nouv Presse Méd 1972;1:2803–2804.
66. Debré R. Louis Pasteur Vallery-Radot (1886–1970). Bull Acad Nat Méd 1971;155:436–448.
67. Pasteur Vallery Radot L. Table chronologique de l'œuvre de Pasteur. In: Pasteur Vallery-Radot L, editor. Œuvres de Pasteur, Vol. 7. Paris: Masson et C^{ie}; 1939. p 473.
68. Anonymous. http://web.pasteur.fr/infosci/archives/ncj1.html.
69. Nicolle J. Maurice Nicolle, un homme de la Renaissance à notre époque. Paris: La Colombe; 1957.
70. Grmek MD. Nicolle, Charles Jules Henri. In: Gillispie CC, editor. Dictionary of Scientific Biography, Vol. XV. New York: Charles Scribner's Sons; 1981. Supplement I, p 453–455.
71. Pasteur Vallery-Radot L. Mémoires d'un Con-conformiste (1886–1966). Paris: Grasset; 1966. p 56, 233–235, 317.
72. Pasteur Vallery-Radot L. Mémoires d'un con-conformiste (1886–1966). Paris: Grasset; 1966. p 47, 55–56.
73. Pasteur L. À Chappuis. In: Pasteur Vallery-Radot L, editor. Correspondance de Pasteur I. Lettres de jeunesse. L'étape de la crystallographie. 1840–1857. Paris: Flammarion; 1940. p 171.
74. Pasteur L. À M. Kestner. In: Pasteur Vallery-Radot L, editor. Correspondance de Pasteur I. Lettres de jeunesse. L'étape de la crystallographie. 1840–1857. Paris: Flammarion; 1940. p 307–308.
75. Pasteur Vallery-Radot L. A Great Life in Brief. New York: Alfred Knopf; 1970. p 32.
76. Pasteur Vallery-Radot L. A Great Life in Brief. New York: Alfred Knopf; 1970. p 55.
77. Pasteur Vallery-Radot L. A Great Life in Brief. New York: Alfred Knopf; 1970. p 73.
78. Pasteur Vallery-Radot L. A Great Life in Brief. New York: Alfred Knopf; 1970. p 167.
79. Pasteur Vallery-Radot L. Louis Pasteur: A Great Life in Brief. New York: Alfred Knopf; 1970. p 107.
80. Dubos RJ. Louis Pasteur: Free Lance of Science. Boston: Little, Brown and Company; 1950.
81. Dubos R. Pasteur and Modern Science. New York: Anchor Books; 1960.
82. Pasteur Vallery-Radot L. Les Plus Belles Pages de Pasteur. Paris: Flammarion; 1943.
83. Laurioz P-Y. Louis Pasteur: La Réalité Après la Légende. Paris: Éditions de Paris; 2003.
84. Jaeger FM. The George Fisher Baker Non-resident Lectureship in Chemistry at Cornell University. I. Spatial Arrangements of Atomic Systems and Optical Activity. New York: McGraw-Hill Book; 1930. p 33–42.
85. Robbins LE. Louis Pasteur and the Hidden World of Microbes. New York: Oxford University Press; 2001. p 21–35.
86. Bernal JD. Molecular asymmetry. In: Bernal JD. Science and Industry in the Nineteenth Century. London: Routledge and Kegan Paul; 1953. p 181–219.
87. Chappuis C. Notice Louis Pasteur. Bulletin de l'Association des anciens élèves de l'école normale 1896;52–66.
88. Partington JR.A History of Chemistry, Vol. IV. New York: St. Martin's Press; 1964. p 749–759.
89. Walden P. The George Fisher Baker Non-Resident Lectureship in Chemistry at Cornell University. Salt, Acids, and Bases: Electrolytes: Stereochemistry. New York: McGraw-Hill Book; 1929. p 325–352.
90. Duclaux É. Pasteur: Histoire d'un Esprit. Paris: Sceaux Charaire; 1896. p 9–42.
91. Jacques J. La Molécule et son Double. La Villette: Hachette; 1992. p 25–45.
92. Pasteur Vallery-Radot L. Images de la vie et de l'œuvre de Pasteur. Paris: Flammarion; 1956.
93. Roberts RM. Serendipity: Accidental Discoveries in Science. New York: Wiley Science Editions; 1989. p 59–65.
94. Ramsay OB. Stereochemistry. London: Heyden; 1981. p 69–80.
95. Kauffman GB, Myers RD. Pasteur's resolution of racemic acid: A sesquicentennial retrospect and a new translation. Chem Educator 1998;3:1–18.
96. Pasteur L. In: Pasteur Vallery-Radot L, editor. Correspondance de Pasteur II. La seconde étape: Fermentations, générations spontanées, maladies des vins, des vers à soie, de la bière. Paris: Flammarion; 1951. p 28–34.

97. Pasteur L. Mémoire sur la Fermentation de l'acide Tartrique. C R Séances Acad Sci 1858;46:615–618.
98. Pasteur L. Recherches sur la dissymétrie dans les produits organiques naturels. In: Pasteur Vallery-Radot L, editor. Œuvres de Pasteur, Vol. 1. Paris: Masson et C^{ie}; 1922. p 314.
99. Geison GL. The Private Science of Louis Pasteur. Princeton: Princeton University Press; 1995. p 259–278.
100. Vallery-Radot M. Pasteur. Paris: Perrin; 1994. p 18–30, 141–147.
101. Debré P. Louis Pasteur. Paris: Flammarion; 1994.
102. Löwy I. Patrice Debré. Louis Pasteur. Isis 2004;95:716.
103. Geison GL. Pasteur, Louis. In: Gillispie CC, editor. Dictionary of Scientific Biography, Vol. X. New York: Charles Scribner's Sons; 1974. p 414.
104. Vallery-Radot M. Pasteur. Paris: Perrin; 1994. p 19.
105. Debré P. Louis Pasteur. Paris: Flammarion; 1994. p 78.
106. Pasteur Vallery-Radot L. A Great Life in Brief. New York: Alfred Knopf; 1970.
107. Vallery-Radot M. Pasteur. Paris: Perrin; 1994. p 113–116.
108. Geison GL. Pasteur, Louis. In: Gillispie CC, editor. Dictionary of Scientific Biography, Vol. X. New York: Charles Scribner's Sons; 1974. p 353.
109. Geison GL. Pasteur, Louis. In: Gillispie CC, editor. Dictionary of Scientific Biography, Vol. X. New York: Charles Scribner's Sons; 1974. p 352.
110. Vallery-Radot M. Pasteur. Paris: Perrin; 1994. p 123–128.
111. Vallery-Radot R. Madame Pasteur. Paris: Flammarion; 1941. p 90.
112. Debré P. Louis Pasteur. Paris: Flammarion; 1994. p 145–146.
113. Debré P. Louis Pasteur. Paris: Flammarion; 1994. p 143–144.
114. Debré P. Louis Pasteur. Paris: Flammarion; 1994. p 145.

Enantiomerically Pure Quaternary Ammonium Salts with a Chiral Alkyl Chain $N(CH_3)(n\text{-}C_3H_7)_2(sec\text{-}C_4H_9)I$: Synthesis and Physical Studies

RUXANDRA GHEORGHE,[1] LISE-MARIE CHAMOREAU,[1] JOSEF KAPITAN,[2] NIKOLAÏ S. OVANESYAN,[3] SERGEI M. ALDOSHIN,[3] LUTZ HECHT,[2] LAURENCE D. BARRON,[2] CYRILLE TRAIN,[1] AND MICHEL GRUSELLE[1]*

[1]*Laboratoire de Chimie Inorganique et Matériaux Moléculaires, UMR-CNRS 7071, IFR 2769, Université Pierre et Marie Curie-Paris 6, F-75252 Paris Cedex 05, France*

[2]*WestCHEM, Department of Chemistry, University of Glasgow, Glasgow G12 8QQ, United Kingdom*

[3]*Institute of Problems of Chemical Physics, Russian Academy of Science, Moscow Region, 142432 Chernogolovka, Russia*

Dedicated to the 160th Anniversary of Louis Pasteur's Discovery

ABSTRACT A pair of enantiomerically pure quaternary ammonium salts with a chiral side chain, methyl-(*R*)-(1-methylpropyl)di(*n*-propyl)ammonium iodide **1** and methyl-(*S*)-(1-methylpropyl)di(*n*-propyl)ammonium iodide **2**, and the related racemate, methyl-(*rac*)-(1-methylpropyl)di(*n*-propyl)ammonium iodide **3**, were synthesized through a reductive alkylation procedure, starting from enantiomerically pure and, also, racemic forms of (*rac*)-(1-methylpropyl)amine. A spectroscopic chiroptical signature in solution was provided by the Raman optical activity spectra of compounds **1** and **2**. The crystallographic structures of **1**, **2**, and **3** were examined by single crystal X-ray diffraction. **1** crystallizes in the tetragonal space group $P4_32_12$ (no. 96), $a = b = 12.826$ (2) Å, $c = 17.730$ (2) Å, $V = 2916.9$ (5) Å^3, $Z = 8$, Flack coefficient 0.04 (2). **2** crystallizes in the tetragonal space group $P4_12_12$ (no. 92), $a = b = 12.842$ (1) Å, $c = 17.749$ (2) Å, $V = 2927.0$ (5) Å^3, $Z = 8$, Flack coefficient 0.05 (2). The crystal structures and space groups for **1** and **2** are enantiomorphs and the crystallographic investigation confirmed the absolute configuration of the stereocenter in both compounds. **3** crystallizes in the monoclinic space group $P2_1/n$ (no. 14), $a = 8.178$ (1) Å, $b = 14.309$ (2) Å, $c = 12.328$ (2) Å, $\beta = 96.811$ (6)°, $V = 1432.4$ (2) Å^3, $Z = 4$. *Chirality 20:1085–1091, 2008.*

KEY WORDS: chirality; ammonium salts; absolute configuration; Raman optical activity; X-ray diffraction

INTRODUCTION

Ammonium cations are a widely studied class of organic cations. During the last 10 years, there has been much interest in chiral ammonium cations that can behave either as asymmetric ionic liquids or phase transfer agents.[1,2] The ability of tetraalkylammonium salts with four different alkyl chains to form mesophases has also been studied.[3]

Our interest in such cations is part of a general strategy to synthesize optically active hybrid molecular magnets.[4] The ultimate goal of this approach is to measure magneto-chiral dichroism[5–8] in a ferromagnetically ordered material. We have focused our attention on the crystallization of optically active oxalate-based magnets of general formula $A^+[M(II)M'(III)(C_2O_4)_3]^-$. Because of the rapid racemization of tris(oxalato)metalate(III) in solution, we chose to develop enantioselective templated-assembly of these compounds starting from resolved template cations.[4] By using resolved bis(bipyridine)phenylpyridineruthenium(II) monocations, we obtained enantiomerically pure three-dimensional bimetallic anionic networks.[9–11] Starting from resolved chiral ferrocenic ammonium cation, we were able to characterize optically active two dimensional bimetallic anionic networks.[10,11] The compounds were obtained as powders because the chiral moiety of the ammonium is lost by hydrolysis during the crystallization process.[11] We intend to extend our study by investigating the ability of other resolved and (configurationally) stable ammonium salts to act as templates in the formation of optically active systems.

Crystallographic data for the structures of **3**, **1**, and **2**, respectively reported in this paper have been deposited with the Cambridge Crystallographic Data (CCDC 666586, 666587, and 666588, respectively).

Contract grant sponsors: University Pierre et Marie Curie-Paris6, CNRS, EPSRC, Russian Academy of Sciences
Contract grant sponsors: DFG Schwerpunktprogramm Molekularer Magnetismus; Contract grant number: SPP 1137
Contract grant sponsor: CNRS/RAS Joint Research Program; Contract grant number: 16332
Contract grant sponsors: RFBR; Contract grant number: 05-03-33026

*Correspondence to: Dr. Michel Gruselle, Laboratoire de Chimie Inorganique et Matériaux Moléculaires, UMR-CNRS 7071, IFR 2769, Université Pierre et Marie Curie-Paris 6, case courrier 42, 4 Place Jussieu, F-75252 Paris Cedex 05, France. E-mail: michel.gruselle@courriel.upmc.fr

Received for publication 10 December 2007; Accepted 10 March 2008
DOI: 10.1002/chir.20577
Published online 12 May 2008 in Wiley InterScience (www.interscience.wiley.com).

We report here the result of the first step we took in this investigation, namely the synthesis, the Raman and Raman optical activity (ROA) studies, as well as the crystallographic analysis of the cationic ammonium precursors. These are quaternary ammonium cations with a chiral alkyl side chain, methyl-(*R*)-(1-methylpropyl)di(*n*-propyl)-ammonium iodide **1** and methyl-(*S*)-(1-methylpropyl)di-(*n*-propyl)ammonium iodide **2**. For comparison, the related racemate, methyl-(*rac*)-(1-methylpropyl)di(*n*-propyl)ammonium iodide **3** is also reported.

MATERIALS AND METHODS

All the chemicals used for the present study were purchased from commercial sources and used without any further purification. Elemental analyses were carried out at the SIARE-UPMC Paris (France) for C, H, and N. The infra red (IR) spectra were recorded in KBr pellets with a Bio-Rad IRFT spectrophotometer in the 4000–200 cm^{-1} range. ^1H NMR spectra were recorded on a Bruker AC 300 spectrometer.

Synthesis

$N(CH_3)(n\text{-}C_3H_7)_2((R)\text{-}sec\text{-}C_4H_9)I$(1). Compound **1** was synthesized starting from the primary (*R*)-(1-methylpropyl)amine, by adapting a three-step procedure already reported in the literature,[3] as follows.

Synthesis of the secondary amine $NH(n\text{-}C_3H_7)((R)\text{-}sec\text{-}C_4H_9)$. A methanolic solution (5 ml) of propanal (1.6 ml, 22 mmol) was added dropwise to an ice-cooled solution of (*R*)-(1-methylpropyl)amine (2 ml, 20 mmol) in methanol (5 ml). After half an hour of stirring at room temperature, the resulting (*R*)-(1-methylpropyl)-*n*-propylimine was reduced with sodium borohydride (0.85 g, 22 mmol), which was added, in small portions, to the ice-cooled solution. The resulting mixture was stirred for 2 h at room temperature, to give (*R*)-(1-methylpropyl)(*n*-propyl)amine. The pH of the solution was set to 14 by adding 20 ml of 1 mol l^{-1} NaOH aqueous solution. The secondary amine was extracted with diethyl ether and purified by distillation (yield 70%).

^1H NMR (300 MHz, $CDCl_3$, TMS): δ/ppm = 2.51 (m, 3 H), 1.45 (m, 3 H), 1.24 (m, 1 H), 0.98 (d, ^2J(H–H) = 6.4 Hz, 3 H), 0.90 (t, ^2J(H–H) = 7.5 Hz, 3 H), 0.87 (t, ^2J(H–H) = 7.5 Hz, 3 H).

Synthesis of the tertiary amine $N(n\text{-}C_3H_7)_2((R)\text{-}sec\text{-}C_4H_9)$. A methanolic solution (2.5 ml) of propanal (1.1 ml, 15.3 mmol) was added dropwise to an ice-cooled solution of (*R*)-(1-methylpropyl)(*n*-propyl)amine (1.59 g, 14 mmol) dissolved in a mixture of methanol (2.5 ml) and dichloromethane (5 ml). After half an hour of stirring at room temperature, sodium triacetoxyborohydride (3.53 g, 16.6 mmol) was added, in small portions, to the ice-cooled solution. After 15 min, three extra portions of propanal (each 0.04 ml, 0.04 equiv.) and $NaBH(OAc)_3$ (each 0.16 mg, 0.05 equiv.) were alternatively added over a total period of 1 h. The resulting mixture was stirred for 3 h at room temperature, to give (*R*)-(1-methylpropyl)di(*n*-propyl)amine. The pH of this solution was set to 14 by adding 36 ml of 1 mol l^{-1} NaOH aqueous solution. The tertiary amine was extracted with diethyl ether and purified by distillation (yield 60.5%).

^1H NMR (300 MHz, $CDCl_3$, TMS): δ/ppm = 2.54 (m, 1 H), 2.28 (m, 4 H), 1.38 (m, 5 H), 1.19 (m, 1 H), 0.87 (3t + 1d, 12 H).

Synthesis of the quaternary ammonium salt $N(CH_3)(n\text{-}C_3H_7)_2((R)\text{-}sec\text{-}C_4H_9)I$. The resulting tertiary amine (1.33 g, 8.5 mmol) was quaternized using iodomethane (0.7 ml, 11 mmol) in toluene (20 ml) at 80°C over a period of 10 h. Methyl-(*R*)-(1-methylpropyl)di(*n*-propyl)ammonium iodide was isolated as a white crystalline powder (yield 76%).

^1H NMR (300 MHz, $CDCl_3$, TMS): δ/ppm = 3.56 (m, 1 H), 3.43 (m, 4 H), 3.20 (s, 3 H), 2.07 (m, 1 H), 1.82 (m, 4 H), 1.60 (m, 1 H), 1.46 (d, 3 H), 1.07 (m, 9 H).

Selected IR bands (KBr): ν = 3008 (s), 2971 (vs), 2938 (s), 2976 (s), 1473 (s), 1394 (m), 1375 (w), 1330 (w), 1187 (w), 1120 (w), 1097 (m), 1036 (w), 990 (w), 980 (w), 949 (m), 935 (m), 884 (w), 844 (w), 753 (s).

Elemental analysis calcd (%) for $C_{11}H_{26}NI$: C 44.00%, H 8.66%, N 4.66%; found: C 42.3%, H 8.57%, N 4.62%.

Single crystals of **1** were obtained by slow diffusion of diethyl ether in a dichloromethane (1.5 ml) solution of methyl-(*R*)-(1-methylpropyl)di(*n*-propyl)ammonium iodide (50 mg).

The same synthetic procedures were applied in the cases of the other two compounds $N(CH_3)(n\text{-}C_3H_7)_2((S)\text{-}sec\text{-}C_4H_9)I$ (**2**) and $N(CH_3)(n\text{-}C_3H_7)_2((rac)\text{-}sec\text{-}C_4H_9)I$ (**3**).

Raman Optical Activity

The Raman and ROA spectra were measured in backscattering in the University of Glasgow using a Chiral*RAMAN* instrument manufactured by BioTools, and described previously.[12] The ROA spectra are presented as scattered circular polarization intensity differences $I_R - I_L$ and the parent Raman spectra as scattered circular polarization intensity sums $I_R + I_L$, where I_R and I_L are the Raman-scattered intensities with right- and left-circular polarization, respectively. The solutions were studied at concentrations ~250 mg/ml at ambient temperature (~20°C) in methanol. They were filtered through 0.22 μm Millipore filters into quartz microfluorescence cells, which were centrifuged gently prior to mounting in the ROA instrument. Residual visible fluorescence from traces of impurities, which can give large backgrounds in Raman spectra, was quenched by leaving the sample to equilibrate in the laser beam for a few hours before acquiring ROA data. Experimental conditions: laser wavelength 532 nm; laser power at the sample ~200 mW; spectral resolution ~10 cm^{-1}; acquisition time ~10 h.

Single Crystal X-Ray Diffraction

A single crystal of each compound was selected, mounted onto a glass fiber, and transferred in a cold nitrogen gas stream at 250 K. Intensity data were collected with a Bruker-Nonius Kappa-CCD with graphite-monochromated Mo–Kα radiation. Unit-cell parameters determination, data collection strategy and integration were carried out with the Nonius EVAL-14 suite of programs.[13] Multi-scan absorption correction was applied.[14] The struc-

tures were solved by direct methods using the SHELXS-86, the SHELXS-97 or the SIR-92 programs.[15–17] All were refined anisotropically by full-matrix least-squares methods using the SHELX-97 software package.[17] For **3,** the occupancy factor of C(10) and C(10b) has been refined leading to 0.69:0.31 ratio. It was then fixed to 2:1.

RESULTS AND DISCUSSION

Two reductive alkylation reactions performed starting from the enantiomerically pure or the racemic forms of *sec*-butylamine, followed by a reaction of quaternization, lead to three iodide salts of quaternary ammonium cations with a chiral side chain: $N(CH_3)(n\text{-}C_3H_7)_2((R)\text{-}sec\text{-}C_4H_9)I$ **1**, $N(CH_3)(n\text{-}C_3H_7)_2((S)\text{-}sec\text{-}C_4H_9)I$ **2** and $N(CH_3)(n\text{-}C_3H_7)_2((rac)\text{-}sec\text{-}C_4H_9)I$ **3**. The reductive alkylation reactions can be performed with various aldehydes.[3,18] On the contrary, the quaternization failed when other iodoalkanes are used because the bulky trialkylamine favors elimination reactions. Nevertheless, this synthetic strategy appears as a general one to obtain a wide variety of enantiomerically pure ammonium salts of both configurations. This last feature contrasts with the strategy that uses compounds from the "chiral pool" as starting materials.[1] Such species can be used for studying the influence of controlled chirality on the formation of mesophases[3] as well as organic reactions using asymmetric ionic liquids[1] or asymmetric phase transfer reagents.[2] In the latter cases, working with either enantiomer of the ammonium cation allows to obtain either enantiomer of the target compound.

The IR spectra of compounds **1**, **2,** and **3** are basically identical. The group of four, strong to very strong, bands located between 2976 and 3008 cm^{-1} are due to the C—H stretching vibrations of the alkyl branches. Another band of strong intensity, situated at around 1460 cm^{-1}, is assigned to the C—H bending vibrations.

The chemical shifts in the ^1H NMR spectra of compounds **1**, **2,** and **3** are identical and consistent with the formation of the ammonium salts. For instance, the ^1H NMR spectrum of **1** shows eight groups of protons. The signals assigned to the protons belonging to the methyl groups are a singlet located at 3.20 ppm (CH_3—N), a doublet at 1.46 ppm (CH_3—CH—; ^2J(H—H) = 6.4 Hz), and two triplets centered at 1.07 ppm (three CH_3—CH_2— groups). The multiplet signals arising from the protons of the β-methylene groups of the two propyl branches are situated at 1.82 ppm, the ones from the α-methylene groups are at 3.43 ppm, and the two diastereotopic protons belonging to the methylene group from the *sec*-butyl chain appear at 1.60 and 2.07 ppm. The multiplet signal due to the proton linked to the carbon stereocenter is located at 3.56 ppm.

It is important to achieve the characterization of the enantiomeric purity and configurational stability of the products in solution. As they are aliphatic ammonium salts, the electronic spectroscopy for such species is dominated by σ—σ* transitions that take place at relatively large energies. Consequently, the natural circular dichroism in the 185–800 nm region, which is the most common technique for analyzing optically active compounds in solution, is not suitable in this case. To get a spectroscopic signature of the absolute configuration of our compounds in solution, we used a vibrational spectroscopy, namely ROA. This technique has been shown to be a powerful method for determining the absolute configuration of aliphatic alkanes.[19] Figure 1 shows the Raman, where the contribution of the solvent (methanol) was subtracted, and ROA spectra of compounds **1** and **2**. Because **1** and **2** are enantiomers, their ROA spectra are of opposite sign and approximately equal magnitude, as expected. A quantitative analysis of the ROA spectra is beyond the scope of this article, and in any event is not required here because the absolute configuration of the stereocenter is known a priori. A qualitative analysis of the ROA spectra[20] of compounds **1** and **2** focuses on vibrational coordinates of groups attached to the asymmetric carbon atom C(8) (cf. Fig. 2) because these are expected to generate the largest ROA signals. We expect groups attached to the nitrogen atom to make only minor contributions to the ROA, but that they will all contribute significantly to the parent Raman spectrum.

Normal modes of vibration involving various deformations of the methyl group linked to the asymmetric carbon atom C(8), together with those from the methylene fragment and the C(8)—H group probably dominate the ROA spectrum. One clear assignment is the 1451/1485 cm^{-1} ROA couplet which originates in the C(8)-methyl antisymmetric deformations, the degeneracy of which is lifted by the chiral environment (no splitting is seen in the parent Raman spectrum; but it is revealed by the ROA couplet). The non-degenerate methyl symmetric deformation might be involved in the 1402 cm^{-1} ROA band. There might also be some involvement of CH_2 deformations in both. Also C(8)—H deformations might be involved in the ∼1285–1331 cm^{-1} ROA bands. C(8)-methyl rocking motions probably contribute to the ∼1110–1174 cm^{-1} and the ∼880–995 cm^{-1} ROA bands, with significant mixing with C(8)—C and C(8)—N^+ stretches.

From ∼565 cm^{-1} and below, the modes will be complicated mixtures of various skeletal deformations, together with methyl torsions at the lower wavenumber end. Although contributions from conformers associated with rotations around the C(8)—N^+ bond and N^+-propyl groups probably complicate the parent Raman spectra, it is possible they do not complicate the ROA so much, again because groups attached to N^+ probably contribute little to the ROA.

Summarized crystallographic data and selected bond distances and angles for compounds **1**, **2**, and **3** are collected in Tables 1 and 2. The molecular structures of **1**, **2**, and **3** are shown in Figure 2, along with the atom numbering scheme. The two enantiomers, **1** and **2**, crystallize in two enantiomorphous tetragonal space groups, $P4_32_12$ (no. 96) and $P4_12_12$ (no. 92), respectively. The crystal structure of compound **3** is achiral in the centrosymmetric monoclinic space group $P2_1/n$ (no. 14). In **1** and **2**, the absolute configuration of the stereocenter was confirmed by the determination of the Flack coefficients.[21] They are equal to 0.04(2) for compound **1**, and 0.05(2) for **2**. Compound **3** crystallizes in a space group containing symmetry opera-

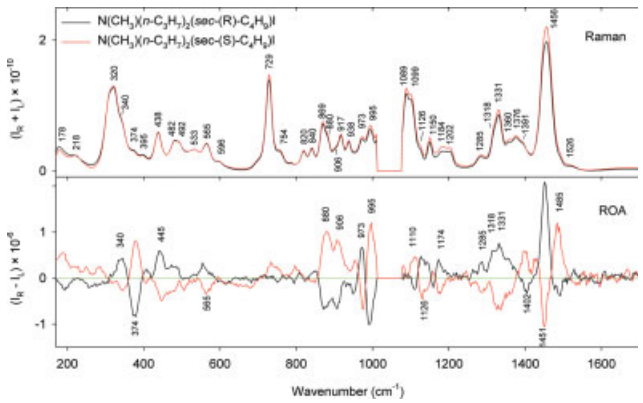

Fig. 1. The Raman (methanol subtracted, baseline corrected) and ROA (baseline corrected) spectra of 1 (black) and 2 (gray/red) in methanol. [Color figure can be viewed in the online issue, which is available at www.interscience.wiley.com.]

tions of the second kind (rotoinversions and glide reflections) forcing the presence of an equal number of (*R*) and (*S*) molecules in the structure: a racemate is formed. The C(10) carbon atom is disordered over two positions, the occupancy factor being 2:1. Hence, it can be bonded to C(9) and C(11) carbon atoms. As a consequence, the two configurations of the carbon stereocenter can be present at the same molecular position.

Following the Wallach's rule,[22–24] the density of the enantiomerically pure compounds **1** and **2** is lower by 1.93% than that of the racemate **3**.

At the molecular level, we restrict ourselves to the description of the structure of **1**. Within experimental errors, the distances and angles in **2** are identical to those of **1** whereas only minor differences are observed between **1** and **3** (Table 2). The bond angles around the nitrogen atom are consistent with a tetrahedral environment (Table 2). The slightly higher values for the angles C(8)—

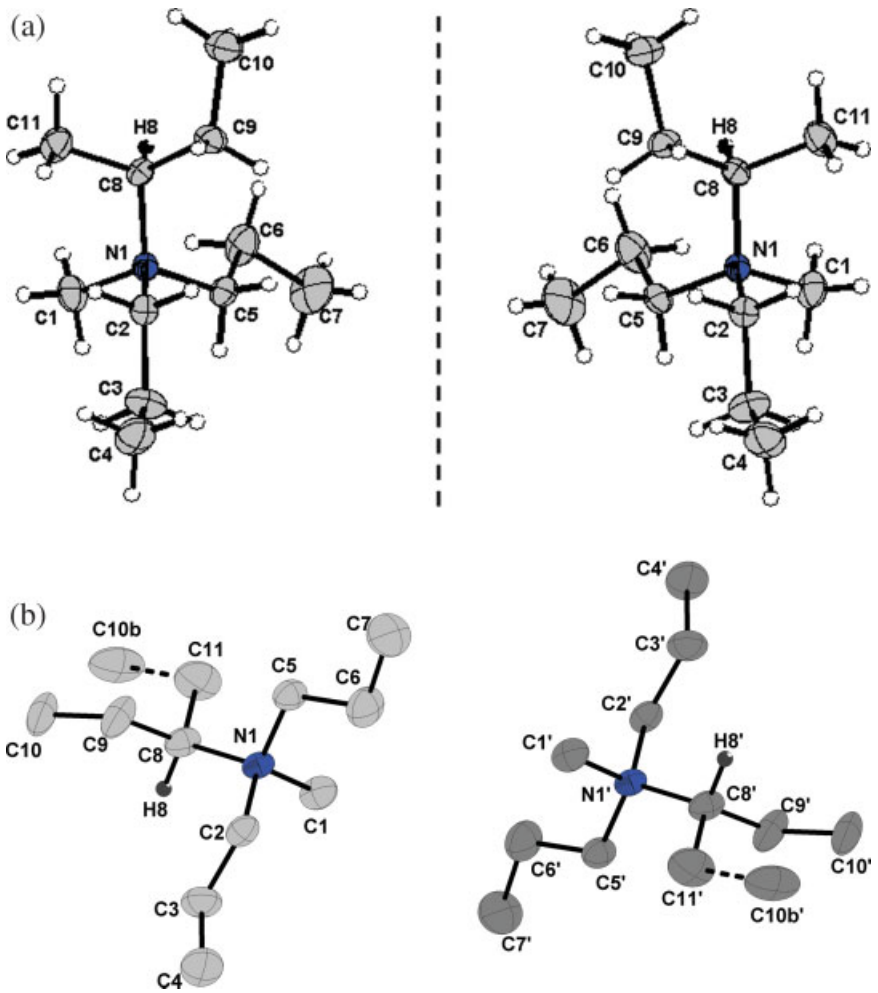

Fig. 2. Ortep view (30% probability) along with the atoms numbering scheme of the molecular crystal structures of quaternary ammonium cations in $N(CH_3)(n\text{-}C_3H_7)_2((R)\text{-}sec\text{-}C_4H_9)I$ 1 (right) and its enantiomer $N(CH_3)(n\text{-}C_3H_7)_2((S)\text{-}sec\text{-}C_4H_9)I$ 2 (left) (**a**) and $N(CH_3)(n\text{-}C_3H_7)_2((rac)\text{-}sec\text{-}C_4H_9)I$ 3 (**b**). In the latter case, the C(10) atom is the most probable position whereas C(10b) is the less probable one (see text). [Color figure can be viewed in the online issue, which is available at www.interscience.wiley.com.]

TABLE 1. Crystallographic data for compounds 1, 2, and 3

	1	2	3
Formula	$C_{11}H_{26}NI$	$C_{11}H_{26}NI$	$C_{11}H_{26}NI$
Formula weight	299.23	299.23	299.23
Crystal system	Tetragonal	Tetragonal	Monoclinic
Space group	$P\,4_3\,2_1\,2$	$P\,4_1\,2_1\,2$	$P\,2_1/n$
Temperature (K)	250 (2)	250 (2)	250 (2)
Unit cell dimensions			
a (Å)	12.826 (2)	12.842 (1)	8.178 (1)
b (Å)	12.826 (2)	12.842 (1)	14.309 (2)
c (Å)	17.730 (2)	17.749 (2)	12.328 (2)
β (°)			96.811(6)
V (Å^3)	2916.9 (5)	2927.0 (5)	1432.5 (2)
Z	8	8	4
D_{calc}(g cm^{-3})	1.363	1.358	1.387
μ (mm^{-1})	2.165	2.157	2.204
F(000)	1216	1216	608
θ_{min}–θ_{max} (°)	3.38–30.00	2.52–30.01	2.84–30.08
Flack coefficient	0.04 (2)	0.05 (2)	–
Reflexions collected/uniques	22448/4252, R_{int} = 0.0422	19051/4268, R_{int} = 0.0512	27582/4179, R_{int} = 0.0538
Data/restraints/parameters	4252/0/124	4268/0/125	4179/1/132
Goodness-of-fit on F^2	1.016	1.006	1.014
Final R_1, wR^2 [$I > 2\sigma$ (I)]	0.0275, 0.0502	0.0321, 0.0540	0.0359, 0.0740
R_1, wR_2 (all data)	0.0578, 0.0573	0.0804, 0.0640	0.0827, 0.0866

N(1)—C(2) and C(8)—N(1)—C(5) formed by the N—C(*sec*-butyl) and the two N—C(propyl) bonds [110.27(15)° and 111.31(16)°)] are likely to be related to the larger steric hindrance between these groups when compared with the smaller methyl group. The two propyl branches have a staggered conformation. The *sec*-butyl chain has a *gauche* conformation, stabilizing the whole molecule by limiting the steric repulsion between the two alkyl groups of the *sec*-butyl branch and the -NMePr$_2$ fragment. The bond angles around the carbon stereocenter (in the range 106.9–112.1°) deviate slightly from the typical sp^3 hybridization angle (109.3°) to optimize the steric repulsion between the four different substituents. The values of the bond lengths vary in a normal regime corresponding to simple C—C (1.51–1.54 Å) and C—N (1.51–1.55 Å) bonds.

TABLE 2. Selected bond distances (Å) and angles (°) for compounds 1, 2, and 3

	1	2	3
N(1)—C(1)	1.509 (3)	1.510 (3)	1.510 (4)
N(1)—C(2)	1.522 (3)	1.517 (3)	1.519 (4)
N(1)—C(5)	1.533 (3)	1.529 (3)	1.522 (4)
N(1)—C(8)	1.550 (3)	1.554 (3)	1.549 (4)
C(2)—C(3)	1.521 (3)	1.527 (4)	1.510 (5)
C(3)—C(4)	1.511 (4)	1.511 (4)	1.525 (5)
C(5)—C(6)	1.526 (3)	1.526 (4)	1.498 (5)
C(6)—C(7)	1.539 (3)	1.543 (4)	1.479 (6)
C(8)—C(11)	1.529 (3)	1.533 (4)	1.519 (5)
C(8)—C(9)	1.535 (3)	1.533 (4)	1.512 (5)
C(9)—C(10)	1.532 (3)	1.539 (4)	1.486 (6)
C(1)—N(1)—C(2)	110.07 (17)	110.0 (2)	108.7 (2)
C(1)—N(1)—C(5)	108.50 (18)	108.4 (2)	109.7 (3)
C(2)—N(1)—C(5)	108.43 (18)	108.5 (2)	108.7 (2)
C(1)—N(1)—C(8)	108.25 (18)	108.1 (2)	108.9 (2)
C(2)—N(1)—C(8)	110.27 (15)	110.37 (19)	111.0 (3)
C(5)—N(1)—C(8)	111.31 (16)	111.4 (2)	109.8 (2)

The quaternary ammonium cations in **1** are related through a 4_3 axis (Fig. 3a). At the supramolecular level, the 4_3 axis generates a right-handed helix along the c axis (see Fig. 3). Because of the 2 axis, the ammonium cations form a second right-handed helix interwoven with the former one (Fig. 3b). In the case of **2**, the ammonium ions are related through a 4_1 axis, leading to two interwoven left-handed helices along the c axis. Within the helix generated by the ammonium cations, the iodide anions are placed in a distorted zig-zag manner, the shortest I···I distance being 7.859(1) Å and the largest 14.797(1) Å. The shortest distance between the equivalent iodide ions "belonging" to neighbouring helices is 7.955(1) Å. The I···N distance is equal to 4.897(2) Å, stabilizing the supramolecular arrangement through electrostatic interactions. In the racemic crystal **3**, the 2_1 axis generates supramolecular helices of the quaternary ammoniums (see Fig. 4). The glide plane generates a second supramolecular helix (see Fig. 4). Because of the location of the C(10) carbon atom mentioned above, a first family of helices is mainly composed (in a 2:1 ratio) of cations of the same configuration. In the family of helices generated by the glide plane, the proportion is reversed. Because X-ray diffraction is not sensitive to short-range order, it is not possible to figure out whether the helices are formed by long sequences of (*R*) molecules followed by long sequences of (*S*) molecules or by a rapid alternation between the (*R*) and (*S*) molecules. The iodine ions are positioned alternatively between the ammonium cations of the same helix, the distance between them being 7.244(2) Å. The shortest distance between the iodide ions "belonging" to helices of opposed chirality is 8.362(4) Å. The shortest distances N···I fall in the range 4.72–4.82 Å.

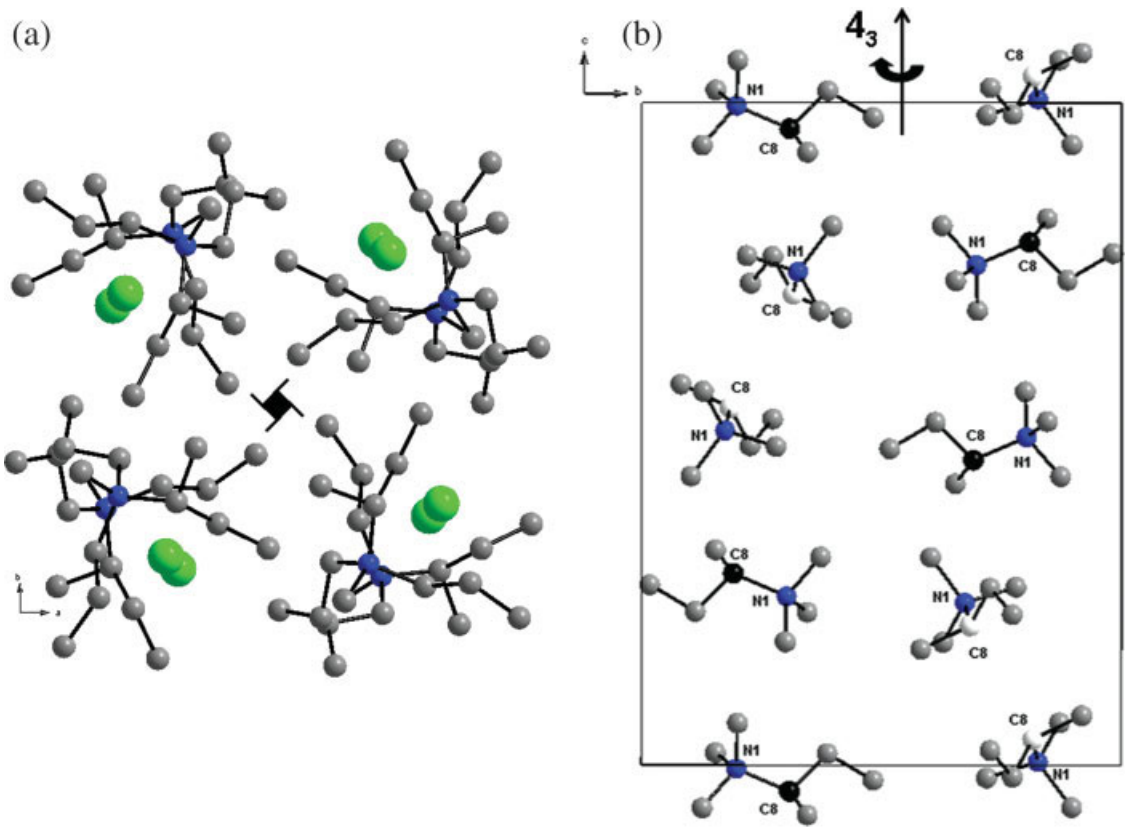

Fig. 3. Packing diagram for crystal 1 illustrating the interwoven helical arrangement of the quaternary ammonium cations at the supramolecular level: (**a**) along the *c* axis and (**b**) along the *a* axis. In (b), for clarity, the iodide ions are not shown and only the first carbon atom of the propyl chains is shown; moreover, the asymmetric carbon atom is colored in black for one helix and in white in the second one (see text). [Color figure can be viewed in the online issue, which is available at www.interscience.wiley.com.]

The comparison between the structures of the enantiomerically pure compounds **1** and **2** and the racemate **3** shows that the handedness of the supramolecular helices in **1** and **2** is indeed entirely determined by the configuration of the carbon stereocenter, whereas no control can be exerted in the case of **3**.

Concluding Remarks

We have described the synthesis of the two enantiomers of methyl(1-methylpropyl)di(*n*-propyl)ammonium iodide starting from the resolved (1-methylpropyl)amine in a three-step procedure with an overall yield of 32%. The synthetic procedure we report can be extended to chiral ammoniums with longer alkyl chains that can be used as asymmetric ionic liquids or phase transfer agents. In contrast with the quaternary ammoniums obtained from the "chiral pool",[1] this strategy allows either enantiomer of the ammonium cation to be synthesized. Thus, it is possible to study the influence of the configuration of the stereocenter both on the chiroptical spectroscopic measurements, as exemplified here by ROA, as well as on the helical crystal packing of the molecular ions, as shown by single crystal X-ray diffraction.

The next step in our general approach of the template enantioselective self-assembly of hybrid 2D and 3D oxa-

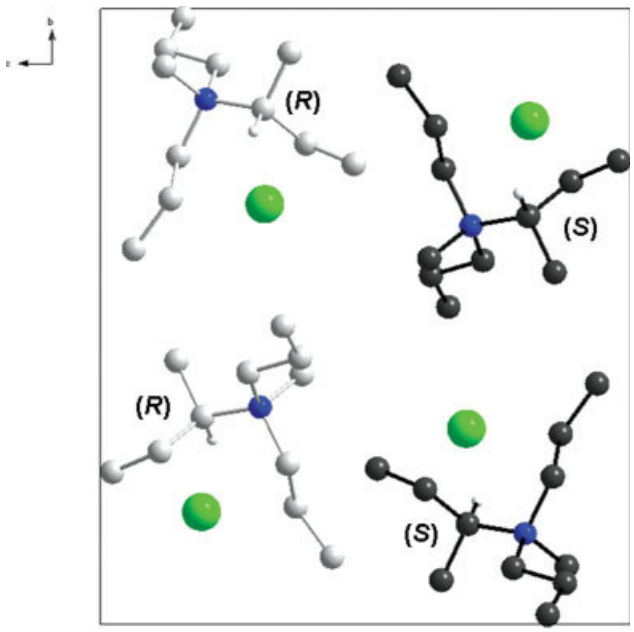

Fig. 4. Packing diagram for crystal 3 along the *a* axis. The configuration of the carbon stereocenters is determined by setting the C(10) atom at its most probable position (see text). [Color figure can be viewed in the online issue, which is available at www.interscience.wiley.com.]

late-based networks[4] will be to test the ability of the resolved methyl(1-methylpropyl)di(*n*-propyl)ammonium cations to build optically active bimetallic honeycomb layers.

LITERATURE CITED

1. Ding J, Armstrong DW. Chiral ionic crystals: synthesis and applications. Chirality 2005;17:281–292.
2. Ooi T, Maruoka K. Recent advances in asymmetric phase-transfer catalysis. Angew Chem Int Ed 2007;46:4222–4266.
3. Soulié C, Bassoul P, Tournilhac F. Cubic. Mesophase in an unsymmetrical alkyl ammonium salt. Synthesis and structural model. Chem Phys Chem 2002;3:1024–1030.
4. Gruselle M, Train C, Boubekeur K, Gredin P, Ovanesyan N. Enantioselective self-assembly of chiral bimetallic oxalate-based network. Coord Chem Rev 2006;250:2491–2500.
5. Barron LD, Vrbancich J. Magneto-chiral birefringence and dichroism. Mol Phys 1984;51:715–730.
6. Rikken GLJA, Raupach E. Observation of magneto-chiral dichroism. Nature (London) 1997;390(6659):493–494.
7. Rikken GLJA, Raupach E. Pure and cascaded magnetochiral anisotropy in optical absorption. Phys Rev E 1998;58:5081–5084.
8. Raupach E, Rikken GLJA, Train C, Malézieux B. Modeling of magneto-chiral enantioselective photochemistry. Chem Phys 2006;26:373–380.
9. Andres R, Brissard M, Gruselle M, Train C, Vaisserman J, Malezieux B, Jamet J-P, Verdaguer M. Rational design of three-dimensional (3D) optically active molecule-based magnets: synthesis, structure, optical and magnetic properties of $\{[Ru(bpy)_3]^{2+}$, ClO_4^-, $[Mn^{II}Cr^{III}(ox)_3]^-\}_n$ and $\{[Ru(bpy)_2ppy]^+$, $[M^{II}Cr^{III}(ox)_3]^-\}_n$, with $M^{II} = Mn^{II}$, Ni^{II}. X-ray structure of $\{[\Delta Ru(bpy)_3]^{2+}$, ClO_4^-, $[\Delta Mn^{II}\Delta Cr^{III}(ox)_3]^-\}_n$ and $\{[\Lambda Ru(bpy)_2ppy]^+$, $[\Lambda M^{II}\Lambda Cr^{III}(ox)_3]^-\}_n$. Inorg Chem 2001;40:4633–4640.
10. Gruselle M, Thouvenot R, Malezieux B, Train C, Gredin P, Demeschik TV, Troitskaya LL, Sokolov VI. Enantioselective self-assembly of bimetallic $[Mn^{II}(\Delta)\text{-}Cr^{III}(C_2O_4)_3]^-$ and $[Mn^{II}(\Lambda)\text{-}Cr^{III}(C_2O_4)_3]^-$ layered anionic networks templated by the optically active (*Rp*)- and (*Sp*)-$[1\text{-}CH_2N(n\text{-}C_3H_7)_3\text{-}2\text{-}CH_3\text{-}C_5H_3Fe\text{-}C_5H_5]^+$ ions. Chem Eur J 2004;10:4763–4769;
11. Shilov GV, Ovanesyan NS, Aldoshin SM, Gruselle M, Train C, Guyard-Duhayon C. J Coord Chem 2004;57:1165–1171.
12. Barron LD, Zhu F, Hecht L, Tranter GE, Isaacs NW. Raman optical activity: an incisive probe of molecular chirality and biomolecular structure. J Molec Struct 2007;834–836:7–16.
13. Duisenberg AJM, Kroon-Batenburg LMJ, Schreurs AMM. An intensity evaluation method: EVAL-14. J Appl Cryst 2003;36:220–229.
14. Blessing RH. An empirical correction for absorption anisotropy. Acta Cryst. A 1995;51:33–38.
15. Sheldrick GM, SHELXS-86. Germany: University of Göttingen; 1986;
16. Altomare A, Cascarano G, Giacovazzo C, Guagliardi A. Completion and refinement of crystal-structures with sir92. J Appl Cryst 1993;26:343–350.
17. Sheldrick GM, SHELXL-97. Germany: University of Göttingen; 1997.
18. Gruselle M, Malézieux B, Train C, Soulié C, Ovanesyan NS. Les cations ammoniums chiraux de type $[R_1R_2R_3R_4N]^+$, de nouveaux templates pour les réseaux bimétalliques à pont oxalate. CR Chimie 2003;6:189–191.
19. Haesler J, Schindelholz I, Riguet E, Bochet CG, Hug W. Absolute configuration of chirally deuterated neopentane. Nature 2007;446:526–529.
20. Barron LD. Molecular light scattering and optical activity. 2nd ed. Cambridge University Press; 2004.
21. Flack HD. On enantiomorph-polarity estimation. Acta Crystallogr Sect A 1983;39:876–881.
22. Wallach O. Zur Kenntniss der Terpene und der ätherischen Oele. Liebigs Ann Chem 1895;286:90–118.
23. Wallach O. Zur Kenntniss der Terpene und der ätherischen Oele. Ueber gebromte Derivate der Carvonreihe. Liebigs Ann Chem 1895;286:119–143.
24. Brock CP, Schweizer WB, Dunitz JD. On the validity of Wallach's rule: on the density and stability of racemic crystals compared with their chiral counterparts. J. Am Chem Soc 1991;113:9811–9820.

Three Different Types of Chirality-Driven Crystallization Within the Series of Uniformly Substituted Phenyl Glycerol Ethers

ALEXANDER A. BREDIKHIN,* ZEMFIRA A. BREDIKHINA, VICTORINA G. NOVIKOVA, ALEXANDER V. PASHAGIN, DMITRY V. ZAKHARYCHEV, AND AIDAR T. GUBAIDULLIN

A.E. Arbuzov Institute of Organic and Physical Chemistry, Russian Academy of Sciences, Kazan, Russian Federation

Dedicated to the 160th Anniversary of Louis Pasteur's Discovery

ABSTRACT Seven chiral arylglycerol ethers 2-R-C_6H_4-O-$CH_2CH(OH)CH_2OH$ (R = H, Me, Et, Allyl, *n*-Pr, *i*-Pr, *tert*-Bu) were synthesized in racemic and scalemic form. The IR spectra, melting points, and enthalpies of fusion for racemic and scalemic samples of every species were measured, the entropies of enantiomers mixing in the liquid state and Gibbs free energies of a racemic compound formation were derived and binary phase diagrams were reconstructed for the whole family. Solid racemic compounds stabilities were ranked for the four substances. Spontaneous resolution was established for the registered chiral drug mephenesin and its ethyl analogue. Metastable anomalous conglomerate, forming crystals having three independent *R** and one independent *S** molecules in the unit cell, is formed during solution crystallization of *tert*-butyl derivative; metastable phase transforms slowly into traditional racemic conglomerate. *Chirality 20:1092–1103, 2008.*

KEY WORDS: spontaneous resolution; anomalous conglomerate; thermochemistry; X-ray diffraction; preferential crystallization; mephenesin

INTRODUCTION

Louis Pasteur's observation of spontaneous resolution of the tartaric acid particular salt followed by triage separation of its enantiomers, in his great 1848 experiment[1], laid the groundwork for the modern science of stereochemistry. Up to now the nature of spontaneous resolution remains something of an enigma, and according to Lluīsa Perez-Garcia and David Amabilino "the understanding and prediction of spontaneous resolution ... remains one of the true challenges for science in the 21st century".[2] Not only has an unquenchable thirst for knowledge made spontaneous resolution so attractive, the practical reasons are every bit as important as the abstract ones. Based on this phenomenon, direct methods for production of single enantiomers, as for instance resolution by entrainment,[3,4] refer to natural limits of resolution effectiveness because of no need of chiral auxiliaries and specialized equipment.

There are different ways to study spontaneous resolution, tracking the little chemical structure variations accompanying the crystallization in the series of closely related chiral compounds is one possibility. The members of such a series must be selected in such a way that every compound would have minimal but regular distinctions from each other. In addition, it would be desirable to have not only qualitative categories like the "conglomerate" or "racemic compound" for characterization of crystalline type, but to introduce a quantitative measure allowing us to rank the observed properties. For this measure one can use the Gibbs free energy changes, ΔG^0, accompanied by the reaction of the racemic compound formation from the enantiopure components, and the values of entropy of mixing of enantiomers in the liquid state, ΔS_1^m. The Gibbs free energy of formation is always negative for a racemic compound, if it can exist, while for a racemic conglomerate this value must be (but not always is) close to zero. So obtained the entropy of mixing has no clear interpretation, but for ideal conglomerate this value must be equal to $R\ln 2$ or 5.75 J K^{-1} mol^{-1}. Both of these thermodynamic characteristics could not be measured directly, but could be calculated on the basis of the chiral substances melting point temperatures and fusion enthalpies T^f and ΔH^f.[3,5] The method of choice for experimental T^f and ΔH^f determination is differential scanning calorimetry (DSC).[6]

As regards the choice of the chemical objects, our recent interests deal with the terminal aryl glycerol ethers $ArO—CH_2CH(OH)CH_2—OH$. The reasons must be pointed out. Firstly, the glycerol ethers and esters are rather common in the family of lipids. Lipids (fats, plasmalogenes, membrane forming glycerolipids, and the like) form the third class, after proteins and carbohydrates, of "life molecules," hence a spontaneous resolution among the lipid-like compounds could be related to the problem of origin of life homochirality.[7] Secondly, many physiologi-

Contract grant sponsor: Russian Fund of Basic Research; Contract grant numbers: 06-03-32508, 07-03-12070
*Correspondence to: A. A. Bredikhin, A.E. Arbuzov Institute of Organic and Physical Chemistry, Arbuzov st., 8, Kazan, 420088, Russia.
E-mail: baa@iopc.knc.ru
Received for publication 7 March 2008; Accepted 20 June 2008
DOI: 10.1002/chir.20648
Published online 2 September 2008 in Wiley InterScience (www.interscience.wiley.com).

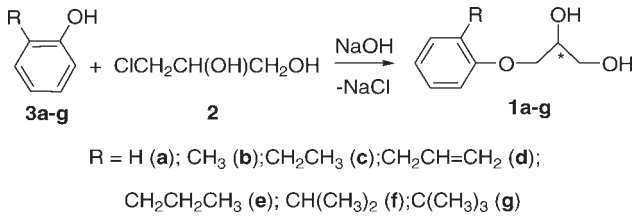

Scheme 1. Synthesis of the chiral *ortho*-substituted phenyl glycerol ethers **1a-g**.

cally active substances, including registered drugs like fungicide chlorphenesin,[8] expectorant guaifenesin,[8] muscle relaxant mephenesin,[8] belong to the series of aryl glycerol ethers, possibly because of their similarity to lipids. Thirdly, the terminal aryl glycerol ethers by simplest chemical manipulations could be transformed to another drugs, in particular to β-adrenoblockers of vast ArO—CH_2-CH(OH)CH_2—NHR family.[9,10] Last, fourthly, it is relatively easy to prepare both racemic and scalemic samples of the aryl glycerol ethers needed for experiments.

Recently, we have studied the crystallization peculiarities in the series of *ortho*-halogen and *ortho*-alkoxyphenyl glycerol ethers.[11,12] The present study is carried out to examine the chirality-driven crystallization of a series of ortho-substituted phenyl glycerol ethers, where the substituent is the hydrogen atom or a hydrocarbon moiety. The availability of both enantiomers of 3-chloropropane-1,2-diol **2** by Jacobsen kinetic hydrolytic resolution of a racemic epichlorohydrin[13] makes it possible to obtain all the series of glycerol ethers **1a–g** through the use of a single process (Scheme 1).

The purposes of this work are to study the melting of the substituted phenyl glycerol ethers as enantiomers, as racemates, and in some cases as mixtures of intermediate compositions by means of DSC; to evaluate stabilities of racemic compounds under experiment; to compare the crystallization peculiarities with the substitution pattern; and to investigate the abilities of conglomerate forming compounds to be resolved by entrainment procedure.

MATERIALS AND METHODS

General

The NMR spectra (600 MHz for ^{1}H and 150.864 MHz for ^{13}C) were recorded on a Bruker Avance-600 spectrometer in $CDCl_3$ with TMS or the signals of the solvent as the internal standard. The IR spectra of the polycrystalline samples of *rac*- and *scal*-compounds under investigations in KBr pellets were recorded on a Bruker IFS-66v Fourier-transform spectrometer.

The X-ray single crystal experiments were carried out on Bruker AXS Smart Apex II and Kappa Apex II diffractometers. Powder X-ray diffraction (PXRD) data were collected on a Bruker *D*8 Advance diffractometer equipped with an Vantec linear PSD, using graphite monochromated Cu Kα (λ 1.54184 Å) radiations, (40 kV, 40 mA).

Optical rotations were measured on a Perkin-Elmer model 341 polarimeter. Throughout the paper the value of specific rotation is given in deg mL g^{-1} dm^{-1}, and the concentration of solutions *c* appears in g (100 ml)$^{-1}$.

Enantiomeric purity was checked by HPLC analysis performed on a Shimadzu LC-20AD system controller, and UV monitor 275 nm was used as a detector. The column used, from Daicel, Inc., was Chiralcel AD-RH (0.46 cm × 15 cm).

All thermal measurements were performed on a Perkin-Elmer Diamond DSC model in aluminum pans using a heating rate of 10 K min^{-1}. Mass of the samples amounted to ~2.5 mg. Temperature scale and heat flux were calibrated against the data for indium, phenol, and naphthalene.

Racemic epichlorohydrin (99%) and 3-(2-methylphenoxy)-propane-1,2-diol (98%) were purchased from Alfa Aesar®; 3-chloropropane-1,2-diol (99+%), phenol (99+%), *o*-cresol (99+%), 2-ethylphenol (99%) were purchased from Acros Organics®; 2-propylphenol (97%), 2-isopropylphenol (98%), 2-*tert*-butylphenol (99%), and 2-allylphenol (98%), were purchased from Lancaster; methyl-*tert*-butyl ether (MTBE, 99.5%) was obtained from Fisher Scientific.

Preparation of 3-Aryloxypropane-1,2-diols

Racemic and enantiopure diols **1a–g** were synthesized by analogy with a published procedure[14] from corresponding phenol **3a–g** and racemic or scalemic 3-chloropropane-1,2-diols, *rac*-**2** and *scal*-**2**, respectively. (−)-(*R*)-**2** {$[\alpha]_D^{20}$ −6.4 (*c* 5, H_2O)} and (+)-(*S*)-**2** {$[\alpha]_D^{20}$ +6.1 (*c* 4.8, H_2O)} were prepared through Jacobsen kinetic hydrolytic resolution of *rac*-epichlorohydrin without modifications.[13]

General procedure. To the solution of corresponding phenol **3a–g** (10 mmol) in ethanol (6 ml) a solution of NaOH (0.5 g, 12.5 mmol) in water (2 ml) was added and the resulting mixture was stirred and heated under reflux for 30 min. Then a solution of 3-chloropropane-1,2-diol **2** (1.3 g, 12 mmol) in ethanol (1 ml) was added, and the mixture was further stirred and heated at reflux for 3 h. After cooling, the mixture was concentrated under reduced pressure followed by addition of water (6 ml) and extraction with CH_2Cl_2 (3 × 20 ml). The combined organic layers were dried over anhydrous Na_2SO_4 and the solvent was removed. The crude diols **1a–g** were usually purified by recrystallization from hexane; (*S*)-aryloxypropanediols were obtained from (+)-(*S*)-**2**, and (*R*)-aryloxypropanediols were obtained from (−)-(*R*)-**2**.

***rac*-3-Phenoxypropane-1,2-diol, *rac*-1a.** Yield: 1.3 g (80%), mp 58–59°C (Ref. 11: mp 56–60°C). An analytical sample was obtained by slow crystallization of crude *rac*-**1a** from a hexane-ether (1:1) mixture. ^{1}H NMR, δ: 2.55 (br.s, 2H, 2 OH), 3.75 (dd, J = 11.7, 5.5 Hz, 1H, 1CH_2O), 3.84 (dd, J = 11.7, 3.8 Hz, 1H, 1CH_2O), 3.99–4.04 (m, 2H, CH_2O), 4.08–4.15 (m, 1H, CHO), 6.91 (dd, J = 8.4, 1.0 Hz, 2 H, $C^{2,6}_{Ar}$ *H*), 6.98 (t, J = 7.4 Hz, 1H, C^{4}_{Ar} *H*), 7.29 (td, J = 7.4, 1.4 Hz, 2H, $C^{3,5}_{Ar}$ *H*). ^{13}C NMR, δ: 63.83 (CH_2OH), 69.28 (CH), 70.57 (CH_2O), 114.71 ($C^{3,5}_{Ar}$), 121.48 (C^{4}_{Ar}), 129.70 ($C^{2,6}_{Ar}$), 158.55 (C^{1}_{Ar}).

(*R*)-3-Phenoxypropane-1,2-diol, (*R*)-1a. Yield: 1.2 g (71%), mp 68–69°C (Ref. 15: mp 62.5–64.5°C); $[\alpha]_D^{20}$ –10.1 (*c* 1, EtOH), $[\alpha]_D^{20}$ −9.7 (*c* 1.0, MeOH) {Ref. 15: $[\alpha]_D^{20}$ −9.5 (*c* 0.5, MeOH), 98.9% ee}, $[\alpha]_D^{20}$ +4.2 (*c* 1, hexane/EtOH, 4:1), $[\alpha]_D^{20}$ + 2.0 (*c* 1, MTBE); 99.6% ee [HPLC; column temperature 29°C; eluent: water/isopropanol = 3.75/1; flow rate 1.0 ml/min; t_R(major) = 7.4 min]; t_R (minor) = 9.6 min]. NMR spectra were identical with spectra of *rac*-**1a**.

(*S*)-3-(2-Methylphenoxy)-propane-1,2-diol, (*S*)-1b. Yield: 1.4 g (77%), mp 90–91°C (Ref. 16: mp 91–92°C); $[\alpha]_D^{20}$ −19.3 (*c* 1.2, hexane/i-PrOH, 4:1) {Ref. 17: $[\alpha]_D^{20}$ −19.3 (*c* 0.9, hexane/i-PrOH, 4:1)}, $[\alpha]_D^{20}$ −12.8 (*c* 1.1, MTBE); 99.8% ee [HPLC; column temperature 40°C; eluent: water/isopropanol = 3/1; flow rate 1.0 ml/min; t_R(major) = 8.3 min]. ^{1}H NMR (600 MHz) δ = 2.20 (br.s, 1H, OH), 2.23 (s, 3H, CH_3), 2.70 (br.s, 1H, OH), 3.78 (dd, *J* = 11.8, 6.1 Hz, 1H, 1CH_2), 3.85 (dd, *J* = 11.8, 3.7 Hz, 1H, 1CH_2O), 4.04–4.07 (m, 2H, CH_2O), 4.11–4.14 (m, 1H, CH), 6.82 (d, *J* = 7.9 Hz, 1H, C^6_{Ar} *H*), 6.88 (t, *J* = 7.4 Hz, 1H, C^4_{Ar} *H*), 7.13–7.15 (m, 2H, $C^{3,5}_{Ar}$ *H*).

(*R*)-3-(2-Methylphenoxy)-propane-1,2-diol, (*R*)-1b. Yield: 1.4 g (77%), mp 90–91°C; $[\alpha]_D^{20}$ +19.3 (*c* 1.2, hexane/i-PrOH, 4:1) {Ref. 17: $[\alpha]_D^{20}$ +19.8 (*c* 0.9, hexane/i-PrOH, 4:1)}, $[\alpha]_D^{20}$ +12.8 (*c* 1.1, MTBE); 99.9% ee [HPLC; column temperature 40°C; eluent: water/isopropanol = 3/1; flow rate 1.0 ml/min; t_R(major) = 7.1 min].

***rac*-3-(2-Ethylphenoxy)-propane-1,2-diol, *rac*-1c.** Yield: 1.5 g (76%), mp 51–53°C (Ref. 18: mp 56–57°C). ^{1}H NMR, δ: 1.23 (t, *J* = 7.6 Hz, 3H, CH_3), 2.67 (2H, *J* = 7.6 Hz, C$H_2$$CH_3$), 3.30 (br.s, 1H, OH), 3.53 (br.s, 1H, OH), 3.78 (dd, *J* = 11.5, 6.3 Hz, 1H, 1CH_2O), 3.87 (dd, *J* = 11.5, 3.7 Hz, 1H, 1CH_2O), 4.01–4.05 (m, 2H, CH_2O), 4.03–4.07 (m, 1H, CH), 6.76 (d, *J* = 8.4 Hz, 1H, C^6_{Ar} *H*), 6.85 (t, *J* = 7.3 Hz, 1H, C^4_{Ar} *H*), 7.06–7.09 (m, 2H, $C^{3,5}_{Ar}$ *H*). ^{13}C NMR, δ: 14.20 (CH_3), 23.22 (*C*$H_2$$CH_3$), 63.93 ($CH_2$OH), 69.03 (CH), 70.71 ($CH_2$O), 111.41 ($C^6_{Ar}$), 121.18 ($C^4_{Ar}$), 126.90 ($C^5_{Ar}$), 129.09 ($C^3_{Ar}$), 132.66 ($C^2_{Ar}$), 156.14 ($C^1_{Ar}$).

(*S*)-3-(2-Ethylphenoxy)-propane-1,2-diol, (*S*)-1c. Yield: 1.3 g (68%), mp 68–70°C; $[\alpha]_D^{20}$ −14.5 (*c* 1, hexane/EtOH, 4:1); $[\alpha]_D^{20}$ −12.3 (*c* 1.0, MTBE); 99.9% ee [HPLC; column temperature 29°C; eluent: water/isopropanol = 3/1; flow rate 1.0 ml/min; t_R(major) = 18.1 min]. NMR spectra were identical with spectra of *rac*-**1c**.

(*R*)-3-(2-Ethylphenoxy)-propane-1,2-diol, (*R*)-1c. Yield: 1.4 g (72%), mp 68–70°C; $[\alpha]_D^{20}$ +11.9 (*c* 1.0, MTBE); 99.3% ee [HPLC; column temperature 29°C; eluent: water/isopropanol = 3/1; flow rate 1.0 ml/min; t_R (major) = 15.6 min].

***rac*-3-(2-Allylphenoxy)-propane-1,2-diol, *rac*-1d.** Yield: 1.6 g (75%), mp 41–43°C (hexane) (Ref. 9: mp 43–44°C).

(*S*)-3-(2-Allylphenoxy)-propane-1,2-diol, (*S*)-1d. Yield: 1.4 g (70%), mp 57–58° (hexane); $[\alpha]_D^{20}$ −2.7 (*c* 0.6, EtOH); $[\alpha]_D^{20}$ −7.2 (*c* 1.0, MTBE); {Ref. 9: mp 47–49°C; $[\alpha]_D^{20}$ −2.1 (*c* 2.8, EtOH)}; 99.9% ee [HPLC; column temperature 29°C; eluent: water/isopropanol = 3/1; flow rate 0.6 ml/min; t_R (minor) = 28.2 min, t_R(major) = 33.4 min]. ^{1}H NMR δ: 2.63 (broad s, 1H, OH), 3.03 (broad s, 1H, OH), 3.34–3.42 (m, 2H, —CH_2—CH=), 3.73 (dd, *J* = 11.5, 5.5 Hz, 1H, CH_2O), 3.81 (dd, *J* = 11.4, 3.3 Hz, 1H, CH_2O), 4.01–4.08 (m, 2H, CH_2O), 4.11–4.19 (m, 1H, CH), 4.98–5.05 (m, =CH_2), 5.92–6.02 (m, 1H, =CH), 6.82 (d, *J* = 8.1 Hz, 1H, C^6_{Ar} *H*), 6.92 (t, *J* = 7.3 Hz, 1H, C^4_{Ar} *H*), 7.12–7.19 (m, 2H, $C^{3,5}_{Ar}$ *H*). ^{13}C NMR δ: 34.58 (*C*H_2—CH=), 63.87 (OCH_2), 69.38 (OCH_2), 70.78 (CH), 111.82 (C^6_{Ar}), 115.30 (CH=*C*H_2), 121.27 (C^4_{Ar}), 127.54 (C^5_{Ar}), 130.20 (C^3_{Ar}), 137.27 (*C*H=CH_2), 128.73 (C^2_{Ar}), 156.34 (C^1_{Ar}).

***rac*-3-(2-Propylphenoxy)-propane-1,2-diol, *rac*-1e.** Yield: 1.6 g (76%), mp 52.5–53.5°C (hexane); (Ref. 19: mp 52–53°C). ^{1}H NMR, δ: 0.97 (t, 3H, CH_3, *J* = 7.3 Hz), 1.61–1.65 (m, 2H, C$H_2$$CH_3$), 2.61 (t, *J* = 7.3 Hz, 2H, C$H_2$$CH_2$), 2.80 (br.s, 2H, OH), 3.69 (dd, *J* = 11.5, 5.8 Hz, 1H, CH_2O), 3.78 (dd, *J* = 11.5, 3.7 Hz, 1H, CH_2O), 3.95–3.98 (m, 2H, CH_2O), 4.03–4.07 (m, 1H, CH), 6.73 (d, *J* = 7.8 Hz, 1H, C^6_{Ar} *H*), 6.83 (dd, *J* = 6.8, 7.3 Hz, 1H, C^4_{Ar} *H*), 7.04–7.07 (m, 2H, $C^{3,5}_{Ar}$ *H*). ^{13}C NMR, δ: 14.07 (CH_3), 23.07 (CH_2), 32.24 (OCH_2), 63.90 (CH_2O), 69.07 (CH_2O), 70.71 (CH), 111.46 (C^6_{Ar}), 121.04 (C^4_{Ar}), 126.94 (C^5_{Ar}), 130.06 (C^3_{Ar}), 131.08 (C^2_{Ar}), 156.22 (C^1_{Ar}).

(*R*)-3-(2-Propylphenoxy)-propane-1,2-diol, (*R*)-1e. Yield: 1.5 g (71%), mp 67–69°C (hexane); $[\alpha]_D^{20}$ +14.9 (*c* 1, hexane/ EtOH, 4:1); $[\alpha]_D^{20}$ = +11.9 (*c* 1.0, MTBE); 99.9% ee [HPLC; column temperature 28°C; eluent: water/isopropanol = 3/1; flow rate 1.0 ml/min; t_R(major) = 28.9 min, t_R(minor) = 33.2 min]. NMR spectra were identical with spectra of *rac*-**1e**.

***rac*-3-(2-Isopropylphenoxy)-propane-1,2-diol, *rac*-1f.** Yield: 1.8 g (88%), mp 80–81°C (hexane). ^{1}H NMR, δ: 1.16 (d, 6H, CH_3, *J* = 6.8 Hz), 2.20 (br. s, 2H, OH), 3.20–3.25 (m, 1H, CH), 3.71 (dd, *J* = 11.5, 5.6 Hz, 1H, CH_2O), 3.80 (dd, *J* = 11.5, 3.7 Hz, 1H, CH_2O), 3.98–4.01 (m, 2H, CH_2OH), 4.05–4.09 (m, 1H, CH), 6.77 (d, *J* = 8.1 Hz, 1H, C^6_{Ar} *H*), 6.89 (t, *J* = 7.3 Hz, 1H, C^4_{Ar} *H*), 7.08 (t, *J* = 7.3 Hz, 1H, C^5_{Ar} *H*), 7.15 (d, *J* = 7.3 Hz, 1H, C^3_{Ar} *H*). ^{13}C NMR, δ: 22.70 (CH_3), 26.87 (CH), 63.89 (OCH_2), 69.29 (CH_2O), 70.64 (CH), 111.54 (C^6_{Ar}), 121.37 (C^4_{Ar}), 126.20 (C^5_{Ar}), 126.68 (C^3_{Ar}), 137.00 (C^2_{Ar}), 155.47 (C^1_{Ar}).

(*R*)-3-(2-Isopropylphenoxy)-propane-1,2-diol, (*R*)-1f. Yield: 1.6 g (76%), mp 71–72°C (petroleum); $[\alpha]_D^{20}$ +13.7 (*c* 1, hexane/i-PrOH, 4:1); $[\alpha]_D^{20}$ +10.7 (*c* 1.0, MTBE) {Ref. 14: $[\alpha]_D^{20}$ +14.1 (*c* 1, hexane/i-PrOH, 4:1)}; 99.0% ee [HPLC; column temperature 21.5°C; eluent: water/isopropanol = 3.75/1; flow rate 0.8 ml/min; t_R(major) = 67.2 min, t_R(minor) = 86.1 min]. NMR spectra were identical with spectra of *rac*-**1f**.

***rac*-3-(2-*tert*-Butylphenoxy)-propane-1,2-diol, *rac*-1g.** Yield: 1.4 g, 63%, mp 68–71°C (hexane/benzene). (Ref. 20: mp 56°C). ^{1}H NMR, δ: 1.41 (s, 9H, CH_3), 2.35 (br.s, 2H, OH), 3.82 (dd, *J* = 11.5, 6.0 Hz, 1H, CH_2O), 3.92 (dd, *J* = 11.5, 3.7 Hz, 1H, CH_2O), 4.07–4.12 (m, 2H, OCH_2), 4.21–4.24 (m, 1H, CH), 6.91 (d, *J* = 7.8 Hz, 1H, C^6_{Ar} *H*), 6.95 (dd, *J* = 7.3, 7.8 Hz, 1H, C^4_{Ar} *H*), 7.20 (t, *J* =

TABLE 1. Resolution by entrainment of *rac*-mephenesin 1b (500 cm^3 H_2O, 25 mg crystal seeds on every run, crystallization temperature 25°C ± 0.5°C)

Run	Added amount of (*R,S*)-**1b**, (g)	Operation amount of (*R*)- and (*S*)-**1b**[a], (g)		Resolution time (min)	(*R*)- and (*S*)-**1b** obtained		
		(*R*)-**1b**	(*S*)-**1b**		Yield (g)	ee (%)[b]	YE (g)[c]
1	9.0[d]	5.50	4.50	95	(*R*) 1.82	97.0	1.77
2	1.80	4.63	5.37	80	(*S*) 1.66	95.4	1.60
3	1.64	5.41	4.59	75	(*R*) 1.50	98.5	1.47
4	1.48	4.68	5.32	80	(*S*) 1.55	92.7	1.48
5	1.53	5.39	4.61	75	(*R*) 1.62	95.0	1.56
6	1.60	4.63	5.37	85	(*S*) 1.54	97.0	1.50

[a]The operation amounts in even runs 2–6 were calculated based on the results in odd runs 1–5, respectively.
[b]ee: enantiomeric excess (HPLC).
[c]YE: Yield of enantiomer; YE (g) = [Yield (g) × ee (%)]/100 − 0.025 (seed weight).
[d]Additional amount of (*R*)-**1b** 1.0 g.

7.3 Hz, 1H, C^5_{Ar} *H*), 7.32 (d, *J* = 7.8 Hz, 1H, C^3_{Ar} *H*). ^{13}C NMR, δ: 30.16 (CH_3), 34.93 (*C*Me_3), 64.12 (OCH_2), 69.15 (CH_2O), 70.95 (CH), 112.42 (C^6_{Ar}), 121.10 (C^4_{Ar}), 126.97 (C^5_{Ar}), 127.28 (C^3_{Ar}), 138.24(C^2_{Ar}), 157.34 (C^1_{Ar}).

(*S*)-3-(2-*tert*-Butylphenoxy)-propane-1,2-diol, (*S*)-1g. Yield: 1.5 g (67%), $[\alpha]^{20}_D$ −10.5 (*c* 1, hexane/EtOH, 4:1); $[\alpha]^{20}_D$ −9.5 (*c* 1.0, MTBE). 99.3% ee [HPLC; column temperature 21°C; eluent: water/isopropanol = 3/1; flow rate 0.8 ml/min, t_R(major) = 50.5 min]. NMR spectra were identical with spectra of *rac*-**1g**.

(*R*)-3-(2-*tert*-Butylphenoxy)-propane-1,2-diol, (*R*)-1g. mp 94–95°C (hexane); $[\alpha]^{20}_D$ +10.5 (*c* 1, hexane/EtOH, 4:1); $[\alpha]^{20}_D$ +9.5 (*c* 1.0, MTBE). 99.7% ee [HPLC; column temperature 21°C; eluent: water/isopropanol = 3/1; flow rate 0.8 ml/min, t_R (major) = 46.3 min].

Resolution of Racemic 3-(2-Methylphenoxy)-propane-1,2-diol (Mephenesin, rac*-1b) by Preferential Crystallization (Entrainment)*

Racemic mephenesin *rac*-**1b** (9.0 g) and (*R*)-**1b** (1.0 g) was dissolved in 500 ml of water at 53–55°C. The solution was cooled to 28°C and seeded with finely pulverized (*R*)-**1b** (25 mg). After stirring the mixture for 95 min at 25°C ± 0.5°C, precipitated (*R*)-**1b** was collected by filtration (1.82 g after drying; 97% ee) (Table 1, run 1). The extra portion of *rac*-**1b** (1.80 g) was then dissolved in the mother liquor at 55°C; the resulting solution was cooled to 28°C. After the addition of (*S*)-**1b** (25 mg) as seed crystals to the solution, and stirring the mixture for 80 min at 25°C ± 0.5°C, (*S*)-**1b** (1.66 g after drying; 95% ee) was collected by filtration (run 2). Further resolution was carried out at 25°C ± 0.5°C by adding amended amounts of *rac*-**1b** to the filtrate in a manner similar to that described above. The detailed conditions are given in Table 1. A high degree of enantiomeric purity of collected diols can be achieved by simple recrystallization. For example, a portion of (*R*)-**1b** (1.62 g, 95% ee) was dissolved in the boiling hexane (64 ml). After cooling the solution to −2°C, the crystallized (*R*)-**1b** was collected by filtration (yield 1.24 g; 99.5% ee).

*Resolution of Racemic 3-(2-Ethylphenoxy)-propane-1,2-diol (*rac*-1c) by Preferential Crystallization*

Racemic diol *rac*-**1c** (1.0 g) and (*S*)-**1c** (0.1 g) was dissolved in 115 ml of water at 53–55°C. The solution was cooled to 25°C and seeded with finely pulverized (*S*)-**1c** (2.5 mg). After stirring the mixture for 70 min at 20°C ± 0.5°C, precipitated (*S*)-**1c** was collected by filtration (0.20 g after drying; 90% ee). The extra portion of *rac*-**1c** (0.2 g) was then dissolved in the mother liquor at 55°C; the resulting solution was cooled to 25°C. After the addition of (*R*)-**1c** (2.5 mg) as seed crystals to the solution, and stirring the mixture for 80 min at 20°C ± 0.5°C, (*R*)-**1c** (0.18 g after drying; 89% ee) was collected by filtration.

*X-ray Diffraction Experiments for 3-(2-*tert*-Butylphenoxy)-propane-1,2-diols, 1g*

The X-ray diffraction data for crystals of compounds *rac*-**1g** and (*S*)-**1g** were collected on a Bruker AXS Smart Apex II and Kappa Apex II [(*S*)-**1g**] diffractometers in the ω and φ-scan modes, using graphite monochromated Mo *K*α λ 0.71073 Å (*rac*-**1g**) and Cu Kα λ 1.54184 Å [(*S*)-**1g**] radiations. Data were corrected for the absorption effect using SADABS program.[21] The structures were solved by direct method and refined by the full matrix least-squares using SHELXTL[22] and WinGX[23] programs. All nonhydrogen atoms were refined anisotropically. The positions of hydrogen atoms were located from the Fourier electron density synthesis and were included in the refinement in the isotropic riding model approximation. Illustrations were made using PLATON.[24]

Crystallographic data (excluding structure factors) for the structures reported in this article have been deposited in the Cambridge Crystallographic Data Centre as supplementary publication nos. CCDC 691121 for *rac*-**1g**, and 691122 for (*S*)-**1g**. Copies of the data can be obtained free of charge upon application to the CCDC (12 Union Road, Cambridge CB2 1EZ U.K. Fax: (internat.) +44-1223/336-033; E-mail: deposit@ccdc.cam.ac.uk).

Room-temperature powder X-ray diffraction data were collected in the Bragg–Brentano mode with a flat-plate

sample. The sample was lightly ground and loaded into a standard sample holder, which was kept spinning (30 rpm) throughout the data collection. Patterns were recorded in the 2θ range between 3° and 50°, in 0.008° steps, with a step time of 2 sec. Five powder patterns were collected and summed for each sample.

Crystallographic Data for (S)*-3-(2-*tert*-Butylphenoxy)-propane-1,2-diol,* (S)*-1g*

The single crystal picked out from the crop of the aforementioned *scal*-**1g** with a specific rotation value of $[\alpha]_D^{20}$ −9.5 (c 1.0, MTBE) was used for single crystal experiment. Formula $C_{13}H_{20}O_3$, colorless prism of dimensions 0.35 × 0.24 × 0.14 mm^3, formula weight 224.29 g mol^{-1}, monoclinic, a = 26.5455(8), b= 6.9990(3), c= 16.6275(6) Å, β = 124.359(2)°, V = 2550.23(16) $Å^3$, T = 293 K, space group C 2 (No. 5), Z 8, μ(Cu-K_α) 6.57 cm^{-1}, F(000) = 976, d_{calc} = 1.168 g cm^{-3}, 4917 reflections measured, 2106 unique (R_{int} = 0.0673), 1961 observed with Fo > 4σ (Fo), 378 parameters. The final R1(F^2) was 0.0480 (>2σI) and wR2(all data) = 0.1291. Goodness-of-fit on F^2 was 1.025, largest diff. peak and hole are 0.203 and −0.194 e·$Å^3$. The final value −0.10(3) of Flack enantiopole parameter[25,26] proved the expected *S* absolute configuration.

The finely pulverized portion from the same bulk sample was used for PXRD experiments.

Crystallographic Data for rac*-3-(2-*tert*-Butylphenoxy)-propane-1,2-diol,* rac*-1g*

The single crystal picked out from the crop of freshly crystallized *rac*-**1g** was used for determination of crystal and molecular structure of primary racemate. The eutectic character of the crop and the metastability of this crystal modification (see text) are the important reasons precluding the high quality crystal growth. Nevertheless the experiment with this crystal enables us to evaluate some important features of primary racemate structure. Formula $C_{13}H_{20}O_3$, colorless prism of dimensions 0.70 × 0.46 × 0.12 mm^3, formula weight 224.29 g mol^{-1}, triclinic, a = 6.6876(11), b = 14.659(2), c = 14.648(2) Å, α = 70.083(2)°, β = 76.777(2)°, γ = 76.785(2)°, V = 1296.3(4) $Å^3$, T = 293 K, space group P 1 (No. 1), Z 4, μ(Mo Kα) 0.80 cm^{-1}, d_{calc} = 1.149 g cm^{-3}, F(000) = 488, 10,227 reflections measured, 9387 unique (R_{int} =0.0173), 3565 observed with Fo > 4σ (Fo), 556 parameters. The final R1(F^2) was 0.0900 (>2σI) and wR2 (all data) = 0.2970. Goodness-of-fit on F^2 was 0.927, largest diff. peak and hole are 0.343 and −0.223 e·$Å^3$.

The finely pulverized portion from the same bulk sample was used for PXRD experiments.

RESULTS AND DISCUSSION

IR Spectroscopy Investigations of the Racemic and Scalemic Samples of the Compounds 1a–g

For initial evaluation of the crystallization type of our compounds, we compared the IR spectra of the racemic

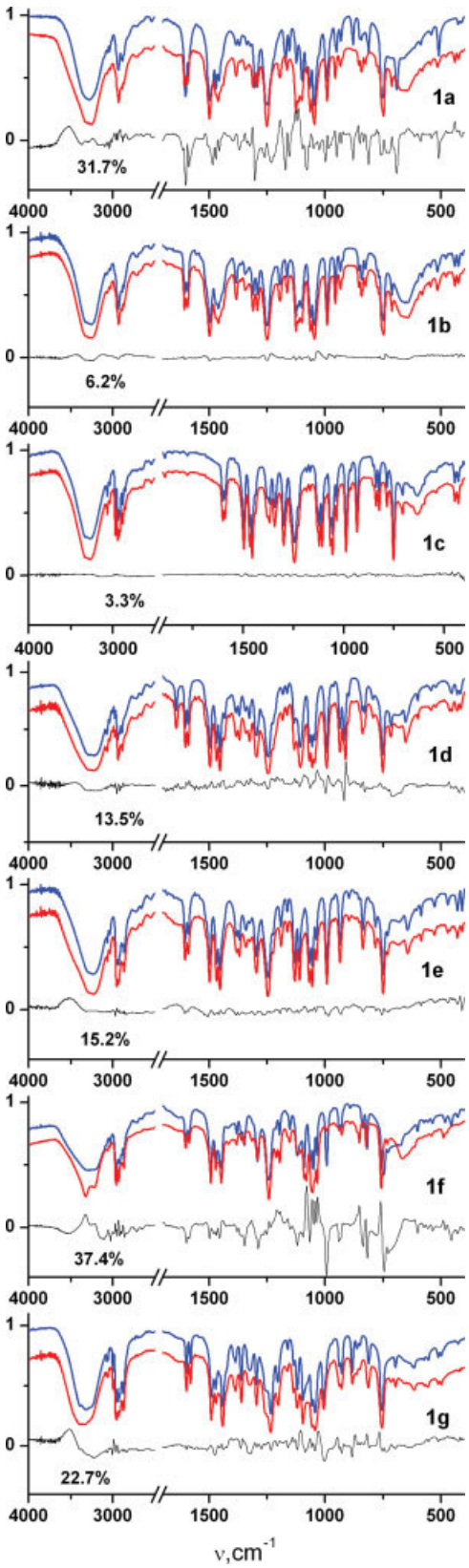

Fig. 1. IR spectra of the crystalline samples **1a–g**. Red curves—racemates, blue curves—scalemates, black curves are differential curves (see text). [Color figure can be viewed in the online issue, which is available at www.interscience.wiley.com.]

TABLE 2. DSC measured melting point (T^f) and enthalpy of fusion (ΔH^f) of racemic (low index R) and enantiopure (low index A) compounds 1a–f and calculated thermodynamic characteristics for these substances, calculated and measured eutectic (low index eu) fusion temperature and eutectic enantiomeric composition (x mole fraction of a predominant enantiomer)

Comp.	T^f_A (°C)	T^f_R (°C)	ΔH^f_A (KJ mol^{-1})	ΔH^f_R (KJ mol^{-1})	T^f_{eu}, calc. (°C)	T^f_{eu}, exp. (°C)	x_{eu}	ΔS^m_1 (J K^{-1} mol^{-1})	ΔG^0 (J mol^{-1})
1a	68.3	58.5	31.8	28.0	56.5[a]	56.3	0.68	2.59	−994
1b	91.0	70.6	34.4	32.2	70.1[b]	70.6	0.50	5.42	−51
1c	68.9	50.9	35.0	34.8	50.7[b]	50.9	0.50	5.68	−21
1d	58.0	41.7	28.8	27.8	41.3[a]	41.7	0.58	4.44	−389
1e	67.3	53.3	31.9	29.5	52.6[a]	53.0	0.60	3.89	−561
1f	71.8	80.5	30.6	31.5	67.5[a]	67.7	0.87	−2.22	−2765

[a]Calculated as intersection for Schröder-Van Laar and Prigogine-Defay curves branches.
[b]Calculated as intersection for two Schröder-Van Laar curves branches.

and highly enantiomerically enriched crystalline samples of **1a–g** in KBr pellets, since the IR spectra of an optically active and the racemic form should be identical for the normal conglomerate formative compounds. To substantiate this comparison, the spectra were subjected to a procedure of normalization and baseline correction. For this purpose, coefficients that minimize the difference $\ln(A_s) - [a_0 + a_1\nu + \ln(A_r)a_2]$, where $\ln(A_s)$ and $\ln(A_r)$ are the extinctions (transmission logarithms) of the scalemic and racemic samples, respectively; ν is the IR radiation frequency corresponding to A, and a_n are the desired regression coefficients, were selected by the least-squares method. It was reasonable to introduce the regression terms $a_1\nu$ to correct the spectral differences caused by the nonspecific (not related to particular absorption bands) interaction of IR radiation with matter (probably, by radiation scatter on heterogeneities of the sample). It should be noted that the use of polynomials of higher powers (quadratic and cubic) for the generation of differential spectra does not improve the statistical parameters characterizing regression. The ratio between the mean-square deviation of the differential curves and the averaged mean-square deviation of spectral curves for the racemate and scalemate, that is, the ratio of error to variation (%), was used as a quantitative characteristic for differential curves, and this namely quantities are cited in Figure 1.

Figure 1 shows good coincidence between the pairs of spectra for compounds **1b** and **1c** under visual comparison; the same is almost true for the allyl and normal propyl derivatives **1d,e**, whereas the spectra of racemic and enantiopure crystalline samples for unsubstituted compound **1a**, isopropyl, and *tert*-butyl substituted phenyl glycerol ethers **1f,g**, differ noticeably. A similar pattern can be observed for the differential curves: for compounds **1b** and **1c**, and to a certain extent for compounds **1d,e**, differences between the spectra of the racemate and enantioenriched sample are about the same level as instrumental background. At the same time they are rather substantial for compounds **1a,f,g**. Thus, IR-test is consistent with the conglomerate nature of mephenesin **1b**; and the great probability exists that normal racemic conglomerate is also formed by ethyl derivative **1c**. The question of crystalline type for other investigated compounds needs further consideration.

Thermochemical Investigations and Phase Behavior of the Compounds 1a–f

The results obtained for the temperature (T^f) and the enthalpy of fusion (ΔH^f) of the pure enantiomers (low index A) and the pure racemates (low index R) of aryl glycerol ethers **1a–f** are presented in Table 2.

In the idealized case, to construct the liquidus of the binary melting phase diagram in the region of a pure component fusion, it is enough to have data on the fusion temperature and enthalpy of fusion for an enantiomerically pure sample. In this case the liquidus line is described by Schröder-Van Laar equation, which is usually used in the simplified form[3]

$$\ln x = \frac{\Delta H^f_A}{R}\left(\frac{1}{T^f_A} - \frac{1}{T^f}\right) \quad (1)$$

where x is the mole fraction of one of the enantiomers in the mixture (the mole fraction of another enantiomer is $x' = 1 - x$); R is the universal gas constant ($R = 8.3170$ J K^{-1} mol^{-1}). The liquidus lines of the phase diagrams for the compounds **1a–f**, which were calculated by eq. 1 using experimental data for enantiomerically pure diols, are presented in Figure 2 (blue lines). The same figures show the experimentally obtained liquidus points drawn by circles. For samples of diols with an intermediate enantiomeric composition, the experimental DSC thermograms contain additional peaks with the almost constant temperature T^f_{eu} which corresponds to the melting point of the eutectics. These experimental characteristics are put on the plot as solid circles too. It is significant that for the compounds **1b** and **1c** experimental liquidus points, including points for racemates, practically fall on the Schröder-Van Laar curves.

The experimental data for racemates, T^f_R and ΔH^f_R, allow to construct another type of a theoretical curve describing liquidus line for congruent melting of binary molecular compounds.

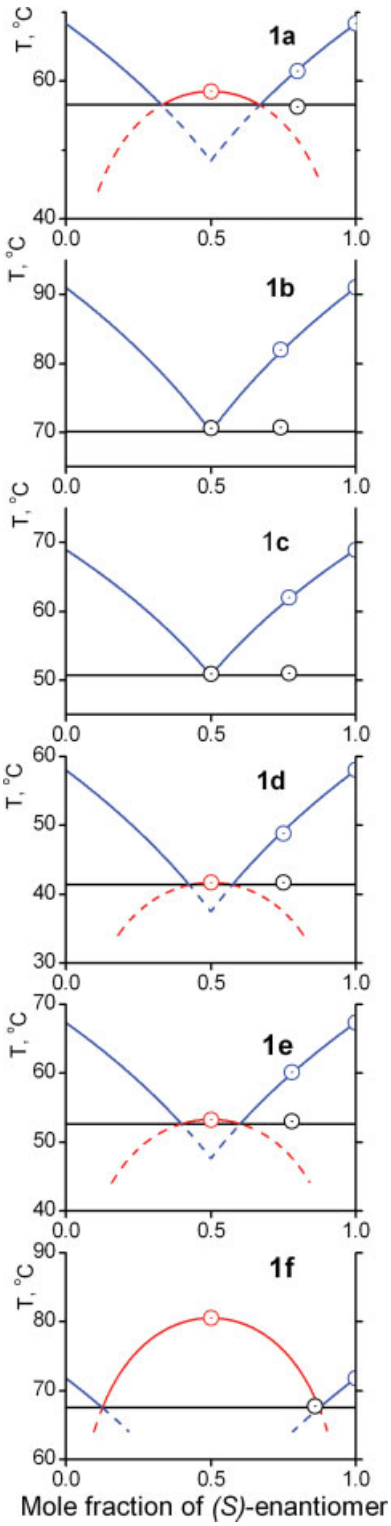

Fig. 2. Experimental (circles) points and calculated (solid lines fragments) binary melting phase diagrams for compounds **1a–f**. [Color figure can be viewed in the online issue, which is available at www.interscience.wiley.com.]

In this case, the liquidus line obeys the Prigogine–Defay equation, which is usually used in the simplified form[3]

$$\ln 4x(1-x) = \frac{2\Delta H^{f}_{R}}{R}\left(\frac{1}{T^{f}_{R}} - \frac{1}{T^{f}}\right) \quad (2)$$

The liquidus lines of the phase diagrams for the compounds **1a–f**, which were calculated by eq. 2 using experimental data for racemic diols, are presented in Figure 2 by red lines.

From Figure 2 it will be obvious that the end of fusion temperatures (colored circles position) for compounds **1a, d–f** are accurately and completely described by combination of theoretical curves of both types. Hence, complete melting phase diagrams could be reproduced by solid liquidus lines fragments with the addition of probable solidus lines (black straight lines which are drawn parallel to the *x*-axis).

Inspecting the forms of so-built phase diagrams one can suppose that the methyl and ethyl substituted phenyl glycerol ethers **1b,c** crystallize as racemic conglomerates, whereas the unsubstituted phenyl glycerol ether **1a** and its allyl and propyl derivatives **1d–f** forms solid racemic compounds. There are other points in favor of this distribution of the crystallization types, we mean the calculated values of entropy of mixing for the liquid enantiomeric compounds, ΔS^{m}_{l}, and the free energy of formation of racemic compounds in the solid state, ΔG^{0}.

Based on a thermodynamic cycle involving the solid and liquid phases of the enantiomers and racemic species, formulas for the ΔG^{0} and ΔS^{m}_{l} calculations were proposed by Grant and coworkers.[5]

$$\Delta G^{0}_{T^{f}_{R}} = -\frac{(T^{f}_{R} - T^{f}_{A})\Delta H^{f}_{A}}{T^{f}_{A}} - T^{f}_{R} R \ln 2 \quad (\text{if } T^{f}_{R} - T^{f}_{A} < 0) \quad (3a)$$

$$\Delta G^{0}_{T^{f}_{A}} = -\frac{(T^{f}_{R} - T^{f}_{A})\Delta H^{f}_{R}}{T^{f}_{R}} - T^{f}_{A} R \ln 2 \quad (\text{if } T^{f}_{R} - T^{f}_{A} > 0) \quad (3b)$$

$$\Delta S^{m}_{l} = \frac{\Delta H^{f}_{R}}{T^{f}_{R}} - \frac{\Delta H^{f}_{A}}{T^{f}_{A}} - \frac{\Delta H^{f}_{R} - \Delta H^{f}_{A}}{T^{f}_{R} - T^{f}_{A}} \ln \frac{T^{f}_{R}}{T^{f}_{A}} \quad (4)$$

The values of ΔS^{m}_{l} and ΔG^{0} calculated by the formulas (3) and (4) are presented in Table 2. The entropy of mixing for enantiomers **1b** and **1c** in the liquid state is equal to 5.42 and 5.67 J K^{-1} mol^{-1}, which is slightly less but close to the value of 5.75 J K^{-1} mol^{-1} (Rln2) for an ideal conglomerate. The near zero value for ΔG^{0} also points on the same feature of chiral **1b** and **1c**.[3,5] The relatively high negative value for ΔG^{0} for unsubstituted and isopropyl derivatives **1a** and **1f** is a good diagnostic for a stable racemic compounds formation in the crystalline state.[5] The intermediate ΔS^{m}_{l} and especially ΔG^{0} values for diols **1d** and **1e** exclude a conglomerate formation, and are compatible with the assumption of (rather unstable) racemic compound formation.

Further information about the compounds under investigation could be picked up by inspection of the binary phase diagram characteristics. The case at hand is the composition of the eutectic. The last is the special point on the binary (or

ternary) phase diagram where the three phases, liquid (melt or solution) and two solid (either two individual enantiomers or enantiomer and racemic compound) exist in equilibrium. If the enantiomeric excess of the eutectic point (ee_{eu}) is exactly equal to zero, we are dealing with a conglomerate forming compound. For this compound the direct resolution approaches could be realized and enantiomeric composition of any scalemic (nonracemic) sample could be enriched to any desirable degree by fraction crystallization. If the eutectic ee lies between 0 and 1 ($0 < ee_{eu} < 100\%$), we are dealing most likely with a racemic compound forming substance. For this system, the standard direct resolution is impossible, but if the ee of the starting sample is lower than ee_{eu}, the predominant enantiomer can be enriched in the liquid phase (mother liquor) to the eutectic ee extent, whereas the precipitate will tend to be racemate. If the solution of the starting material has an ee higher than the ee_{eu}, a pure predominant enantiomer or mixtures of enantiomers with an ee higher than the eutectic ee can be crystallized out. Equilibrium crystallization of the sample with ee = ee_{eu} could not change its enantiomeric composition in either the precipitate or in the filtrate form.

The eutectic compositions for the glycerol ethers **1a–f** are presented in Table 1. From this it follows that the sample could be enantioenriched by crystallization provided that an enantiomeric excess of it is about or more than 74% (**1f**), 36% (**1a**), and 20% (**1e**). For the allyl derivative **1d** the ee $\geq$ 6% is sufficient for enantioenrichment, and at last for methyl and ethyl derivatives a sample could be racemic for the purpose; in other words, the compounds **1b** and **1c** could be potentially resolvable by direct methods. We have particularly inspected this possibility.

Resolution of Racemic 3-(2-Methylphenoxy)-propane-1,2-diol (Mephenesin, rac*-1b) and 3-(2-ethylphenoxy)-propane-1,2-diol (*rac*-1c) by Entrainment Procedure*

The entrainment effect, that is the preferential crystallization of an enantioenriched crop induced by seeding with enantiopure crystals of the oversaturated solution of a conglomerate forming (almost) racemic chiral compound, was first discovered by Pasteur's student Gernez.[27,28] Racemates resolution by entrainment[4] is a gratifying labor since success allows one to obtain easily both enantiomers without resorting to any enantiopure auxiliaries. But even in the case of conglomerate forming substances it is not always easy to use the benefits of a spontaneous resolution. Coquerel and coworkers[4,29] are of the opinion that almost half of conglomerate forming compounds would demonstrate poor entrainment characteristics.

Discovering two new conglomerates in the family of aryl glycerol ethers we decided to examine their abilities for preferential resolution. This task was all the more interesting since *rac*-3-(2-methylphenoxy)-propane-1, 2-diol, *rac*-**1b** is a well-known skeletal muscle relaxant, mephenesin.[8] We used water for the resolution as the most cheap and "green" solvent, and by analogy with our own successful effective entrainment procedure for another chiral drug, guaifenesin.[10]

In the case of ethyl derivative **1c** we have just demonstrated entrainment effect. As shown earlier, two runs (one cycle) are sufficient to obtain from 1.2 g racemate (*R*)- and (*S*)-**1c** samples of about 0.2 g each. The quality of both specimens are good enough, and making sure that the compound **1c** is quite capable of preferential crystallization we made no attempts to improve sample enantiopurity and to optimize experimental conditions for the resolution.

For monitoring the entrainment abilities of mephenesin **1b** during seed-induced crystallization of oversaturated slightly nonracemic water solutions we have used mother liquor enantiomeric composition. Unfortunately, the optical rotation of water mephenesin solutions is too low to use polarimetry for these purposes. So we made use of chiral liquid chromatography for monitoring this process. During the course of crystallization we have collected the aliquots (10 μl) of mother liquor at regular intervals. The aliquots were mixed with 1 ml of Pr^iOH, and portions of 20 μl of the solutions were analyzed with the Chiralcel AD-RH column. All investigated solutions of mephenesin of different initial concentrations but of equal starting enantiomeric enrichment behave uniformly in the main features. During the crystallization process primary enantiomeric excess of solute (~9%) decreased to zero, changed sign, and mounted to initial absolute value (even exceeded this value for high initial concentrations). The mother liquor enantiomeric composition (and the composition of deposited crystals as well) then asymptotically tended to racemic. Varying initial concentration, temperature gap, and crystallization time we have adopted the conditions for the satisfactory resolution of racemic mephenesin. An example of successful resolution of near racemic **1b** is illustrated in Table 1.

Over the course of the resolution a supersaturated solution of *rac*-**1b**, including a small excess of (*R*)-**1b**, was prepared by heating, and then cooling to 25°C. A small amount of seed crystals of (*R*)-**1b** was added and the stirred solution was allowed to crystallize for about 85 min. The weight of (*R*)-**1b** obtained after filtration was more than the common weight of the initial excess of the (*R*)-enantiomer and seed added. *rac*-**1b** was added to the mother liquor in order that the overall quantity of **1b** in the solution could be recovered. The mixture was heated until the solid was completely dissolved and then cooled to 25°C. After the solution had been seeded with (*S*)-**1b** and stirred for about 85 min, precipitated (*S*)-**1b** was collected in a similar manner. The cycle was repeated several times.

As evident from Table 1, three cycles (six runs) of entrainment resolution using ordinary laboratory equipment and no resolving agents are sufficient enough to obtain from ~17 g of *rac*-**1b** (*R*)- and (*S*)-**1b** samples of about 5 g each. The quality of each nonracemic specimen is good enough, and single recrystallization is sufficient to obtain (*R*)- and (*S*)-**1b** diols with enantiomeric excess higher than 99%.

*Crystallization Features of 3-(2-*tert*-Butylphenoxy)-propane-1,2-diol 1g*

Both racemic (Fig. 3, curve 1, Fig. 4, curve 1) and enantiopure (Fig. 4, curve 5) polycrystalline samples of 3-(2-*tert*-butylphenoxy)-propane-1,2-diol **1g** obtained by crystal-

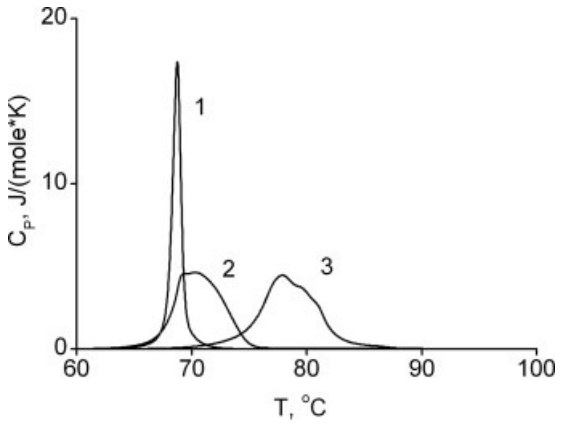

Fig. 3. DSC traces for the racemic samples of 3-(2-*tert*-butylphenoxy)-propane-1,2-diol **1g**; 1—"primary racemate" obtained by solution crystallization of racemic **1g**; 2—the same sample after several weeks aging; 3—artificial recemate obtained by mixing of approximately equal amounts of (*R*)- and (*S*)-**1g**.

lization from the solutions of corresponding composition are melted reproducibly giving the single narrow DSC traces with good linear fronts. This fact provides a way of estimating the temperature and the enthalpy of fusion for the pure enantiomer and the pure racemate of *tert*-butyl derivative **1g** as $T^{f}_{A} = 94.5^{\circ}$, $\Delta H^{f}_{A} = 32.2$ KJ mol^{-1}, $T^{f}_{R} = 67.9^{\circ}$C, $\Delta H^{f}_{R} = 19.3$ KJ mol^{-1}. The first pair of the experimental characteristics allows reconstructing Schröder-Van Laar branches of the phase diagram and estimating (as the position of their intersection) the fusion temperature of hypothetical conglomerate, $T^{f}_{congl.} = 72.2^{\circ}$C. This value is sufficiently above the experimental one for racemate. In the control experiment the racemic sample prepared by mixing of (almost) equal amounts of the pure enantiomer crystals has begun melting at near theoretical temperature T^{f}_{congl} (Fig. 3, curve 3). After several weeks aging of the sample of "primary racemate" (obtained by direct crystallization from a racemate solution) at an ambient temperature, its DSC melting trace splits, and a higher melting component could be observed (Fig. 3, curve 2), while no changes were detected in the melting of pure enantiomer samples of the same age.

The anomalous behavior of the "primary racemate" sets one thinking about additional metastable crystal forms in the system under investigation.[30] The shapes of the DSC traces for intermediate enantiomeric purity samples prepared by drying the solutions of proper composition (Fig. 4) provide support for this conclusion.

Thermograms for the mixtures of intermediate compositions (Fig. 4, curves 2–3) show simultaneous presence of three melting peaks. The low temperature one is identical by appearance and position to the melting of "primary racemate." The peak is traceable in a wide range of compositions; the peak characteristic temperature is therewith kept constant. This suggests that no individual compound but some eutectic mixture melting is the thermoinitiated process behind the low temperature peak appearance. This eutectic is not coincident with the above studied traditional racemic conglomerate formed by enantiopure crystals, and is formed by some other metastable (with respect to a homochiral) solid phase(s).

It can be inferred that all the facts under discussion are understood by reference to so-called anomalous racemate[3,31] formation during the (solution) crystallization of the racemic or the intermediate composition samples of **1g**. According to Jacques et al.,[3] anomalous racemate is an addition molecular compound in which crystals contain two enantiomers with a stoichiometry differing from the usual 1:1 ratio. We have anticipated that the above discussed "primary racemate" of *tert*-butylphenyl glycerol ether **1g** is in fact the racemic conglomerate formed by enantiomeric crystals of such anomalous racemate. To all appearance, despite the fact of less thermodynamic stability, the formation of this crystal modification is kinetically favorable. Therefore, during the racemate crystallization from a solution only the "anomalous conglomerate" (this is a more accurate expression for this case and the other examples of the sort than "anomalous racemate") precipitates.

If a solution contains an excess of one of enantiomers, the precipitate, alongside with anomalous conglomerate, contains individual enantiomer crystals. The presence of this phase manifests itself by appearance of the third high temperature peak on the DSC traces (Fig. 4). However, the possibility of the stable enantiopure solid phase generation from the metastable phase(s) immediately in the course of thermoscanning must not be ruled out. For the high enantiomeric purity samples ($x > 0.8$) the anomalous racemate melting peak virtually goes to level (Fig. 4, curve 4). Evidently in this case two crystal phases present in the sample, namely, one enantiomorph of the anomalous racemate and a pure enantiomer.

Bearing all these facts in mind we embarked on a series of control experiments using X-ray diffraction approaches. First of all we have established the molecular and crystal structure of *scal*-**1g** crystallized from an enantiopure (by HPLC) sample of the *tert*-butylphenyl glycerol ether by

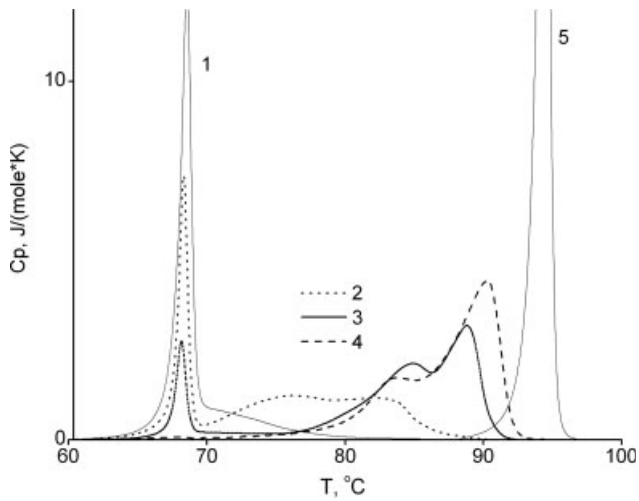

Fig. 4. DSC traces for the varying composition samples of 3-(2-*tert*-butylphenoxy)-propane-1,2-diol **1g**; $x = 0.6$ (1); $x = 0.7$ (2); $x = 0.8$ (3); $x = 0.9$ (4); $x = 1.0$, pure enantiomer (5). Here x—mole fraction of a predominant enantiomer.

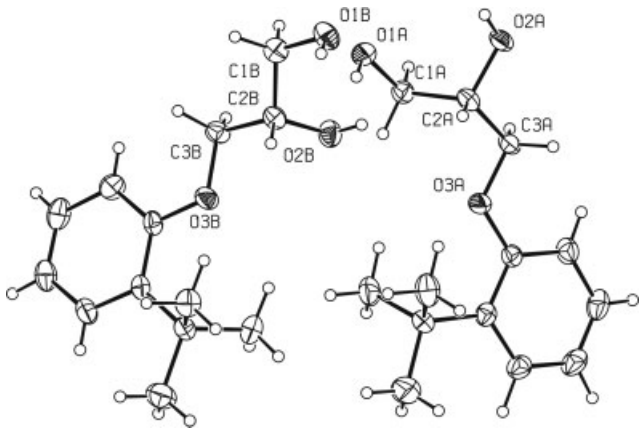

Fig. 5. ORTEP drawing of the independent part of the unit cell for (*S*)-**1g** crystal. Displacement ellipsoids are drawn at the 50% probability level; H atoms are represented by circles of arbitrary size.

single crystal X-ray analysis. Leaving out the details, we will point to Figure 5 where the independent part (two molecules) of the unit cell of *scal*-**1g** is depicted. The powder X-ray diffractogram has been simultaneously obtained from the bulk sample of the *scal*-**1g** (Fig. 7d); the experimental PXRD pattern has coincided completely with the theoretical one (Fig. 7c).

When a single crystal picked up from the bulk sample of "primary racemate" was examined by X-ray diffraction analysis two possibilities for interpretation of the experimental diffraction pattern were aroused. The automatically offered one fitted with achiral space group *Iba*2 (No. 45) with a sufficiently disordered position of all OH groups and low refinements parameters. The disorder could be diminished by lowering the crystal symmetry as far as *P*1 space group. In this case the unit cell consists of four independent molecules with the first three of them having an opposite configuration than the fourth one has. There are no crystallographic reasons to decide between these two possibilities. We have yielded to chiral *P*1 group based on the foregoing thermodynamic arguments. The case of achiral group presumes the existence of an individual racemic compound in the solid primary racemate and consequently the lowering of a fusion temperature of the sample after the enantiopure component was added owing to new eutectic formation. This is not the case as it was established in the experiments (see Fig. 4). On the contrary the case of noncentrosymmetrical *P*1 group presumes the crystallization of the *rac*-**1g** primary racemate as a mixture of enantiomorphous crystals having triple excess of one or another enantiomer. This mixture constitutes a eutectic by itself, and owing to this fact has a possibility to keep a constant melting temperature with the advent of additional component.

Figure 6 demonstrates an independent part of the *P*1 unit cell for the crystal picked up from the primary racemate bulk sample. The calculated PXRD pattern for this cell as well as for an experimental one for the freshly crys-

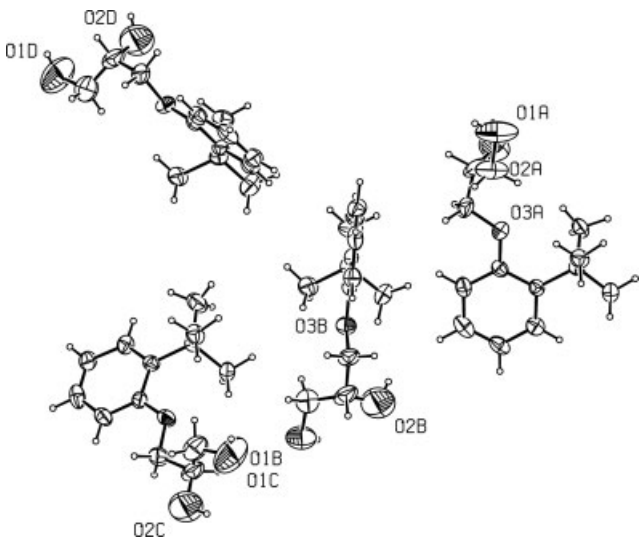

Fig. 6. ORTEP drawing of the independent part of the unit cell for *rac*-**1g** crystal. Displacement ellipsoids are drawn at the 30% probability level; H atoms are represented by circles of arbitrary size.

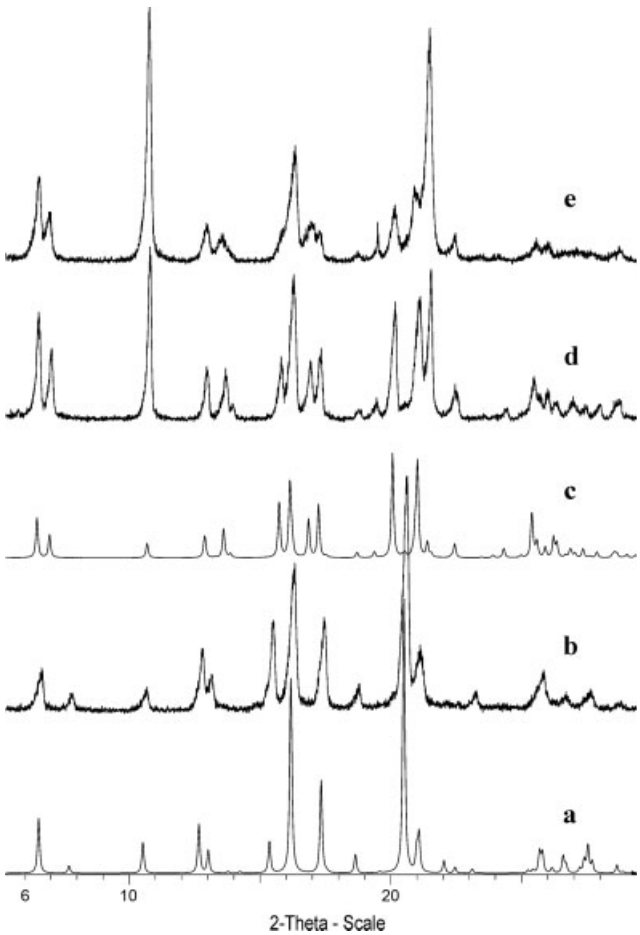

Fig. 7. Powder X-ray diffractograms for compound **1g**: (**a**) calculated from single crystal X-ray data based upon *P*1 unit cell parameters of primary racemate; (**b**) experimental pattern of freshly crystallized primary racemate; (**c**) calculated from single crystal X-ray data for enantiopure crystal; (**d**) experimental pattern for bulk enantiopure sample; (**e**) experimental pattern of bulk racemic sample after 2 months of aging.

tallized bulk sample of *rac*-**1g** are reproduced in Figure 7 (a and b correspondingly); both patterns are coincident with one another. Figure 7e demonstrates the PXRD pattern for the same *rac*-**1g** bulk sample after ~2 months of aging under ambient temperature. It will readily be seen that this curve coincides almost completely with the above discussed curve (Fig. 7d) for the enantiopure sample. And this is direct evidence of solid phase change from metastable primary crystals (anomalous conglomerate) to stable normal conglomerate formed by enantiopure components.

CONCLUSIONS

The seven aryl glycerol ethers **1a–g** studied in this work have very close chemical structure and differ only in the uniformly positioned (*ortho* phenoxyl position) far removed from the chiral centers substituents. All the substituents, hydrogen atom, alkyl, or allyl groups, are alike in polarity, are not capable of strong hydrogen bond formation, and are distinguishable mainly in size and conformational properties. Nevertheless these seemingly second-order distinctions were found to be sufficient for considerable changes in the crystallization characteristics of the different racemic members of the family.

Thus, three racemates out of the series of seven, H-, *n*-Pr-, and *i*-Pr-derivatives **1a,e,f**, crystallize as typical racemic compounds if not identical in thermodynamic characteristics. Allyl derivative **1d** forms rather unstable racemic compound. It is not improbable that the change of crystallization conditions will change the crystallization type in this case. Two substances **1b** and **1c** turn out to be typical conglomerates. The property of their spontaneous resolution could be used as the basis for an effective production of these compounds in a single enantiomer form. This is particularly of importance because one of these substances, **1b**, is the registered drug mephenesin.

Finally, the series is closed by the *tert*-butyl derivative **1g**, a racemate of which manifests rare if not unique types of spontaneous resolution. It seems reasonable to say that the metastable form, resulting during solution crystallization, and the stable form, to which metastable one transforms as times goes by, both are the eutectic mixtures of scalemic crystals. Metastable eutectic, i.e. the conglomerate of enantiomorphous crystals enriched with one or another enantiomer, arising as a result of spontaneous resolution of the anomalous racemate, turns into the eutectic of enantiopure crystals.

Thus, in this work the queer character of a spontaneous resolution has been demonstrated once again, the number of known conglomerate forming substances has been enlarged, and the uncommon variant of spontaneous resolution of metastable anomalous racemate has been found out.

LITERATURE CITED

1. Pasteur L. Sur les relations qui peuvent exister entre la forme cristalline, la composition chimique et le sens de la polarisation rotatoire. Ann Chim Phys 1848;24:442–460.
2. Perez-Garcia L, Amabilino DB. Spontaneous resolution, whence and whither: from enantiomorphic solids to chiral liquid crystals, monolayers and macro- and supramolecular polymers and assemblies. Chem Soc Rev 2007;36:941–967.
3. Jacques J, Collet A, Wilen SH. Enantiomers, racemates and resolutions. Malabar, FL: Krieger Publishing; 1994. 447 p.
4. Coquerel G. Preferential crystallization. Top Curr Chem 2007;269:1–51.
5. Li ZJ, Zell MT, Munson EJ, Grant DJW. Characterization of racemic species of chiral drugs using thermal analysis, thermodynamic calculation, and structural studies. J Pharm Sci 1999;88:337–346.
6. Höhne GWH, Hemminger WF, Flammersheim H-J. Differential scanning calorimetry. Berlin-Heidelberg-New York: Springer Verlag; 2003. 298 p.
7. Avalos M, Babiano R, Cintas P, Jimenez JL, Palacios JC. Symmetry breaking by spontaneous crystallization—is it the most plausible source of terrestrial handedness we have long been looking for?—A reappraisal. Orig Life Evol Biosphere 2004;34:391–405.
8. O'Neil MJ, editor. The Merck Index, 14th ed. Whitehouse Station, NJ: Merck and Co; 2006.
9. Bredikhina ZA, Savel'ev DV, Bredikhin AA. Cyclic sulfites—the key intermediates in the synthesis of 1-alkylamino-3-aryloxypropan-2-ols from glycidol. Russ J Org Chem 2002;38:213–219.
10. Bredikhina ZA, Novikova VG, Zakharychev DV, Bredikhin AA. Solid state properties and effective resolution procedure for guaifenesin, 3-(2-metoxyphenoxy)-1,2-propanediol. Tetrahedron: Asymmetry 2006;17:3015–3020.
11. Zakharychev DV, Lazarev SN, Bredikhina ZA, Bredikhin AA. Crystallization of chiral compounds 3. 3-Phenoxypropane-1,2-diol and 3-(2-halophenoxy)propane-1,2-diols. Rus Chem Bull Int Ed 2006;55:230–237.
12. Bredikhin AA, Bredikhina ZA, Zakharychev DV, Konoshenko LV. Spontaneous resolution among chiral glycerol derivatives: crystallization features of *ortho*-alkoxysubstituted phenyl glycerol ethers. Tetrahedron: Asymmetry 2007;18:1964–1970.
13. Schaus SE, Brandes BD, Larrow JF, Tokunaga M, Hansen KB, Gould AE, Furrow ME, Jacobsen EN. Highly selective hydrolytic kinetic resolution of terminal epoxides catalyzed by chiral (salen)Co^{III} complexes. Practical synthesis of enantioenriched terminal epoxides and 1,2-diols. J Am Chem Soc 2002;124:1307–1315.
14. Egri G, Kolbert A, Balint J, Fogassy E, Novak L, Poppe L. Baker's yeast mediated stereoselective biotransformation of 1-acetoxy-3-aryloxypropan-2-ones. Tetrahedron: Asymmetry 1998;9:271–283.
15. Kitaory K, Furukawa Y, Yoshimoto H, Otera J. CsF in organic synthesis. Regioselective nucleophilic reaction of phenols with oxiranes leading to enantiopure β-blockers. Tetrahedron 1999;55:14381–14390.
16. Bredikhin AA, Bredikhina ZA, Lazarev SN, Savel'ev DV. Systematic search for conglomerates among glycerol aromatic monoethers: guaifenesin and mephenesin are the cases. Mendeleev Commun 2003;13:104–105.
17. Theil F, Weidner J, Ballschuh S, Kunath A, Schick H. Kinetic resolution of acyclic 1,2-diols using a sequential lipase-catalyzed transesterifications in organic solvents. J Org Chem 1994;59:388–393.
18. Lambooy JP. Physiologically active substituted α-glyceryl phenyl ethers. J Am Chem Soc 1951;73:349–350.
19. Yale HL, Pribyl EJ, Braker W, Bergeim FH, Lott WA. Muscle-relaxing compounds similar to 3-(*o*-toloxy)-1,2-propanediol. I. Aromatic ethers of polyhydroxy alcohols and related compounds. J Am Chem Soc 1950;72:3710–3716.
20. Auzou G, Rips R, Derappe C, Peyroux J. Anxiolytic activity derived from a myorelaxant structure. *tert*-Butylphenol derivatives. Eur J Med Chem Chim Ther 1974;9:548–554.
21. Sheldrick GM. SADABS, Program for empirical X-ray absorption correction. Bruker-Nonius, 2004.
22. Sheldrick GM. SHELXTL v.6.12, Structure determination software suite, Bruker AXS, Madison, WI, 2000.

23. Farrugia LJ. WinGX 1.64.05. An integrated system of Windows programs for the solution, refinement and analysis of single crystal X-ray diffraction data. J Appl Crystalogr 1999;32:837–838.
24. Spek AL. Single-crystal structure validation with the program *PLATON*. J Appl Cryst 2003;36:7–13.
25. Flack HD. On enantiomorph polarity estimation. Acta Crystallogr Sect A 1983;39:876–881.
26. Flack HD, Bernardinelli G. Reporting end evaluating absolute structure and absolute configuration determination. J Appl Crystallogr 2000;33:1143–1148.
27. Gernez. Séparation des tartrates gauches et des tartrates droits à l'aide des solutions sursaturées. Compt Rend 1866;63: 843.
28. Gernez. Verfahren zur Scheidung rechtsdrehend- und linksdrehendweinsaurer Salze. Ann Chem Pharm 1867;143:376.
29. Dufour F, Perez G, Coquerel G. A Priori assessment of the maximum possible entrainment effect attainable during preferential crystallization. The case of the simultaneous resolution of (±)-ephedrine and (±)-mandelic acid. Bull Chem Soc Jpn 2004;77:79–86.
30. Coquerel G. Review on the heterogeneous equilibria between condensed phases in binary systems of enantiomers. Enantiomer 2000;3:481–498.
31. Levkin PA, Torbeev VY, Lenev DA, Kostyanovsky RG. Homo- and heterochirality in crystals. Top Stereochem 2006;25:81–134.

Vibrational Circular Dichroism and IR Spectral Analysis as a Test of Theoretical Conformational Modeling for a Cyclic Hexapeptide

PETR BOUR,[1,2] JOOHYUN KIM,[1] JOSEF KAPITAN,[1,2] ROBERT P. HAMMER,[3] RONG HUANG,[1] LING WU,[1] AND TIMOTHY A. KEIDERLING[1]*

[1]*Department of Chemistry, University of Illinois at Chicago, Chicago, Illinois*
[2]*Institute of Organic Chemistry and Biochemistry, Academy of Sciences, Prague 6, Czech Republic*
[3]*Department of Chemistry, Louisiana State University, Baton Rouge, Louisiana*

ABSTRACT A model cyclohexapeptide, cyclo-(Phe-^{D}Pro-Gly-Arg-Gly-Asp) was synthesized and its IR and VCD spectra were used as a test of density functional theory (DFT) level predictions of spectral intensities for a peptide with a nonrepeating but partially constricted conformation. Peptide structure and flexibility was estimated by molecular dynamics (MD) simulations and the spectra were simulated using full quantum mechanical (QM) approaches for the complete peptide and for simplified models with truncated side chains. After simulated annealing, the backbone conformation of the ring structure is relatively stable, consisting of a normal β-turn and a tight loop (no H-bond) which does not vary over short trajectories. Only in quite long MD runs at high temperatures do other conformations appear. MD simulations were carried out for the cyclic peptide in water and in TFE, which match experimental solvents, as well as with and without protonation of the Asp carboxyl group. DFT spectral simulations were made using the annealed structure and were extended to include basis set variation, to determine an optimal computational approach, and solvent simulation with a polarized continuum model (PCM). Stepwise full DFT simulation of spectra was done for various sequences with the same backbone geometry but based on (1) solely Gly residues, (2) Ala substitution except Gly and Pro, and (3) complete sequences with side chains. Additionally, a selection of structures was used to compute IR and VCD spectra with the optimal method to determine structural variation effects. The side chains, especially the Asp—COOH and Arg—NH_2 transitions, had an impact on the computed amide frequencies, IR intensities and VCD pattern. Since experimentally these groups would have little chirality, due to conformational variation, they do not impact the observed VCD spectra. Correcting for frequency shifts, the Ala model for the cyclopeptide gives the clearest representation of the amide VCD. The experimental sign pattern for the amide I' band in D_2O and also the sharper, more intense amide I VCD band in TFE was seen to some degree in one conformer with Type II′ turns, but the data favor a mix of structures. *Chirality 20:1104–1119, 2008.*

KEY WORDS: peptide conformational spectral interpretation; infrared absorption; vibrational circular dichroism; density functional theory; molecular dynamics; solvent effects

INTRODUCTION

Vibrational spectroscopy has a long history in the conformational analyses of peptide structures.[1] Originally empirical correlations of IR amide I and II frequency positions were first used to discriminate helical and sheet-like peptides, then extended to protein studies, after which Raman analyses of amide I and III frequencies were applied to proteins. More recently the chiroptical variants of both were utilized to distinguish protein conformations and to deconvolve components of mixed structures as found in globular proteins.[2–6] Of the structural types, α-helices and β-sheets yield the more characteristic vibrational transitions, since they are repeating structures of some

Contract grant sponsor: National Science Foundation; Contract grant numbers: CHE-0316014, CHE-0718543 to TAK
Contract grant sponsor: American Chemical Society; Contract grant numbers: 42027-AC4 to RPH
Contract grant sponsor: Grant Agency of the Czech Republic; Contract grant numbers: 203/06/0420, 202/07/0732 to PB
Contract grant sponsor: Grant Agency of the Academy of Sciences; Contract grant number: A400550702 to PB
Contract grant sponsor: John Simon Guggenheim Fellowship to TAK
*Correspondence to: Timothy A. Keiderling, Department of Chemistry, University of Illinois at Chicago, Chicago, Illinois. E-mail: tak@uic.edu
Received for publication 2 September 2007; Accepted 7 February 2008
DOI: 10.1002/chir.20560
Published online 27 May 2008 in Wiley InterScience (www.interscience.wiley.com).

uniformity in amide conformation, resulting in excitonic bands of higher intensity and characteristic chirality. This has led to a number of useful analyses and, for peptides, to some exceptionally detailed spectral assignments, recently enhanced by use of isotopic labeling to create localized transitions.[7–18] A key element of peptide conformational studies is use of chiroptical techniques such as circular dichroism (CD) and more recently vibrational CD (VCD) and Raman optical activity (ROA), the latter of which can have useful sensitivity to isotopic variants.[4–6,14,19–21] Here chirality is not used to determine absolute configuration, which is, of course, known from the synthetic method used (e.g. employing L-amino acids), but is useful to determine oligomer conformation which can be uniform (as in helices or sheets) or highly variable, lacking repeating character, particularly in ϕ, ψ torsions. Conformational chirality is most strongly evident for the amide properties which would otherwise be locally achiral without interresidue coupling in the oligomer.

A major conformational contribution to globular protein structure comes from the various turn structures by which a strand can reverse itself in space and make the protein or peptide more compact. By its very nature these are not repetitive and thus do not give a uniform contribution to the spectrum nor create extended exciton coupled modes. Spectral characterization of turns has been a long term goal in conformational analyses, with most attention on tight β-turns that reverse the strand direction and form a H-bond from position i (C=O) to $i + 3$ (N—H).[22–27] Creating viable experimental models of stable turn peptides is challenging as well. If a turn is part of a linear peptide chain there will be considerable local conformational fluctuation unless some other construct constrains it, thereby creating a large energy barrier to transformation. One method to constrain a turn is formation of a hairpin, a topic that has prompted extensive studies involving both peptide design and spectral analyses.[26,28–42] For a turn-focused study, hairpins have the disadvantage that most of the residues in the peptide are not in the turn (yet contribute to spectral overlap, thereby obscuring the turn contribution), and those in the termini (which are open and frayed) often have considerable fluctuation.

Another option for turn modeling is to form small cyclic peptides, where the turn is constrained by the rest of the peptide or by another linker acting as a bridge.[24,25,43,44] One approach to this would be to make disulfide linked sequences,[45–50] and another has been to use mimetics.[24,51–55] A cyclic peptide is also constrained, and can form β-turns or other structures, depending on sequence and ring size. While large cyclic peptides can form a closed hairpin with designed turns, the problem of sorting out spectral responses arises when many of the residues have conformations other than that of the targeted turn.[36,56,57] Cyclic pentapeptides tend to form γ-turns with β-turns, somewhat mixing up the picture.[58] On the other hand cyclic hexapeptides can form more symmetrical structures with one cross-strand H-bond plus two β-turns or loops which may or may not close to form additional cross-strand H-bonds.[25,59–62] Many of these have been characterized and offer an opportunity to determine characteristic turn spectral behavior in a constrained environment and with minimal interference from "extra" residues.

One of the best ways for the detailed interpretation of peptide vibrational spectra is via density functional theory (DFT)-based computations. For large molecular systems these pose a difficulty since such computations become too large and added approximations must be made. We have had great success modeling spectra for regular structures by focusing on local interactions.[9,13,17,32,40,63,64] However in a cyclic or turn structure, the local interactions can be separated in a sequence due to cross-strand interactions. This has required us to develop methods of transferring properties obtained with computations for smaller molecules onto larger ones to obtain force field (FF), atomic polar and axial tensor (APT and AAT) values to determine IR and VCD frequencies and intensities.[40,65,66] An extension of this method has proven to be useful for simulation of the Raman and ROA spectra as well.[67,68] On the other hand, with current computational capabilities, a cyclic hexapeptide is small enough that we can do a complete FF, APT, and AAT computation, even including side chains. It is also an appropriate structure for extended MD trajectory calculations to explore conformational variations that can occur at different temperatures. Because of the cyclic constraints, these still result in a limited ensemble of conformations, which in turn can provide the basis for ab initio computations of their spectral properties.

Thus, to pursue such tests of peptide conformation—spectroscopic property correlation, we have chosen a cyclic peptide, c(FpGRGD), where p = ^{D}Pro, whose sequence suggests (based on previous NMR results) that stable Type II′ turn geometries will be formed.[62] We have explored the conformational space of this peptide with MD calculations at various temperatures and with different solvents and states of ionization (pH). We have simulated the spectra at the full DFT level for several model structures using both an all atom approach and a "stripped" structure where residues other than Pro and Gly (i.e. R,D,F) are substituted with Ala. This has allowed us to look at the effects of the fluctuation in the trajectory on the spectral results. These we then compared with experimental spectra of compounds we have synthesized. Use of such a limited size model system of restricted conformation has made possible the combination of MD and QM approaches without resorting to the transfer methods we have employed for larger peptides.

EXPERIMENTAL AND THEORETICAL METHODS

Peptide Synthesis

The c(FpGRGD) peptide was synthesized on an ABI Pioneer Peptide Synthesizer according to the manufacturer's protocols for the synthesis of backbone cyclized peptides. These protocols take advantage of three-dimensional orthogonal protection schemes[69] based on base-labile Fmoc, acid-labile (TFA) side-chain group, and allyl (Al) groups, which are piperidine and TFA-stable and removed with Pd(0) catalysts. This scheme for on-resin

synthesis of backbone amide and side-chain amide cyclized peptides was first systematically described by Barany and coworkers.[70] In this case, side-chain anchoring is desired to allow for on-resin backbone cyclization. For this sequence, anchoring is most conveniently offered through the side-chain of Asp, i.e., Fmoc-Asp(OH)-OAl is attached to an Wang-type linker (PAC-PEG-PS; commercially available from ABI) to provide the starting point for this synthesis. Coupling of the remaining residues utilized four equivalents each of Fmoc-protected amino acid (e.g., Fmoc-Arg(Pbf)-OH), TBTU, and HOBt (final concentration of each = 0.25 M) dissolved in 0.5 M DIEA in DMF for 1 h. On-resin cyclization was accomplished by first removing the final F_{moc}-group from the Phe-residue and then cleaving the allyl ester of the C-terminal Asp with a two-fold excess of $(Ph_3P)_4Pd$ in a solution containing 5% acetic acid and 2.5% *N*-methylmorpholine in $CHCl_3$. The allyl cleavage solution is recycled for 2 h and then the resin is washed with a solution of 5% DIEA and 0.5% sodium diethyldithiocarbamate in DMF to remove trace metal ions. The backbone amide bond formation between the amino group of Phe and carboxyl of Asp was accomplished with a four-fold excess of PyAOP dissolved in 0.5 M DIEA in DMF. PyAOP is utilized here to prevent guanidylation of the amino group which can occur with amidine-based coupling agents like TBTU and HATU.[71]

Experimental Spectroscopy

IR spectra were measured with a Digilab FTS-60A FTIR spectrometer (Varian, Randolf, MA) and VCD with a dispersive instrument developed at UIC and described extensively in the literature.[72] Samples were prepared by dissolving the cyclic peptide in D_2O with 0.1 M DCl and lyophilizing (twice) to eliminate TFA and redissolving (~45 mg/ml in D_2O, pH = 2). Alternatively, samples were dissolved without exchange in TFE or DMSO-d6 (~46 mg/ml) or with exchange in TFE-OD. The solutions were placed in cells composed of two CaF_2 windows separated by a Teflon spacer (50 or 100 μm), which were clamped in a brass ring and placed in a temperature-controlled holder of our own design.

Comparative ATR-IR spectra of dried peptide films deposited from H_2O and from D_2O were measured to encompass a wider spectral region. Samples were originally prepared at pH = ~2.6 or ~7.0 (to obtain spectra with contributions of either protonated and deprotonated Asp sidechains) by dissolving lyophilized peptide in H_2O or D_2O, then 7.5 μl was deposited onto the ATR crystal surface, and dried under N_2 flow. IR spectra were obtained at room temperature using a Pike Miracle ATR (3 bounce, ZnSe) and the internal DTGS detector by averaging 128 scans. Conversion to absorbance was done by referencing to an empty ATR cell.

For comparison, fluorescence and CD spectra (in the UV region) were obtained with a J-Y Fluoromax 3 and a JASCO J-815 dichrometer, respectively. Temperature for CD measurements was varied by flow from a Neslab RT-7 bath through a sample holder under instrument control.

Molecular Dynamics Conformational Studies

We initially performed test MD computations on a protonated variant of the cyclic peptide (i.e. with the Asp—COOH and Arg—$NHC(NH_2)_2^+$ side chains) as well as on the zwitterionic form (with Asp —CO_2^- and $NHC(NH_2)_2^+$). The protonated form is relevant to many of our experimental conditions and thus is analyzed in detail. The Amber 8.0, Gromacs (www.gromacs.org/) and Tinker programs were used for MD simulations.[73] General conformational behavior was explored with the Amber99[74] and OPLS-AA force fields in large solvent boxes (32 Å with Amber 8.0, zwitterion in H_2O and DMSO, 40 Å with Gromacs for the protonated form in H_2O), where several MD runs of 10–60 nsec were performed. The common TIP3P water[75] and OPLS-AA TFE force field were used with a particle-mesh Ewald (PME) summation.

Simulated annealing was run with Tinker software using an Amber 99 force field (from 1000 to 300 K) for the protonated form and was followed by running short MD trajectories at 300 K with the same FF. From these trajectories, 10 MD configurations were selected for ab initio computation, by sampling every 100 psec from a 1 ns trajectory, run at 300 K, NpT ensemble, with 1 fsec time steps. MD computations were realized on various Linux-based computers.

Ab Initio Vibrational Spectral Computations

Selected conformations from the MD trajectories above were used for DFT determinations of vibrational spectroscopic properties, calculated with the Gaussian 03 software package.[76] Some conformers were fully optimized, but for most of them a constrained normal mode optimization method[77,78] was used to retain the MD conformation by fixing coordinates for modes less than 300 cm^{-1}. In this way, the higher-frequency modes, presumably important for the spectra, could be relaxed while having a minimal impact on the MD determined conformation (primarily dependent on low frequency torsional modes, Figure 1). For optimized structures the force fields (FF), atomic polar and axial tensors (AAT, APT) were calculated. In most cases the BPW91/6-31G** functional and basis set was used with the COSMO solvent correction (exceptions will be noted). Some of the DFT computations were simplified by reducing the R (Arg), D (Asp), and F (Phe) side chains to $—CH_3$, i.e. substituting with Ala, but retaining G (Gly) and P (Pro) residues, which enabled DFT exploration of amide spectral features, which are of prime interest to the IR and VCD, for more conformations with alternate structures. Also some tests were done on a fully Gly substituted sequence ($cGly_6$) whose conformation was constrained to one set of MD determined ϕ, ψ values. Additionally, computations to determine optimal methods were performed on the $cGly_6$ model peptide in vacuum with the B3LYP/6-31G** to test the impact of using a hybrid functional and with BPW91/6-311++G** to test the effect of a basis set containing diffuse functions. While DFT calculations for cyclic model peptides without side chains could be calculated on a Linux cluster with 32-bit/2GB nodes, computations on hexapeptides with full side chain representations

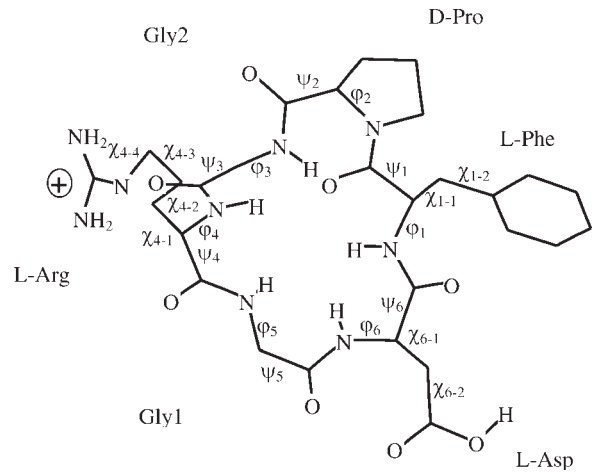

Fig. 1. Definition of the c(FpGRGD) cyclic hexapeptide torsion angles and numbering scheme.

were run on 64-bit PCs with up to 16 GB RAM. Simulated spectra of both protonated and deuterated peptides were generated with these DFT-level parameters using our own supplementary programs.

RESULTS

Experimental Spectral Data

ECD (electronic circular dichroism in the UV range) spectra were measured for the peptide in H_2O and TFE at neutral and acidic pH. The spectra (shown in Fig. 2) have a negative broad feature with a minimum at ~202 nm which while not characteristic of any standard model peptide secondary structure, presumably reflects the turn geometry modified by the Phe-^{D}Pro-Gly linkage. The pattern is roughly similar to that seen by Vass et al.[25] in their study of similar cyclic peptides, in which it was recognized that although the CD resembled that of a disordered structure, that could not be correct (since it is cyclic). They also noted this CD is not typical of known β-turns and thus might be more complex due to conformational averaging. This suggestion is further supported by the CD bands we have reported for the NG4 and ^{D}PG4 peptides (Ac-VNGK-NH_2, disordered, and Ac-^{D}PNGK-NH_2, Type I′ turn, respectively) being of the opposite sign.[38] There is little effect of acidic pH on the spectra, but the TFE data did have an extra negative band at ~193 nm. Similarly, the fluorescence of this cyclic peptide with either 250 or 280 nm excitation, while different, is similar in both solvents, but in TFE is much broader, suggesting some quenching mechanism (data not shown).

IR and VCD spectra were measured for the cyclic peptide in D_2O, TFE-OH, TFE-OD and DMSO, at different pH values, and ATR-IR spectra were measured on dried films taken from H_2O and D_2O solutions at high and low pH, to obtain both protonated and H/D exchanged samples and to observe the effects of protonation of the Asp side chain. Because of its small size and nonregular geometry, the Phe-^{D}Pro linkage, and the Asp and Arg side chains, this cyclic peptide gives rise to several partially resolved bands in the amide I region that may (at some level) be associated with local modes. The positions and relative intensities of these are sensitive to pH, and the TFE results to H/D exchange. The solution phase IR spectra are broader in D_2O than in the organic solvents, but accounting for the linewidth differences, the D_2O and TFE data are consistent, but are shifted in frequency with D_2O being lower (Table 1 and Fig. 3, where the D_2O and TFE results are compared). The DMSO and TFE-OD data are not shown.

Again allowing for frequency shift and line broadening, and correcting for some variation in baseline, the VCD spectra of all three solution phase samples have the same fundamental coupled oscillator-like (alternating sign sequence) VCD pattern. Within the amide I profile, a dominant strong couplet appears, which is correlated to the higher wavenumber absorption component. The bandshape is negative then positive with decreasing frequency (at 1671 and 1647 cm^{-1}, respectively, in D_2O, while in TFE the corresponding negative band has two components at 1692 and 1680 cm^{-1} and the positive band is at 1651 cm^{-1}). Typically a weaker nega-

TABLE 1. Comparison of observed amide I frequencies and intensities for c(FpGRGD) in D_2O and TFE

D_2O				TFE			
IR		VCD		IR		VCD	
Frequency (cm^{-1})	Intensity (A)	Frequency (cm^{-1})	Intensity (10^{-5} ΔA)	Frequency (cm^{-1})	Intensity (A)	Frequency (cm^{-1})	Intensity (10^{-5} ΔA)
1710[a]	0.09	1701	0.1	1725[a]	0.08		
		1671	−1.1			1692	−1.9
1648	0.40	1647	1.8	1674	0.78	1680	−2.0
						1651	3.5
1622	0.38	1622	−0.4	1634	0.56	1632	(–)[c]
1587	0.16	1601	8.4			1631	1.0
				1530[b]	0.22	1523[b]	2.5

[a]Mostly due to Asp−COOH.
[b]Amide II band in TFE−OH.
[c]Negative band between two positives.

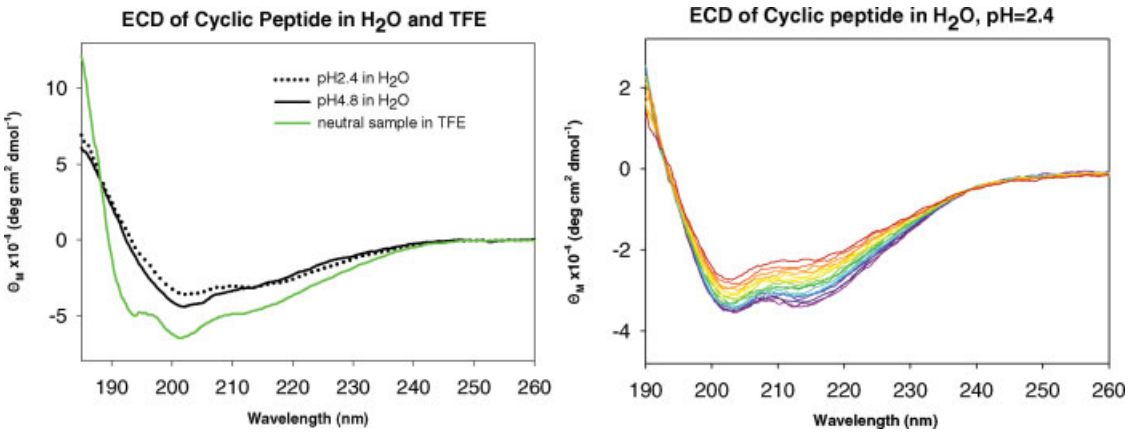

Fig. 2. ECD spectra of the c(FpGRGD) hexapeptide in H_2O at low (dotted line) and neutral pH (black solid line) and in TFE (green line) at room temperature (left) and in H_2O (acidic pH) from 5 to 85°C (right), where violet/blue (more intense) are the low temperatures and orange/red the hot. [Color figure can be viewed in the online issues, which is available at www.interscience.wiley.com.]

tive and positive VCD are seen to the low wavenumber side of the amide I, with the negative component corresponding to the prominent lower wavenumber absorption band (Table 1 and Fig. 3, right side).

The ATR-IR for low pH samples (see Fig. 4) has an amide I band with a maximum at ~1625 cm^{-1} and a shoulder at ~1650 cm^{-1}, which are altered in relative intensity from the solution phase data. They also show a broad amide II band at ~1525 cm^{-1} that shifts to ~1450 cm^{-1} on H/D exchange. A presumed amide III band occurs at ~1280 cm^{-1} but is quite dispersed and obscured by overlap with side-chain modes (as evident from comparison of H_2O and D_2O spectra, see inserts in Fig. 4). At neutral pH, the Asp—COO^- band gives a broad band from 1530–1580 cm^{-1} and at low pH the Asp—COOH is at ~1710 cm^{-1}.

MD-Derived Geometry

The torsional angles for the definition of the cyclic peptide conformation are defined in Figure 1. For VCD and IR, the backbone conformation is most relevant and will be the focus of the discussion in this article. While side chain conformational fluctuations were also analyzed, they are most relevant for Raman spectral studies, which will be discussed separately with relevant experimental data and Raman simulations.

An overall equilibrium between conformations could only be sampled with MD using relatively long time simulations. Important conformational transitions such as the flipping motion of the ^{D}Pro-Gly turn between Type I′ and II′ turns could only be observed, even for 100 nsec runs, with higher temperatures and certain force fields. In particular, Amber99 showed no transitions from conformations started having a Type I′ turn, but OPLS led to conformers with Type II′-like turns at long times. Only by use of high temperature simulations could such transitions be revealed in the MD trajectories. In Figure 5a, the time dependent conformational fluctuations showing such a transition are illustrated in terms of changes in the radius of gyration (R_g) and dihedral angles sampled during a trajectory obtained at 450 K. While the R_g does not vary drastically, as would be expected for a cyclic molecule, the Pro dihedral angles, ϕ_2, ψ_2, have a sharp transition in ψ_2 from ~0° to ~ −130° and back during the 14 nsec trajectory (Fig. 5b). This is consistent with a change from approximately Type I′ to II′ for the Pro-Gly turn. More or less concerted with that change is a flip of the Gly5 ϕ_5 from 110°

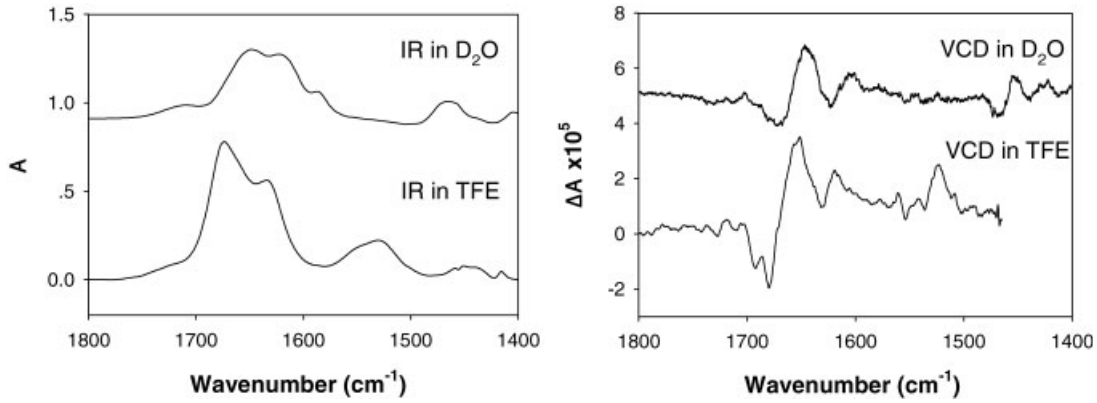

Fig. 3. Experimentally obtained IR (left) and VCD (right) spectra of the c(FpGRGD) hexapeptide in (top) D_2O (pH = 2) and (bottom) TFE.

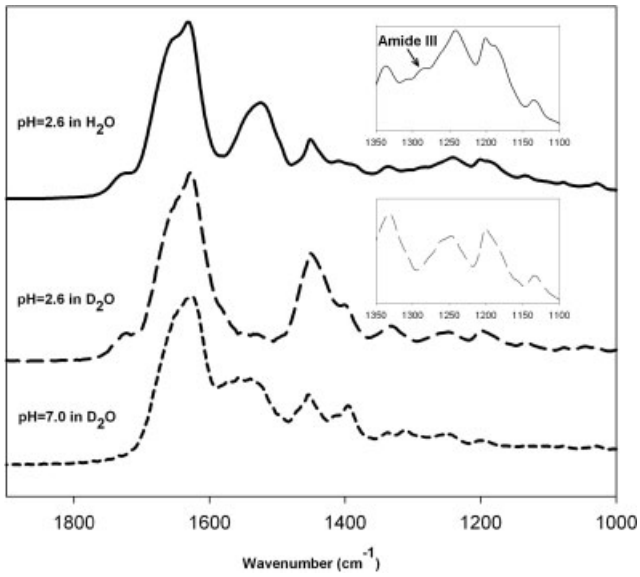

Fig. 4. ATR-IR spectra for films of the c(FpGRGD) peptide deposited from H_2O (top, solid line) or D_2O at pH 2.6 (middle, dashed) or 7.0 (bottom, short dash). Inserts show expanded amide III regions.

to -140°, but the ψ_5 value is more variable, indicating that this turn has a less well-defined conformation (Fig. 5c).

Figure 6 shows the corresponding distributions of dihedral angles derived from the same trajectory for each residue, F1,p2,G3,R4,G5,D6 in the order Figures 6a–6f, respectively. Overall, the observed conformational fluctuations suggest that this cyclic peptide has stable mixed structures most often composed of two turns and a (very short) anti-parallel β-strand structure. The two turns are achieved in the ^{D}Pro2-Gly3 sequence (numbering as in Fig. 1), with the dihedral angles corresponding to the ^{D}Pro2 and the Gly3 residues being close to values expected for tight β-turn Type I′ ($\phi_2\sim60$, $\psi_2\sim30$, $\phi_3\sim90$ and $\psi_3\sim0^\circ$) or Type II′ ($\phi_2\sim60$, $\psi_2\sim-120$, $\phi_3\sim-80$ and $\psi_3\sim0^\circ$) values. The other turn, composed of the Gly5-Asp6 residues, is quite distorted from these ideal values, but may also have two dominant conformational populations. However, they are not β-turns, in that three N—H groups (F1,D6,G5) tend to point in toward the center of the turn, rather than forming a H-bond with a C=O. Two residues, Phe1 and Arg4, form an elemental anti-parallel sheet structure, but as seen in Figure 5d, both cross-strand H-bonds are infrequently formed, presumably due to the distortion at the second, non-β-like turn (Gly5-Asp6). In particular, the dihedral angles of the Phe1 residue are consistent with an anti-parallel β-strand structure (Fig. 6a), but the Arg4 has a broader distribution in ψ.

The MD-derived structures described above are consistent with the results of our simulated annealing calculations (see below) which also converged on a cyclic structure with a Type I′ turn and a distorted, non-H-bonded turn at the Gly-Asp end. The MD results show a definite dispersion in the structures the ring can achieve, but also imply substantial barriers between them. The question remains if the structures can be discriminated or the equilibrium studied spectroscopically. This is a challenge for the QM spectral simulations.

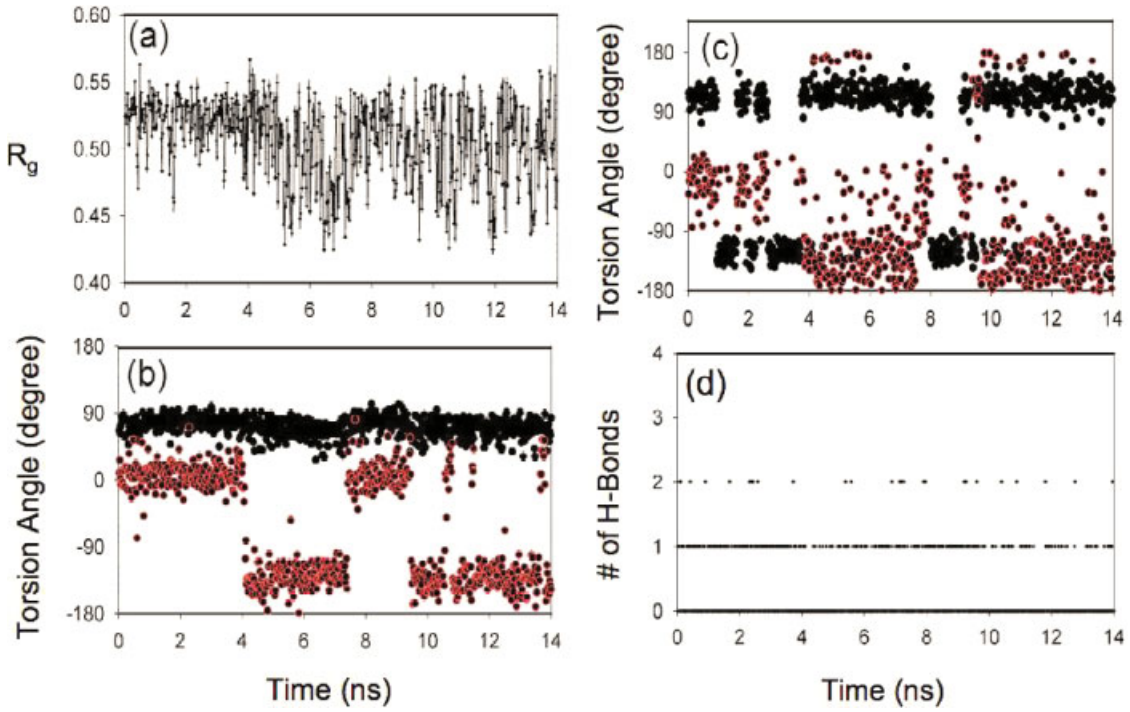

Fig. 5. Time-dependent equilibrium conformational fluctuation. MD trajectory carried out at 450 K with a total simulation time 14 nsec illustrating changes in the: (**a**) radius of gyration (R_g) of the entire peptide; (**b**) dihedral angles (ϕ_2 = black, upper, single value trace, ψ_2 = red) of the ^{D}Pro residue in the ^{D}Pro-Gly turn; (**c**) dihedral angles (ϕ_5 = black, mostly upper trace, ψ_2 = red) of the Gly5 residue in the Gly-Asp turn; and (**d**) number of H-bonds among the backbone amide groups. [Color figure can be viewed in the online issue, which is available at www.interscience.wiley.com.]

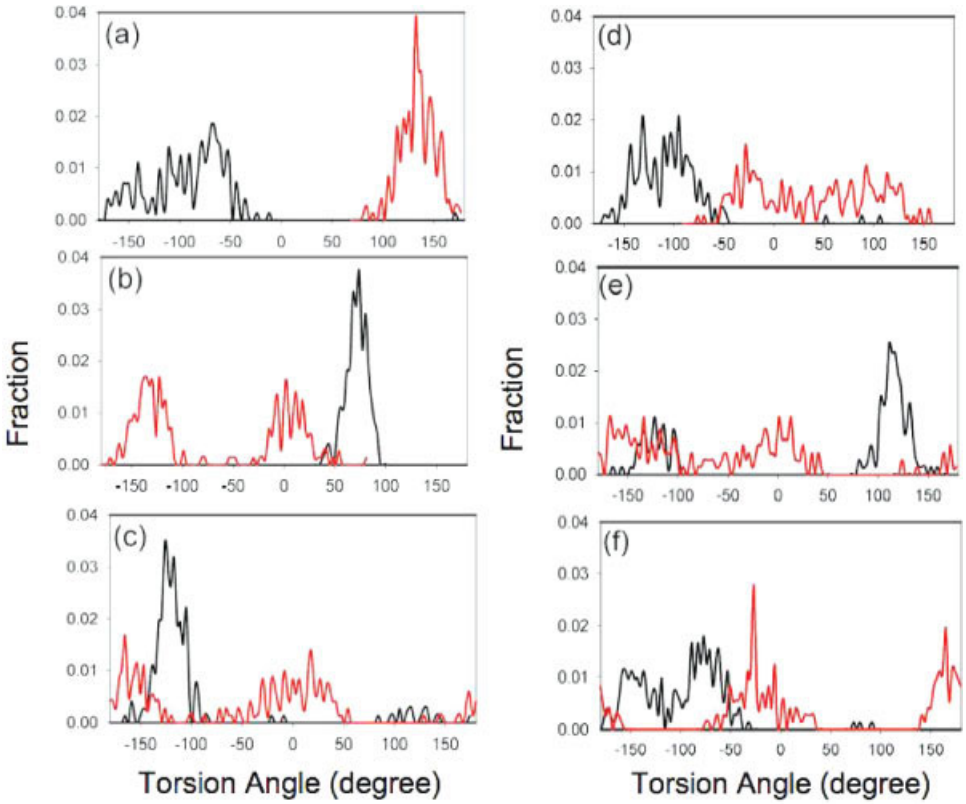

Fig. 6. Relative distribution of dihedral angles of each residue in the same 450 K trajectory as Figure 5. Values indicate fraction of population distribution in a degree. The black line is for ϕ, and the red line is for ψ. Residues are: (**a**) Phe1, $\phi \sim -70$ to -150, (**b**) DPro2, $\phi \sim 80$, (**c**) Gly3, $\phi \sim -120$, (**d**) Arg4, $\phi \sim -100$ to -130, (**e**) Gly5, $\phi \sim 120$ and -120, (**f**) Asp6, $\phi \sim -80$ and -150. [Color figure can be viewed in the online issue, which is available at www.interscience.wiley.com.]

Simulated Annealing

The conformational distributions evident in the MD runs described above indicate typical structures to select for further study. The equilibrium obtained for the peptide backbone geometry conformation by simulated annealing with the Amber99 force field was conserved at 300 K, but the side-chain conformations varied widely. The torsion angles (defined in Fig. 1) of the main cyclic peptide chain for a 1 nsec MD trajectory subsequent to the annealing had rms deviations within 9–17° of the average values as summarized in Table 2. Not surprisingly, the Gly residue moved most ($\Delta\tau \sim 15°$) while the flexibilities of the other residues were smaller, $\Delta\tau \sim 10$–$13°$; the most rigid being the proline residue. The peptide backbone flexibility appears to be moderated by the side chain characteristics. The cyclic peptide thus again resembles two Type I′ β-turns, one induced by the Pro-Gly, while the charged amino acids partially stabilize the structure by formation of intramolecular hydrogen bond bridges.

The MD trajectories were influenced by the starting geometry and the computational scheme, presumably due to the constraints of the ring, which can lock the peptide into a local minimum for a considerable time at low temperatures. High temperature simulations show that rapid transitions between Type II′ and I′ turns are possible (see Fig. 5b) if one uses a cutoff for long range interaction correc-

TABLE 2. Average torsional angles and their dispersion obtained from simulated annealing

Backbone	*F*		*P*		*G*		*R*		*G*		*D*	
Torsion[a]	ϕ_1	ψ_1	ϕ_2	ψ_2	ϕ_3	ψ_3	ϕ_4	ψ_4	ϕ_5	ψ_5	ϕ_6	ψ_6
$<\tau>$	−141	157	62	16	74	20	−134	10	168	−56	−136	−21
$<\Delta\tau>$	9	9	10	11	15	15	13	12	12	17	13	14
Sidechain	*F*		*R*				*D*					
Torsion	$\chi_{1\text{-}1}$	$\chi_{1\text{-}2}$	$\chi_{4\text{-}1}$	$\chi_{4\text{-}2}$	$\chi_{4\text{-}3}$	$\chi_{4\text{-}4}$	$\chi_{6\text{-}1}$	$\chi_{6\text{-}2}$				
$<\tau>$	−97	98	68	−175	−68	−179	−62	−84				
$<\Delta\tau>$	12	14	9	22	9	45	13	17				

[a] $<\tau>$, average torsional value; $<\Delta\tau>$, root mean square deviation.

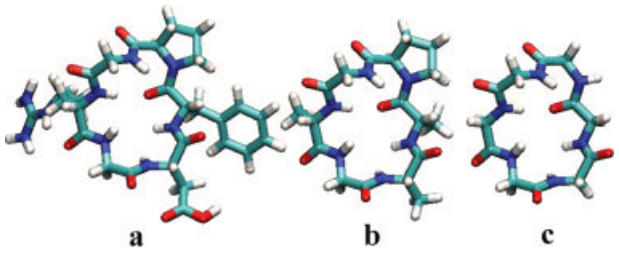

Fig. 7. Geometry of the full c(FpGRGD) peptide in a Type I′ turn form (**a**, left), its "alanine" (**b**, middle) and "all-glycine" (**c**, right) analogues taken for the spectra computations (based on the A-4 conformer of Table 2). [Color figure can be viewed in the online issue, which is available at www.interscience.wiley.com.]

tions. Simulated annealing can overcome these relatively large barriers to conformational transition, making the resulting structures a reasonable representation for the solution structure. Since we have chosen to employ ^{D}Pro-Gly to stabilize one turn, it is not surprising that the structures differ from previously determined cyclic hexapeptide NMR results. The force fields chosen for our simulations probably also contribute to the deviation.

Quantum Mechanical Spectral Modeling

For spectral modeling we randomly selected 10 MD peptide geometries (A1-10) from a 1 nsec Tinker/Amber simulation of the positively charged form. These structures all had an approximate Type I′ turn at the ^{D}Pro-Gly residues plus the distorted tight loop characteristic of the highly annealed sample. Graphical representations of a typical version of the Type I′ containing structure (A-series) are shown in Figure 7, with and without side chains. To give some idea of the consistency of the ring backbone conformation and the variation of the sidechains, we plotted an overlapped version of these 10 structures in Figure 8a. These structures were partially DFT optimized at the BPW91/6-31G** level with a COSMO representation of the solvent and with constraints along normal coordinates for modes <300 cm^{-1}.[77,78] Final torsion angles for this set are given in Table 3 (columns labeled A1–A10).

The alternate turn conformation did not occur during this short MD run, thus to provide a comparison, four Type II′ conformers (B-series) were constructed from an MD simulation of the zwitterionic state (structures B1–B4 in Table 3). Use of the MD structures with restricted COSMO optimization resulted in more separation of the cross-strand parts of the B-type ring, so that while the N—H and C=O remained directed at each other; the distances became too large for H-bonding. Thus the solvent corrected QM structure and the MD in solution structures are related in having weaker (longer) cross-strand H-bonds. If these B structures were instead fully optimized in vacuum without constraint, the H-bonds were formed, i.e. the ring tightened up on itself, and systematic changes in ϕ, ψ angles are clear. For the A structures, such a contraction is not seen, and the vacuum structures and ϕ, ψ angles are similar to the COSMO structures, which may be due to the unusual loop formed at the Gly5-Asp6 segment which cannot form an H-bond. Two examples of full minimization in vacuum are indicated as B-1_{vac} and A-4_{vac} in Table 3. As is clear from Table 3, the variation in the ϕ, ψ angles for the respective Type II′ and I′ conformations is not large among these selected conformations and we thus expect their spectra to be relatively consistent for the amide modes. Surprisingly, in Figure 8, the overlaid A structures show more variation at the ^{D}Pro-Gly Type I′ turn end than the other end, while the B structures are more closely overlapped on both ends. This is not evident in the Table 3 comparison and probably indicates a coupling of different motions to relax the molecules, which could be symptomatic of convergence to a multiple minimum. However the change between Type I′ and II′ turns, i.e. between the A and B series, is substantial and affects all of the torsion angles, indicating that change is global. The question remains as to its impact on spectra.

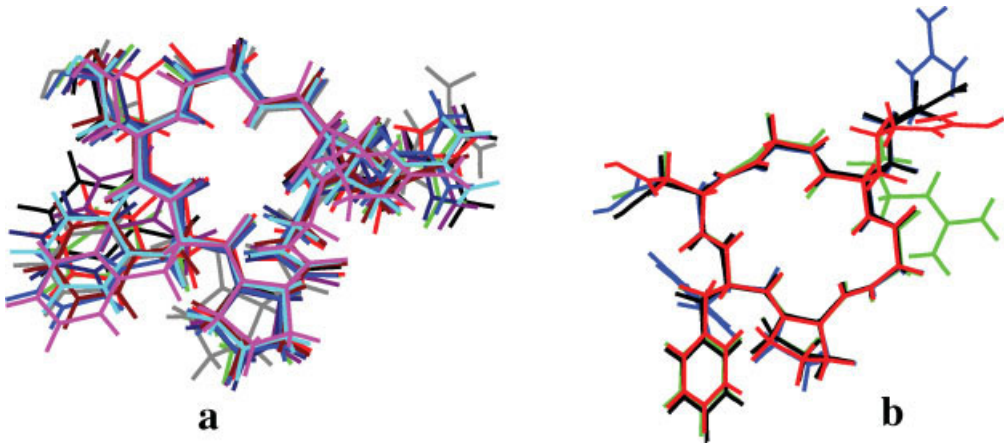

Fig. 8. For the c(FpGRGD) peptide, overlap of (**a**-left) 10 structures derived from a 1 nsec MD trajectory after simulated annealing (A1-10, Table 3) which maintain a Type I′ turn at the ^{D}Pro-Gly linkage and (**b**-right) four structures (B1-4) which have a Type II′ turn on both ends (^{D}Pro-Gly and Gly-Asp) and potential (but long) anti-parallel cross-strand H-bonds. [Color figure can be viewed in the online issue, which is available at www.interscience.wiley.com.]

TABLE 3. Torsion angles of c(FpGRGD) MD conformations selected for ab initio computations

	Type II′ turns				Type I′ turns										Vacuum	
τ	B-1	B-2	B-3	B-4	A-1	A-2	A-3	A-4	A-5	A-6	A-7	A-8	A-9	A-10	A-4$_{vac}$	B-1$_{vac}$
ϕ_1	−153	−137	−145	–154	−126	−148	−143	−139	−133	−141	−146	−144	−143	−146	−132	−113
ψ_1	130	132	159	125	165	132	163	156	170	156	160	160	153	169	152	101
ϕ_2	73	81	71	79	57	63	56	52	74	47	46	65	62	73	53	65
ψ_2	−142	−143	−151	–139	25	28	19	23	15	12	30	11	9	16	24	−107
ϕ_3	−93	−86	−85	−84	59	60	66	70	69	92	39	66	92	78	72	−109
ψ_3	−10	−22	−23	−19	13	39	39	35	16	18	60	33	37	14	33	20
ϕ_4	−143	−148	−146	–150	−124	−153	−145	−145	−138	−141	−143	−138	−168	−143	−144	−148
ψ_4	120	121	118	156	9	20	13	7	3	20	−6	10	3	−10	10	118
ϕ_5	92	103	109	82	178	173	160	−170	164	161	171	168	−179	−177	−174	70
ψ_5	−134	−144	−146	–135	−71	−73	−61	−58	−23	−51	−27	−67	−76	−47	−55	−129
ϕ_6	−111	−95	−91	–114	−132	−151	−127	−132	−153	−143	−146	−126	−132	−130	−137	−101
ψ_6	16	−12	−12	12	−27	6	−32	−22	−44	−15	−29	−28	−15	−35	−25	13

Peptide Vibrational Modes

The amide mode frequencies are sensitive to the basis set and functional approximation used. In order to evaluate the impact of this variance, and to determine an appropriate level for pursuing our various cyclic peptide computations, we arbitrarily chose a single structure and did a number of test computations varying the approximations used. For the model in Figure 7c, where all residues are substituted by Gly, but the ϕ, ψ torsional angles of A-4 in Table 3 were maintained, IR and VCD were computed at the B3LYP/6-31G**, BPW91/6-31G** and BPW91/6-311++G** levels, all with the COSMO solvent correction, and are compared in Figure 9. The relative IR intensities and VCD band shapes of the main amide bands are conserved for all levels of theory used, but their frequencies show a steady decrease for this variation of DFT methods, which is most distinct for the amide I, as expected. There are differences in the hybrid (B3LYP) functional results including a band at ~1350 cm^{-1}, but there are few IR or VCD data for comparison with these predictions especially since the side chains will dominate this region for real systems. Such considerations can be important for the Raman interpretations, which will be considered separately.

The most important characteristic, the amide I-II gap is also reduced by changing from the hybrid functional (B3LYP, where the gap is ~220 cm^{-1}) to BPW91, and even further by use of the diffuse orbitals (6-31++G**) bringing the average amide I–II separation down to ~140 cm^{-1} in (Fig. 9c), which approaches the experimental value of ~100 cm^{-1}. (It should be noted that, without inclusion of explicit solvent, we would not expect to achieve the experimental amide I-II separation value in our DFT-based simulations.[17,21,79]) The B3LYP functional contains the Hartree-Fock exchange term and is computationally somewhat slower than BPW91, which thus costs more time and offers no advantage (actually poses a disadvantage) for these amide centered modes of prime consideration in peptide IR and VCD spectra. Although the results are better, computations with the basis set containing the diffuse functions (++) are much slower than with 6-31G**, which can become prohibitive for realizing calculations with larger peptides. For example, with the cGly$_6$

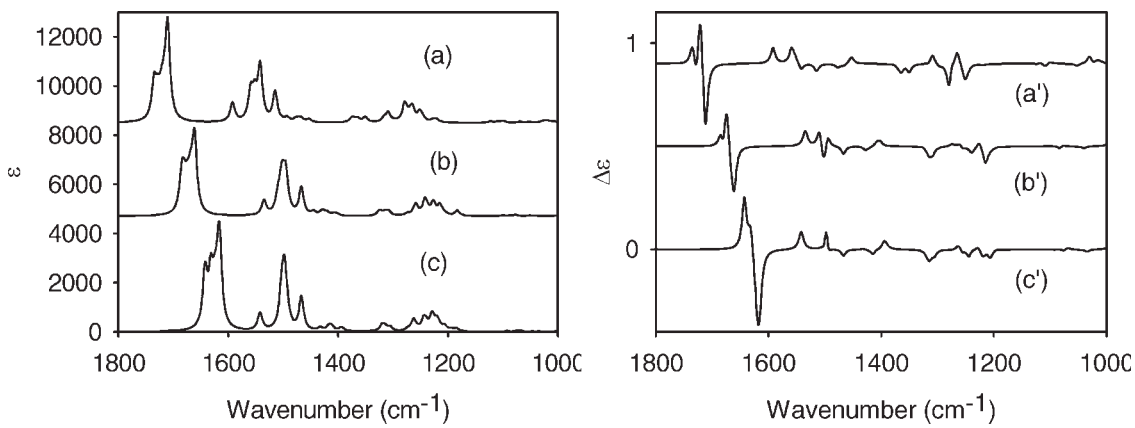

Fig. 9. Absorption (left) and VCD (right) spectra of the glycine analogue of the c(FpGRGD) peptide, cGly$_6$, simulated for the A-4 conformation at the B3LYP/COSMO/6-31G**(**a**,**a**′), BPW91/COSMO/6-31G** (**b**,**b**′), and BPW91/COSMO/6-311++G** (**c**,**c**′) levels.

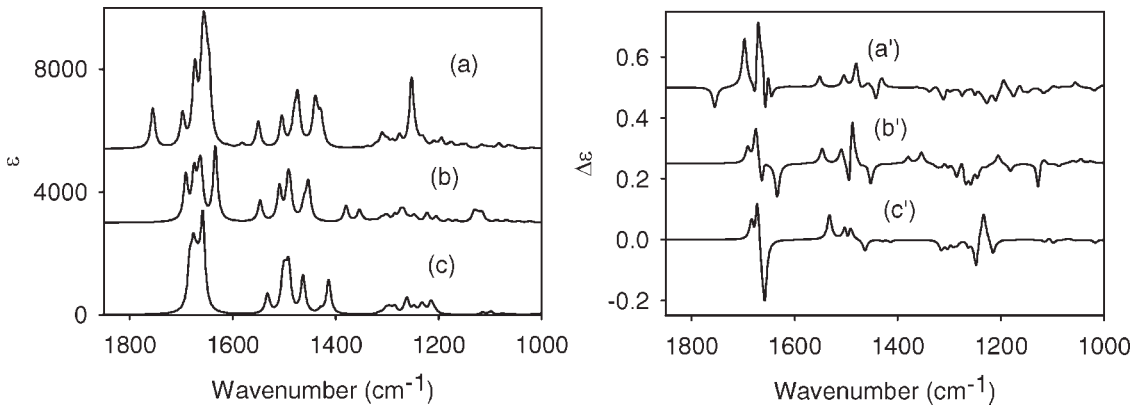

Fig. 10. Comparison of absorption (left) and VCD (right) spectra simulated for the full c(FpGRGD) peptide (**a**,**a**′) and its Ala-like, c(ApGAGA), (**b**,**b**′) and glycine, $cGly_6$, (**c**,**c**′) derivatives at the BPW91/COSMO/6-31G** level. See Figure 7 for the respective geometries. For (c,c′) the glycine CH_2 were Cα H/D exchanged to form L-d_1Gly. These results can be compared to the experimental IR and VCD data in Figure 3.

peptide, addition of diffuse functions expanded the basis set by ~50% and the time for the frequency calculation increased fivefold on our computers. Since the relative dispersion and intensity patterns found with 6-31++G** level computations are preserved in both the IR and VCD spectra with the smaller basis set, we consider the BPW91/6-31G** method to be an acceptable compromise that allows us to compute larger peptide systems and qualitatively estimate the impact of factors, such as structure, flexibility and molecular environment. Detailed mixing of local modes does vary somewhat yielding small differences in quantitative mode intensities, but a consistent qualitative pattern is maintained, which results in very similar overall IR and VCD amide I and II bandshapes. Since the general basis set dependent patterns are established, we can incorporate reasonable corrections for known frequency error systematics (diagonal FF elements), if it is desired to better align predictions with the experimentally observed dispersion. Furthermore, since it is established that the solvation effects are the main error in these computed frequencies, the virtue of basis set expansion without solvent correction is debatable.[68,79–81]

Since the BPW91/COSMO/6-31G** calculational level is seen to be most efficient for the targeted amide modes, a series of computations were then directed at modeling the impact of the side chains on the spectral shapes. We compared the DFT computed spectra of the whole peptide (including side chains) with that of its Ala analogue, c(ApGAGA),where side chains, except for Pro and Gly, were replaced by $-CH_3$, and finally with the simplified $cGly_6$ analogue (as illustrated in Figure 7). The A-4 conformation was again arbitrarily selected for these tests. We chose a specific conformer, because, while the angles in Table 1 represent the average geometry well, they cannot yield a realistic geometry since the angles were averaged independently. IR and VCD spectra computed for the three cyclic peptide analogues (Figs. 7a–7c) are thus plotted in Figures 10a–10c. Using the $cGly_6$ spectra (Figs. 10c and 10c′) as a reference, we can assess the impact of the side chain perturbations on the amide I, II, and III vibrations. Since the Gly CH_2 group scissor motion overlaps the amide II in this DFT-derived FF (vacuum), the molecule was modified to be pseudo chiral by changing the mass of the appropriate H to 2, i.e. H/D exchange yielding the L-d_1-Gly variant, thereby modifying the scissor mode into a C_α—H (and C_α—D) wag that would be normally present in these residues. The impact of this correction was relatively small, as can be seen by comparing Figures 9b and 9b′ with Figures 10c and 10c′.

For $cGly_6$, the amide I mode spectrum has the least dispersion for the three structures used in this comparison, and less than seen experimentally, having a computed maximum at 1662 cm^{-1} and shoulder at 1680 cm^{-1}. Incorporating the D-Pro residue and substituting Ala for the other three non Gly residues (Fig. 7b) leads to splitting of the amide I band and development of a distinct low frequency component (computed at ~1632 cm^{-1}) due to the Phe1-Pro2 tertiary amide.[38] The amide I modes in the Ala-based peptide are relatively uncoupled, each assignable to a specific amide from G5 on the high frequency side to p2 then A6(D),G3,and A4(R) overlapped to A1(F), resulting in a dispersion perhaps slightly larger than seen experimentally. The amide II band also showed an increase in dispersion for the Ala model (Fig. 10b), which may correlate to its mixing with Ala—CH_3 modes and the Pro—CH_2 modes that are actually calculated as partially interspersed with the lowest amide II components. Amide III modes are also affected by the side chains and couple with the methyl motion as well as the C_α—H deformation. These frequencies are dispersed between 1205–1274 cm^{-1} in this model while the C_α—H bands are mostly higher, but their IR intensities are so low as to make the spectrum in this region non-descript, just a series of poorly resolved features spread over 100 cm^{-1}.

Finally, by incorporating realistic side chains (Fig. 10a) into the computation, distinct new modes are seen corresponding to the added functional groups. However, the amide I vibrations actually become less dispersed, and the amide I modes become more mixed, each assignable to 2 or more local amides. While the C=O stretching vibration of the Asp—COOH group is computed at 1756 cm^{-1}, the highest amide I component is again dominantly G5 with p2+R4 modes forming the next feature and F1 + D6 the

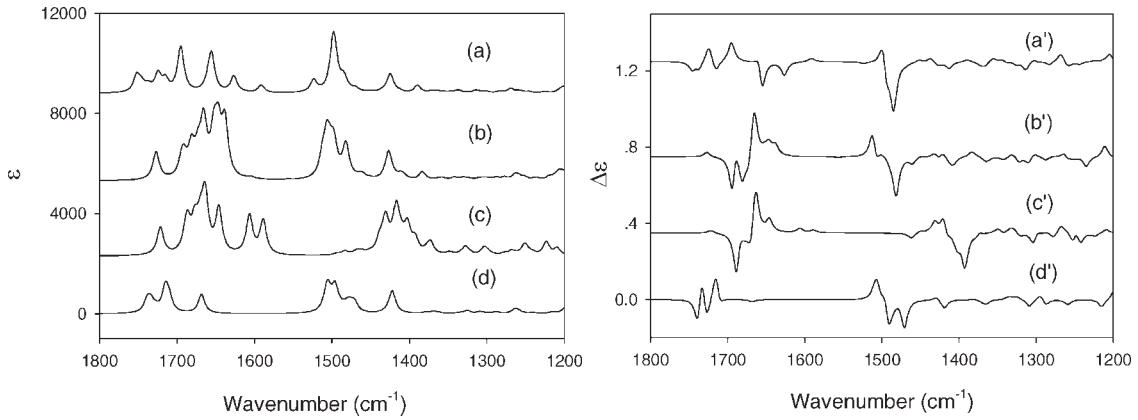

Fig. 11. Left—predicted IR spectra of the c(FpGRGD) B-1 conformer calculated with BPW91/6-31G* (**a**) in vacuum, (**b**) with COSMO, and (**c**) the full c(FpGRGD) peptide N-deuterated as compared to (**d**) for c(ApGAGA), Ala side chains only, in vacuum. Note that (a) and (d), the results in vacuum are in general alignment, if the absence of the Arg and Asp side chain contributions in c(ApGAGA) are taken in consideration. Right—the corresponding calculated VCD spectra, with (**a′–d′**) same conditions as on the left.

main peak. The Arg4 side chain vibrations are computed at ~1646–52 cm^{-1}, forming the low frequency shoulder on the amide I in Figure 10a, and these effectively push up the (Phe1-^{D}Pro2) amide frequencies. The amide II mode for the peptide with sidechains in (Fig. 10a) appears more dispersed but with the same intensity pattern as for the simplified models (Figs. 10b and 10c), even though it is highly overlapped with Phe and other $—CH_2$ based modes. Those side chain modes often have less dipole strength, so their impact on the IR is smaller making the observed pattern reflect the intensity dominance of the amide modes. Only highly dipolar side chains like Asp and Arg contribute to the IR at a level that is significant for single residues. However, the C—N stretch mode of the F1-p2 amide is computed at ~1420 cm^{-1} with relatively high dipole strength in most simulations. As noted above for the $cGly_6$, the amide III region does have most of its IR intensity from overlapping side chain modes, since it has only very weak amide vibrations. The computed full c(FpGRGD) spectrum has strong Asp side chain C—O—H bending (1253 cm^{-1}) and C—O stretching (1310 cm^{-1}) IR transitions in this region.

The VCD spectra (Figs. 10a′–10c′) differ more between the various side chain representations. However, some common patterns can be recognized, such as the dominant amide I negative couplet, distorted to a (+,+,−) pattern from high to low frequency for these A-type conformers. The lower negative band is stretched out due to the Phe1-Pro2 amide shift down in frequency for the Ala model (Fig. 10b′) and is further distorted by addition of the Arg4 overlap in the full side chain calculations (Fig. 10a′). The main difference in the amide I is that the overall positive couplet VCD which clearly dominates the spectra for the Gly and Ala models is obscured in the full calculation, where it apparently loses a negative component due to band overlap. In VCD simulations the chiral contributions of Arg4, Asp6, and Phe1 will be computationally overestimated, since in solution their side chains will sample many conformations, but these calculations necessarily select out just one of them. This plus the fact that they are also calculated to lie high in wavenumber (in both relative and absolute senses) means they interfere in the computational analysis of the amide I VCD spectrum. While the overall amide VCD pattern can still be determined from the full peptide calculations it does not adequately resemble the experimental one for the amide I.

The amide II VCD has more variation with the side chain approximation used, perhaps because amide II motion can be coupled to the methyl C-H bending modes, but remains net positive, while the amide III region has many broadly dispersed bands but is net negative. Either of these might agree with the experiment, but the data are too broad and weak to be certain. Dependence of the IR and VCD spectra on the side chains is often ignored, normally replacing them with methyls or hydrogens for QM spectral simulation.[12,38,82,83] Such an approach works well for homopeptides or for periodic peptide structures, such as sheets or helices, where the perturbations are uniform, thus leading to an overall shift of the spectrum maintaining relative relationships. Variable side chains can cause difficulty in modeling irregular cyclopeptide spectra,[40,66] but with careful assignment, their impact can be taken into account, since they mainly shift the amide frequencies, or serve to disperse the amide character among nearby modes, rather than change its nature or chirality.

Solvent Correction Model Comparison

After having assessed the role of the side chains we compared models for the effect of the solvent on the vibrational spectra. Fundamentally in all cases where we compare the same molecules with and without COSMO correction for solvent effects, the COSMO amide I results are shifted down in frequency and the dispersion is compressed as compared to vacuum (contrast Figs. 11a and 11b). That added dispersion (~150 cm^{-1}) in vacuum is accompanied by (at least partial) reversion to localized oscillator modes, which includes decoupling the Arg side chain modes from the amide I when the side chains are represented. (For the B-1 conformer, Arg modes are com-

puted at ~1655 cm^{-1} and 1695 cm^{-1} partially interspersed with the amide modes in vacuum but are lower in frequency and less dispersed using COSMO correction. In A-4, the relationship is different in detail but qualitatively the same, COSMO being lower than in vacuum, but there resulting in Arg side chain vibrations overlapping amide modes in both cases.) A similar decoupling, at least partially, of the amide I modes occurs on H/D exchange of the amide to yield the amide I′ modes, as can be seen in Figures 11b and 11c. While the dispersion does not change very much on *N*-deuteration, the Arg side chain modes shift down by ~50 cm^{-1}, and the amide pattern clarifies. This is commonly the situation that would be seen in peptides dissolved in D_2O.

To visualize these solvent effects, we changed our focus structure from that of the previous figures and plotted in Figure 11 the computed IR and VCD spectra for the B-1 conformer for c(FpGRGD) with all side chains included in (a) in vacuom and with COSMO, both (b) protonated and (c) *N*-deuterated and below that plotted (d) the computed spectra for the all Ala, c(ApGAGA), version (but again in vacuum) for the same ring geometry. With these computations for the B-ring geometry (two Type II′ turns), we can see some regularity. The highest mode is again the Asp—COOH, followed by the amide I modes whose highest component is the Pro amide, followed by mixtures of the D6, G5, and R4 amides with increasing intensity to the maximum intensity amide mode which is centered on the G3 amide, and finally a weaker F1 amide is shifted down in frequency (due to the Phe-^{D}Pro tertiary amide bond). Overlapping the F1 amide I are the Arg side chain modes which shift further down on deuteration and (partly) in vacuum, as noted above. Amide II modes in the B structures are more tightly clustered than for the A series resulting in more intensity for the overlapped cluster. This is particularly evident in the in vacuom representation, where amide II modes are often predicted to have anomalously high intensity without solvent correction.[21] To lower frequency is a distinct intense F1-p2 C—N stretch, predicted at ~1420 cm^{-1}.

This shift to a representation of the B conformers, in contrast to Figures 9 and 10, was chosen to show the differences in spectra for the two forms which is especially evident in the VCD. Here the dominant pattern seen is a positive amide I couplet, with negative VCD for the lower intensity, higher frequency p2 mode and positive for the intense G3 mode. The other modes also contribute, and with increased mixing tend to have opposing signs, resulting in added couplet (or oscillating) bands, but maintaining a positive couplet overall pattern. The Ala representation for the B-1 conformer in fact results in an alternating sign pattern for the amide I modes (Fig. 11d′) that is in qualitative agreement with the experimental pattern seen in D_2O. This underlying oscillation has a tendency to result in two high frequency negative components being apparent in the VCD, much as seen in TFE experimentally, when the computed dispersion is contracted in the COSMO version for the full peptide. Another facet of this B-series conformation is that the Asp—COOH mode is less separated from the amide I than for the A series, but this characteristic is quite dependent on method. Clustering of the amide II modes seems to result in a negative couplet pattern with the lower frequency negative component being dominant, and quite intense, which does not fit the experimental pattern. The amide II mode is likely to be affected by H-bonding to the solvent, which will vary considerably for different residues. The F1-p2 C—N stretch is also predicted to be negative in this conformation.

DISCUSSION

This study of a model cyclic peptide demonstrates the chirality that develops for a sequence with an averaged set of constrained conformations, as measured with VCD. The VCD spectra of amide I bands have no local character and result from the coupling of locally achiral groups in a chiral conformation. The constraint persists through conformational averaging due to the relative weighting of favored structures. Thus the important issue for interpretation of spectra in terms of conformation is proper modeling of this coupling. Here we showed that the peptide can be adequately represented by its backbone if one keeps in mind the necessary corrections that will be imposed by the side chains, such as spectral overlap and shifting of the base frequencies. This is most easily done if Gly and Pro residues, which are the most distinct vibrational variants, are kept as explicit components of the structure and if other residues are represented as L-Ala, with the proper chirality.

There are certainly solvent effects on the spectra, as can be seen by comparing our IR and VCD data for the cyclic peptide in TFE and water (even more so in DMSO, data not shown). However, the results are qualitatively consistent. This fits the MD results which show that the amide backbone does not change much unless one uses a very high temperature trajectory. The qualitative sign pattern of the VCD transitions is preserved in both spectra. The computed patterns for the B-series in vacuom and with COSMO mostly reflect the observed amide I spectra and actually are somewhat better predicted with the COSMO on the full c(FpGRGD) peptide than the minimal (Ala-based) side-chain simulation. But the qualitative agreement for the amide I is apparent in both levels of computation, while that for the amide II is not. The qualitative success of the Ala prediction arises because the side chains do not contribute much to the amide I VCD pattern, but they do shift the frequencies, much as solvation does, and in this case they distort the low frequency side (due to Arg mode overlap). Use of VCD predicted for just a single structure means that this shift arises from a perturbation due to a fixed, arbitrary stereochemical relationship, whereas the sidechains in solution are highly flexible. Substituting Ala in the prediction means such effects, while ignored, are also effectively averaged. None-the-less the frequency impact remains and one must be aware of it to compensate in the analysis. As we have established, solvation effects can be compensated in VCD analyses by knowing the general effects and either shifting the mode frequencies or just compensating for them in analysis of the

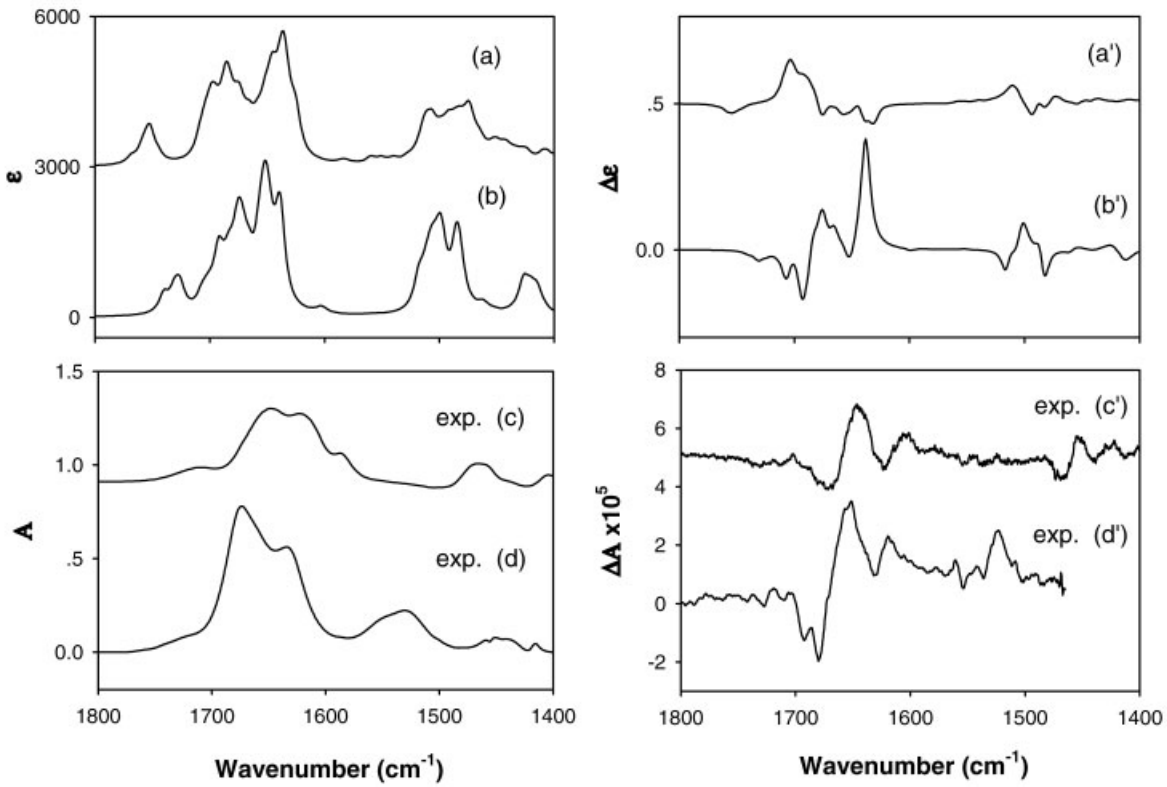

Fig. 12. Comparison of the average IR (left) and VCD (right) spectra for the (**a**) A1-10 Type I′ series and (**b**) B1-4 Type II′ series of computed spectra with the respective experimental spectra in (**c**) D_2O and (**d**) TFE OH.

spectra. The same should be true of flexible side-chain effects. If those effects are tracked by simulation resulting in establishment of behavior patterns, the simpler calculations can lead one to a useful conformational interpretation. The Arg effect is also minimized by N—D substitution which shifts those modes down in wavenumber and reduces overlap with the amide I modes.

Comparison with Experiment

All the spectra we calculated have a dispersed amide I mode typically exhibiting two main overlapped features whose components to lower energy are generally more intense, which reflects the ATR spectral patterns (see Fig. 4) but does not fit the solution results (Fig. 3) as well. The computed spectra of both the A and B series have this pattern, but computationally the A pattern is more dependent on Arg modes being mixed with the amide I. In the A series case, the overall pattern could be seen as two overlapped bands. For the c(FpGRGD) peptide in vacuum or when deuterated, as well as for the Ala version, the original pattern persists despite the increased dispersion and the shift of the Arg modes.

In the experimental spectra, the amide II modes are weak and broad at best, which is consistent with the A-series IR absorbance but not predicted by the B-series pattern. Even with COSMO the amide I–II separation is too large. In our experience, only use of explicit solvent representation in the DFT and a larger basis set including diffuse functions (as suggested above with our Gly_6 comparative calculations in Fig. 9) can overcome this deficiency.[21,66,79] Lower frequency bands do not discriminate between the two structural models, due to low IR intensity; consequently, the IR is seen to be conformationally indeterminant. There are variations in the different conformations found in the MD trajectory, so choosing just one (as done in the above examples using just B-1 or A-4 conformers) biases the result. Averaging over the trajectory should help even out the specific deviations, but this requires computing spectra for individual structural variants. A comparison of the experimental data and the computed average for the selected A and B-forms noted in Table 3 are shown in Figure 12.

VCD does show a distinct difference between the conformers. The B-series has a dominant amide I positive couplet, although when these four spectra are averaged, an anomalously high intensity positive VCD band appears on the low frequency side of the amide I mode. The match of specific modes is far from perfect, and the lower frequency components of the amide I are underrepresented, but the overall sign pattern seen experimentally suggests that the B-conformers must make a major contribution to the conformational mix, and this would in turn indicate that Type

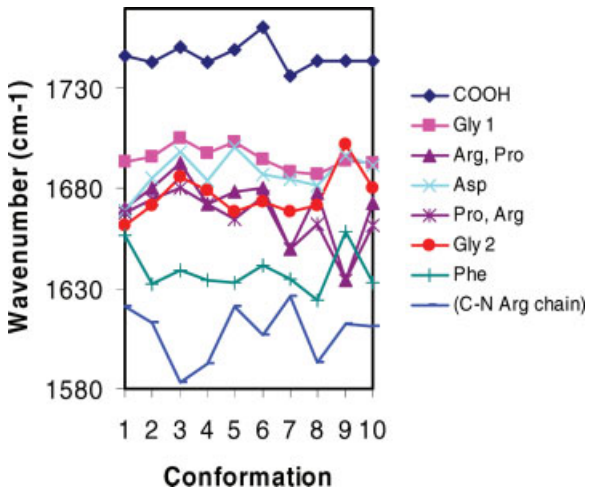

Fig. 13. Calculated amide C=O (and Arg side chain) stretching mode frequencies for 10 A-type conformations of the cyclic peptide selected during the MD run. [Color figure can be viewed in the online issue, which is available at www.interscience.wiley.com.]

II′ turns are important in this cyclic peptide structure. The apparent mis-match in the amide II region noted above for the B-1 conformer is improved by averaging over the four B conformers, making that mode also supportive of this structural assignment. Clearly the only way to find agreement between experiment and theory here is to average computed spectra for many structures. Since our selection of them from the MD trajectory is intrinsically arbitrary, definitive structural analysis is premature, but qualitative conformational determination seems possible. Slight variation (full minimization) of the modeling of the A structures revealed that the VCD pattern is very sensitive to minor geometry variations within one class of the β-turns. Particularly, the increased flexibility of the peptide chain in the vicinity of the glycine residues, observed also for other model oligopeptides,[26] can have a significant impact on the resultant spectral shape.

Going beyond the amide modes, the Asp—COOH mode is experimentally seen as a shoulder on the high frequency side of the amide I, more like the B-series predictions, and the Arg bands are low frequency shoulders (in D_2O, but perhaps higher in organic solvents). Without the COSMO correction, the predicted Asp band would be even more unrealistically high in frequency. The VCD corresponding to this band is very weak and functionally indeterminate in sign. The Arg modes are more difficult to sort out, but apparently are just below the amide I in D_2O and have little VCD contribution. The sum of these observations is that the Ala model offers a representation better suited to assigning the amide modes than do the full side-chain calculations, but that the COSMO corrections remain helpful. This assumption must be used with care. Clearly for peptides containing Arg, there is an upward shift of the F1-p2 frequency, so the Arg has an impact on the amide I, serving to reduce its dispersion. Further, for sorting out these modes, it is very useful to have calculated the spectra at different levels of approximation. By this we mean with varying contributions from the side chains. For a single DFT calculation, the side chain contributions could be shifted by isotopic substitution, which while somewhat difficult (or at least expensive) to realize experimentally, is straightforward to simulate computationally by just changing the masses and reusing the original FF.

We have further attempted to use the empirical corrections for solvent effects that we have previously reported to further correct the spectra for solvent effects (not shown).[81,84,85] Unfortunately, although the corrections did improve the frequencies of the amide I modes, they did not lead to an improved interpretation of the data.

Effect of Molecular Flexibility

Finally, we explore the effect of the conformational flexibility of the peptide on the spectra. This effect, perhaps surprisingly, appears smaller than that of the solvent, at least in the adopted models. For example, for the 10 A-conformations selected during the MD run, amide I frequencies oscillate ($\sim\pm 15\ cm^{-1}$) around average values and the arginine side chain vibration exhibits slightly bigger sensitivity to the conformations. This of course is consistent with the small changes in backbone geometry (see ϕ, ψ values in Table 2), whose impact on amide I frequencies can be seen in Figure 13. There similar normal modes are tracked in different conformers with the aid of the S-vector overlaps, $P_{A_I B_J} = |\sum_{\lambda=1\ldots NAT,\ \alpha=1,3} S^{I,A}_{\lambda\alpha} S^{J,B}_{\lambda\alpha}|$, where $S^{I,A}_{\lambda\alpha}$, is the S-matrix vector for mode I, atom λ and coordinate α in conformation A.[66] The overlaps achieve maximum values (= 1) for identical modes. Occasional change of the transition ordering suggests that the averaging could change the signs of VCD features, which does occur for close lying modes as can be seen in the variations of central frequencies for the 10 conformers, and even sometimes for further separated ones, see conformers A-7 and A-9 as shown in Figure 13. Similar plots could be made for the B-conformers, but they are much more similar and consequently do not offer such exchanges in ordering.

ACKNOWLEDGMENT

We wish to thank Ms. Martha Juban in the LSU Protein Facility for assistance with the peptide synthesis.

LITERATURE CITED

1. Aamouche A, Devlin FJ, Stephens PJ. Determination of the absolute configuration of 1-(2-methylnaphtyl)methyl sulfoxide by vibrational circular dichroism spectroscopy. J Org Chem 2001;66:3671–3677.
2. Beenken WJD, Lischka H. Spectral broadening and diffusion by torsional motion in biphenyl. J Chem Phys 2005;123:144311.
3. Williams RW, Dunker AK. Determination of the secondary structure of proteins from the amide I band of the laser raman spectrum. J Mol Biol 1981;152:783–813.
4. Keiderling TA. Protein and peptide secondary structure and conformational determination with vibrational circular dichroism. Curr Opin Chem Biol 2002;6:682–688.
5. Keiderling TA. Peptide and protein conformational studies with vibrational circular dichroism and related spectroscopies. In: Berova N, Nakanishi K, Woody RW, editors. Circular dichroism: principles and applications, 2nd ed. New York: Wiley-VCH; 2000. p 621–666.

6. Barron LD, Zhu F, Hecht L. Raman optical activity: an incisive probe of chirality and of biomolecular structure and behaviour. Vib Spectrosc 2006;42:15–24.
7. Decatur SM, Antonic J. Isotope-edited FTIR spectroscopy of helical peptides. J Am Chem Soc 1999;121:11914–11915.
8. Barber-Armstrong W, Donaldson T, Wijesooriya H, Silva RAGD, Decatur SM. Empirical relationships between isotope-edited IR spectra and helix geometry in model peptides. J Am Chem Soc 2004;126:2339–2345.
9. Huang R, Kubelka J, Barber-Armstrong W, Silva RAGD, Decatur SM, Keiderling TA. Nature of vibrational coupling in helical peptides: an isotopic labeling study. J Am Chem Soc 2004;126:2346–2354.
10. Silva RAGD, Barber-Armstrong W, Decatur SM. The organization and assembly of a beta-sheet formed by a prion peptide in solution: an isotope-edited FTIR study. J Am Chem Soc 2003;125:13674–13675.
11. Silva RAGD, Nguyen JY, Decatur SM. Probing the effect of side chains on the conformaiton and stability of helical peptides via isotope-edited infrared spectroscopy. Biochemistry 2002;51:15296–15303.
12. Kubelka J, Silva RAGD, Bouř P, Decatur SM, Keiderling TA. Chirality in peptide vibrations. Ab Initio computational studies of length, solvation, hydrogen bond, dipole coupling and isotope effects on vibrational CD. In: Hicks JM, editor. Chirality: physical chemistry. ACS Symposium Series. Vol. 810. Washington DC: American Chemical Society; 2002. p 50–64.
13. Kubelka J, Keiderling TA. The anomalous infrared amide I intensity distribution in ^{13}C isotopically labeled peptide β-sheets comes from extended, multiple-stranded structurres. An ab initio study. J Am Chem Soc 2001;123:6142–6150.
14. Silva RAGD, Kubelka J, Decatur SM, Bouř P, Keiderling TA. Site-specific conformational determination in thermal unfolding studies of helical peptides using vibrational circular dichroism with isotopic substitution. Proc Natl Acad Sci USA 2000;97:8318–8323.
15. Decatur SM. IR spectroscopy of isotope-labeled helical peptides: probing the effect of *N*-acetylation on helix stability. Biopolymers 2000;54:180–185.
16. Starzyk A, Barber-Armstrong W, Sridharan M, Decatur SM. Spectroscopic evidence for backbone desolvation of helical peptides by 2,2,2-trifluoroethanol: an isotope edited IR study. Biochemistry 2005;44:369–376.
17. Bouř P, Keiderling TA. Ab initio modeling of amide I coupling in antiparallel beta-sheets and the effect of 13C isotopic labeling on infrared spectra. J Phys Chem B 2005;109:5348–5357.
18. Decatur SM. Elucidation of residue-level structure and dynamics of polypeptides via isotope-edited infrared spectroscopy. Acc Chem Res 2006;39:169–175.
19. Sreerama N, Woody RW. Protein secondary structure from circular dichroism spectroscopy—combining variable selection principle and cluster analyses with neural network, ridge regression and self-consistent methods. J Mol Biol 1994;242:497–507.
20. Venyaminov SY, Yang JT. Determination of protein secondary structure. In: Fasman GD, editor. Circular dichroism and the conformational analysis of biomolecules. New York: Plenum; 1996. p 69–107.
21. Kubelka J, Huang R, Keiderling TA. Solvent effects on IR and VCD spectra of helical peptides: DFT-based static spectral simulations with explicit water. J Phys Chem B 2005;109:8231–8243.
22. Hollosi M, Majer ZS, Ronai AZ, Magyar A, Medzihradszy K, Holly S, Perczel A, Fasman GD. CD and Fourier transform IR spectroscopic studies of peptides. II. Detection of beta turns in linear peptides. Biopolymers 1994;34:177–185.
23. Vass E, Kurz M, Konat RK, Hollosi M. FTIR and CD spectroscopic studies on cyclic penta- and hexa-peptides. Detailed examination of hydrogen bonding in (beta)- and (gamma)- turns determined by NMR. Spectrochim Acta 1998;54:773–786.
24. Perczel A, Hollosi M. Turns. In: Fasman GD, editor. Circular dichroism and the conformational analysis of biomolecules. New York: Plenum; 1996. p 285.
25. Vass E, Hollosi M, Besson F, Buchet R. Vibrational spectroscopic detection of beta- and gamma-turns in synthetic and natural peptides and proteins. Chem Rev 2003;103:1917–1954.
26. Kim J, Kapitán J, Lakhani A, Bouř P, Keiderling TA. Tight β-turns in peptides. DFT-based study of infrared absorption and vibrational circular dichroism for various conformers including solvent effects. Theor Chem Acc 2008;119:81–97.
27. Krishnan B, Szymanska A, Gierasch LM. Site-specific fluorescent labeling of poly-histidine sequences using a metal-chelating cysteine. Chem Biol Drug Des 2007;69:31–40.
28. Roy RS, Gopi HN, Raghothama S, Karle IL, Balaram P. Hybrid peptide hairpins containing alpha- and omega-amino acids: conformational analysis of decapeptides with unsubstituted beta-, gamma-, and delta-residues at positions 3 and 8. Chem A Eur J 2006;12:3295–3302.
29. Mahalakshmi R, Raghothama S, Balaram P. NMR analysis of aromatic interactions in designed peptide beta-hairpins. J Am Chem Soc 2006;128:1125–1138.
30. Syud FA, Stanger HE, Mortell HS, Espinosa JF, Fisk JD, Fry CG, Gellman SH. Influence of strand number on antiparallel beta-sheet stability in designed three- and four-stranded beta-sheets. J Mol Biol 2003;326:553–568.
31. Karle I, Gopi HN, Balaram P. Infinite pleated beta-sheet formed by the beta-hairpin Boc-beta-Phe-beta-Phe-D-Pro-Gly-beta-Phe-beta-Phe-OMe. Proc Natl Acad Sci USA 2002;99:5160–5164.
32. Setnička V, Huang R, Thomas CL, Etienne MA, Kubelka J, Hammer RP, Keiderling TA. IR study of cross-strand coupling in a beta-hairpin peptide using isotopic labels. J Am Chem Soc 2005;127:4992–4993.
33. Ramirez-Alvarado M, Kortemme T, Blanco FJ, Serrano L. Beta-hairpin and beta-sheet formation in designed linear peptides. Bioorg Med Chem 1999;7:93–103.
34. Lacroix E, Kortemme T, Lopez de la Paz M, Serrano L. The design of linear peptides that fold as monomeric β-sheet structures. Curr Opin Struct Biol 1999;9:487–493.
35. Kortemme T, Ramirez-Alvarado M, Serrano L. Design of a 20-amino acid, three-stranded beta-sheet protein. Science 1998;281:253–256.
36. Hilario J, Kubelka J, Syud FA, Gellman SH, Keiderling TA. Spectroscopic characterization of selected β-sheet hairpin models. Biospectroscopy 2002;67:233–236.
37. Espinosa JF, Syud FA, Gellman SH. Analysis of the factors that stabilize a designed two-stranded antiparallel beta-sheet. Protein Sci 2002;11:1492–1505.
38. Hilario J, Kubelka J, Keiderling TA. Optical spectroscopic investigations of model beta-sheet hairpins in aqueous solution. J Am Chem Soc 2003;125:7562–7574.
39. Koepf EK, Petrassi HM, Sudol M, Kelly JW. WW: an isolated three-stranded antiparallel beta-sheet domain that unfolds and refolds reversibly; evidence for a structured hydrophobic cluster in urea and GdnHCl and a disordered thermal unfolded state. Protein Sci 1999;8: 841–853.
40. Bouř P, Keiderling TA. Vibrational spectral simulation for peptides of mixed secondary structure: method comparisons with the Trpzip model hairpin. J Phys Chem B 2005;109:23687–23697.
41. Bouř P, Buděšínský M, Špirko V, Kapitán J, Šebestík J, Sychrovský V. A complete set of NMR chemical shifts and spin-spin coupling constants for L-alanyl-L-alanine zwitterion and analysis of its conformational behavior. J Am Chem Soc 2005;127:17079–17089.
42. Yasui SC, Pančoška P, Dukor RK, Keiderling TA, Renugopalakrishnan V, Glimcher MJ, Clark RC. Conformational transitions of phosvitin with pH variation. Vibrational circular dichroism study. J Biol Chem 1990;265:3780–3788.
43. Mantsch HH, Perczel A, Hollosi M, Fasman GD. Characterization of β-turns in cyclic hexapeptides in solution by Fourier transform IR spectroscopy. Biopolymers 1993;33:201–207.
44. Vass E, Lang E, Samu J, Majer Z, Kajtar-Peredy M, Mak M, Radics I, Hollosi M. Vibrational spectrocopic detection of H-bonded β- and γ-turns in cyclic peptides and glycopeptides. J Mol Struct 1998;440:59–71.
45. Cochran AG, Tong RT, Starovasnik MA, Park EJ, McDowell RS, Theaker JE, Skelton NJ. Minimal peptides scaffold for beta-turn display: optimizing a strand position in disulfide-cyclized beta-hairpins. J Am Chem Soc 2001;123:625–632.
46. Ravi A, Balaram P. Cyclic peptide disulfides. Consecutive beta-turn conformation of a synthetic model peptide corresponding to the active site of thioredoxin. Biochi Biophys Acta 1983;745:301–309.

47. García-Echeverría C, Siligardi G, Mascagni P, Gibbons W, Giralt E, Pons M. Conformational analysis of two cyclic disulfide peptides. Biopolymers 1991;31:835–843.
48. Russell SJ, Blandl T, Skelton NJ, Cochran AG. Stability of cyclic beta-hairpins: asymmetric contributions from side chains of a hydrogen-bonded cross-strand residue pair. J Am Chem Soc 2003;125:388–395.
49. Ravi A, Prasad BVV, Balaram P. Cyclic peptide disulfides—solution and solid-state conformation of Boc-Cys-Pro-Aib-Cys-S-S-bridge-NH-Me, a disulfide-bridged peptide helix. J Am Chem Soc 1983;105:105–109.
50. Xie P, Zhou QW, Diem M. Conformational studies of β-turns in cyclic peptides by vibrational CD. J Am Chem Soc 1995;117:9502–9508.
51. Gilon C, Mang C, Lohof E, Friedler A, Kessler H. In: Goodman M, Felix A, Moroder L, Toniolo C, editors. Synthesis of peptides and peptidomimetics, Vol. E 22 b. New York: Georg Thieme Verlag Stuttgart; 2003. p 461.
52. Perczel A, Hollosi M, Foxman BM, Fasman GD. Conformational analysis of pseudocyclic hexapeptides based on quantitative circular dichroism (CD), NOE, and X-ray data. The pure CD spectra of Type I and Type II beta-turns. J Am Chem Soc 1991;113:9772–9784.
53. Matter H, Kessler H. Structures, dynamics, and biological activities of 15 cyclic hexapeptide analogs of the alpha-amylase inhibitor tendamistat (HOE 467) in solution. J Am Chem Soc 1995;117:3347–3359.
54. Gardner RR, Liang GB, Gellman SH. Beta-turn and beta-hairpin mimicry with tetrasubstituted alkenes. J Am Chem Soc 1999;121:1806–1816.
55. Kaul R, Angeles AR, Jager M, Powers ET, Kelly JW. Incorporating beta-turns and a turn mimetic out of context in loop 1 of the WW domain affords cooperatively folded beta-sheets. J Am Chem Soc 2001;123:5206–5212.
56. Syud FA, Stanger HE, Gellman SH. Interstrand side chain-side chain interactions in a designed β-hairpin: significance of both lateral and diagonal pairings. J Am Chem Soc 2001;123:8667–8677.
57. Cochran AG, Skelton NJ, Starovasnik MA. Tryptophan zippers: stable, monomeric beta-hairpins. Proc Natl Acad Sci USA 2001;98:5578–5583.
58. Chatterjee J, Mierke D, Kessler H. *N*-methylated cyclic pentaalanine peptides as template structures. J Am Chem Soc 2006;128:15164–15172.
59. Kessler H, Bats JW, Griesinger C, Koll S, Will M, Wagner K. Peptide conformations. 46. Conformational analysis of a superpotent cytoprotective cyclic somatostatin analog. J Am Chem Soc 1988;110:1033–1049.
60. Gierasch LM, Deber CM, Madison V, Niu CH, Blout ER. Conformations of (X-L-Pro-Y)2 cyclic hexapeptides. Preferred beta-turn conformers and implications for beta turns in proteins. Biochemistry 1981;20:4730–4738.
61. Bean JW, Kopple KD, Peishoff CE. Conformational analysis of cyclic hexapeptides containing the D-Pro-L-Pro sequence to fix beta-turn positions. J Am Chem Soc 1992;114:5328–5334.
62. Muller G, Gurrath M, Kurz M, Kessler H. BetaVI turns in peptides and proteins: a model peptide mimicry. Protein Struct 1993;15:235–251.
63. Kubelka J, Keiderling TA. Differentiation of β-sheet forming structures: ab initio based simulations of IR absorption and vibrational CD for model peptide and protein β-sheets. J Am Chem Soc 2001;123:12048–12058.
64. Huang R, Setnička V, Etienne MA, Kim J, Kubelka J, Hammer RP, Keiderling TA. Cross-strand coupling of a β-hairpin peptide stabilized with an Aib-Gly turn using isotope-edited IR spectroscopy. J Am Chem Soc 2007;129:13592–13603.
65. Bouř P, Sopková J, Bednárová L, Maloň P, Keiderling TA. Transfer of molecular property tensors in Cartesian coordinates: a new algorithm for simulation of vibrational spectra. J Comput Chem 1997;18:646–659.
66. Kim J, Huang R, Kubelka J, Bouř P, Keiderling TA. Simulation of infrared spectra for beta-hairpin peptides stabilized by an Aib-Gly turn sequence: correlation between conformational fluctuation and vibrational coupling. J Phys Chem B 2006;110:23590–23602.
67. Kapitán J, Baumruk V, Kopecký VJ, Bouř P. Demonstration of the ring conformation in polyproline by the Raman optical activity. J Am Chem Soc 2006;128:2438–2443.
68. Bouř P. Computations of the Raman optical activity via the sum-over-states expansions. J Comput Chem 2001;22:426–435.
69. Barany G, Albericio F. A 3-dimensional orthogonal protection scheme for solid-phase peptide-synthesis under mild conditions. J Am Chem Soc 1985;107:4936–4942.
70. Kates SA, Sole NA, Johnson CR, Hudson D, Barany G, Albericio F. A novel, convenient, 3-dimensional orthogonal strategy for solid-phase synthesis of cyclic-peptides. Tetrahedron Lett 1993;34:1549–1552.
71. Albericio F, Cases M, Alsina J, Triolo SA, Carpino LA, Kates SA. On the use of PyAOP, a phosphonium salt derived from HOAt, in solid-phase peptide synthesis. Tetrahedron Lett 1997;38:4853–4856.
72. Keiderling TA, Kubelka J, Hilario J. Vibrational circular dichroism of biopolymers. Summary of methods and applications. In: Braiman M, Gregoriou V, editors. Vibrational spectroscopy of polymers and biological systems. Boca Raton: CRC Press; 2006. p 253–324.
73. Ponder JW. Tinker, software tools for molecular design v. 4.2. 2004; Available at: http://dasher.wustl.edu/tinker/.
74. Pearlman DA, Case DA, Caldwell JW, Ross WS, Cheatham TE, Debolt S, Ferguson DM, Seibel G, Kollman PA. AMBER, a package of computer progeams for applying molecular mechanics, normal mode analysis, molecular dynamics and free energy calculations to simulate the structural and energetic properties of molecules. Comp Phys Commun 1995;91:1–41.
75. Jorgensen WL, Chandrasekhar J, Madura JD. Comparison of simple potential fuctions for simulating liquid water. J Chem Phys 1983;79:926–935.
76. Frisch MJ, Trucks GW, Schlegel HB, Scuseria GE, Robb MA, Cheeseman JR, Montgomery JA, Vreven T, Kudin KN, Burant JC, Dapprich S, Millam JM, Daniels AD, Kudin KN, Strain MC, Farkas O, Tomasi J, Barone V, Cossi M, Cammi R, Mennucci B, Pomelli C, Adamo C, Clifford S, Ochterski J, Petersson GA, Ayala PY, Cui Q, Morokuma K, Salvador P, Dannenberg JJ, Malick DK, Rabuck AD, Raghavachari K, Foresman JB, Cioslowski J, Ortiz JV, Baboul AG, Stefanov BB, Liu G, Liashenko A, Piskorz P, Komaromi I, Gomperts R, Martin RL, Fox DJ, Keith T, Al-Laham MA, Peng CY, Nanayakkara A, Challacombe M, Gill PMW, Johnson B, Chen W, Wong MW, Andres JL, Gonzalez C, Head-Gordon M, Replogie ES, Pople. Gaussian 03, Revision C .02. Wallingford CT: Gaussian, Inc.; 2004.
77. Bouř P, Keiderling TA. Partial optimization of molecular geometry in normal coordinates and use as a tool for simulation of vibrational spectra. J Chem Phys 2002;117:4126–4132.
78. Bouř P. Convergence properties of the normal mode optimization and its combination with molecular geometry constraints. Collect Czech Chem Commun 2005;70:1315–1340.
79. Kubelka J, Keiderling TA. Ab initio calculation of amide carbonyl stretch vibrational frequencies in solution with modified basis sets. 1. *N*-methyl acetamide. J Phys Chem A 2001;105:10922–10928.
80. Bouř P, Michalík D, Kapitán J. Empirical solvent correction for multiple amide group vibrational modes. J Chem Phys 2005;122:144501.
81. Bouř P. On the influence of the water electrostatic field on the amide group vibrational frequencies. J Chem Phys 2004;121:7545–7548.
82. Kubelka J, Silva RAGD, Keiderling TA. Discrimination between peptide 3_{10}- and α-helices. Theoretical analysis of the impact of α-methyl substitution on experimental spectra. J Am Chem Soc 2002;124:5325–5332.
83. Bouř P, Kubelka J, Keiderling TA. Quantum mechanical models of peptide helices and their vibrational spectra. Biopolymers 2002;65:45–69.
84. Bouř P, Keiderling TA. Empirical modeling of the peptide amide I band IR intensity in water solution. J Chem Phys 2003;119:11253–11262.
85. Yang S, Cho M. IR spectra of *N*-methylacetamide in water predicted by combined quantum mechanical/molecular mechanical molecular dynamics simulations. J Chem Phys 2005;123:134503.

Highly Enantioselective Organocatalytic Conjugate Addition of Nitromethane to Benzylidene Acetones

GÁBOR SZÁNTÓ,[1]* PETRA BOMBICZ,[2] ALAJOS GRÜN,[1,3] AND ISTVÁN KÁDAS[1]

[1]*Department of Organic Chemistry and Technology, Budapest University of Technology and Economics, Budapest, Hungary*
[2]*Department of X-ray Diffraction, Institute of Structural Chemistry, Chemical Research Center, Hungarian Academy of Sciences, Budapest, Hungary*
[3]*Research Group of Organic Chemical Technology, Hungarian Academy of Sciences, Budapest University of Technology and Economics, Budapest, Hungary*

ABSTRACT Six active 4-aryl-5-nitro-pentan-2-ones were synthesized enantioselectively from the corresponding 5-aryl-butenones by asymmetric Michael addition of nitromethane using an imidazolidine-type enantioselective organocatalyst. The ee ratio of the products were between 67 and 100%, determined by HPLC with Chiracel OD. Molecular and crystal structure of 3,4-methylenedioxy-phenyl-5-nitro-pentan-2-one has been studied by single crystal X-ray diffraction. *Chirality 20:1120–1126, 2008.*

KEY WORDS: organocatalyst; Michael addition; enantioselectivity; crystal structure; enantiomer excess

INTRODUCTION

The asymmetric conjugate addition is one of the most powerful bond-forming reactions to construct enantioenriched, highly functionalized carbon skeletons for total synthesis of natural and biological active compounds (for recent reviews see Refs. 1–6). Its importance is evident by considering that a Michael addition can represent the initiating step of more complex inter- and intramolecular tandem processes. The utility of this reaction is due, in part, to the broad spectrum of nucleophilic donors and electrophilic acceptors that can be employed in the transformation (see Refs. 7–12 for general reviews).

Nitroalkanes are particularly valuable source of stabilized carbanions, as the strongly electron withdrawing nature of the nitro group (pK_a $MeNO_2 < 10$) facilitates generation of the nitronate anion under mild conditions[13] and are suitable nucleophilic donors in Michael addition. Additionally, the nitro group is versatile functional group that can be converted to ketone (Nef reaction), reduced to amine, etc.[14] Although the γ-nitro-ketones which are the products of the conjugate addition of nitroalkanes to enones easily can be synthesized alternatively by the Michael addition of ketones to the corresponding nitroolefins, generally, the first route is preferable because of the better stability of enones than nitro olefins specially for large-scale synthesis.

In the last two decades, a variety of catalyst systems have been developed for the asymmetric conjugate addition of nitroalkanes and in particular nitromethane to chalcones. These include chiral crown ethers,[15–20] chiral Lewis acids,[21] phase transfer catalyst derived from cinchona alkaloids,[22–24] and cinchona alkaloid-derived thiourea catalysts,[25] and aluminum-salen complex.[26]

These methods, however, have good stereoselectivity either only in case of chalcones, or for other enones needed complicate bidentate catalysts (sometimes with metal-complexes) which mostly can be synthesized on lengthy, multistep routes.

Simple metal-free organocatalysts[27–31] having chiral pyrrolidine or imidazolidine skeleton, easily made from such common L-amino acids as L-proline or L-phenylalanine, developed in the last years by several groups,[32–38] seem to be the most successful enantioselective catalysts for a range of reactions. Proline (**1**) has been first used as its rubidium salt in the addition of nitroalkanes to enones with moderate to good enantioselectivities (41–84%).[39–42] The use of proline with amine additives for addition to enones was investigated by Hanessian and Pham[43] than Ley and coworkers improved the method using tetrazole derivatives of proline, in every case with piperazin derivatives as base additives, reaching 72–89% ee.[44–49]

Macmillan and coworkers have introduced the chiral imidazolidinone type catalyst **2** and **3** (Scheme 1), readily available from L-phenylalanine, methylamine, and acetone or pivalaldehyde, respectively,[50–55] but these catalysts have not been used in conjugate addition of nitroalkanes to enones.

Jørgensen and coworkers developed the simple chiral imidazolidine catalyst **4** (Scheme 1), which without any additives gave 34–86% enantioselectivities for conjugate addition of nitroalkanes to simple enones, for example, in case of nitrometane and benzylidene acetone the ee was

Contract grant sponsor: Hungarian Research Foundation; Contract grant number: T 034772.
Contract grant sponsor: National Office for Research and Technology; Contract grant number: MU-00338/2003
*Correspondence to: Gábor Szántó, Department of Organic Chemistry and Technology, Budapest University of Technology and Economics, 1521 Budapest, PO Box 91, Hungary. E-mail: gszanto@mail.bme.hu
Received for publication 27 November 2007; Accepted 22 February 2008
DOI: 10.1002/chir.20567
Published online 27 May 2008 in Wiley InterScience (www.interscience.wiley.com).

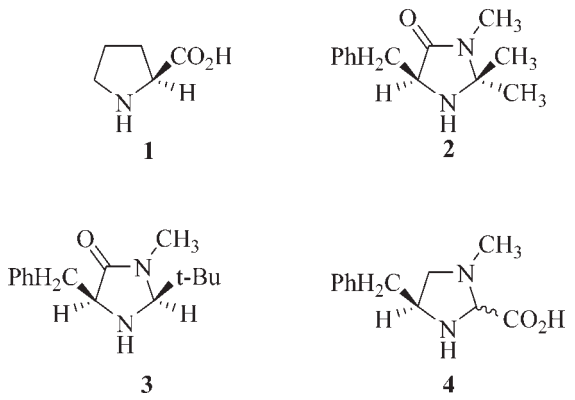

Scheme 1. The metal-free organocatalysts **1–4**.

73%.[56] Their catalyst gave good enantioselectivities in other type Michael reactions, too, for example, they developed a method for the synthesis of the anticoagulant warfarin and analogues.[57–60]

In our ongoing studies directing toward the synthesis of phenantridine alkaloids and their analogues we extended the application of the Jørgensen catalyst **4** for the enantioselective Michael addition of nitromethane to hydroxy, alkoxy, and methylenedioxy substituted benzylidene acetones **5a–f** and have reached in every case similar or better enantioselectivites than can be reached with the unsubstituted enone.[56] The synthesized six active 4-aryl-5-nitropentan-2-ones **6a–f** are suitable intermediates for our alkaloid synthesis (Scheme 2).

4-Aryl-5-nitro-pentan-2-ones as chiral compounds can be synthesized by Michael addition either from the prochiral 4-arylbutenones and nitromethane or from the prochiral β-nitrostyrenes and acetone. Both reactions are known for a long time using unsubstituted[61–69] or substituted[61–71] phenyl derivatives. Although it is obvious that both reactions can be performed enantioselectively; they were not described in the literature until recently.

The alternative way of preparation of the *R*-enantiomer of this compound **(6a)** from nitrostyrene and acetone[26,44–49,72] with bidentate or mixture catalysts was reported recently. The *R*-enantiomer of 4-(4-methoxyphenyl)-5-nitro-pentan-2-one was also synthesized,[26,72] anyhow none of other substituted active nitropentanones were prepared and published until now.

EXPERIMENTAL

General Procedures

Melting points were determined using a Büchi 510 apparatus and are uncorrected. The optical rotation was measured with the help of a Perkin-Elmer 241 polarimeter at 20°C. NMR spectra were obtained in $CDCl_3$ on a Brucker DRX-500 instrument. Mass spectra were obtained on a Varian MAT312 instrument. Column chromatography was carried out using 70–230 mesh silica gel (Merck). The ee values were determined by HPLC (detector: JASCO UV-1575, pump: PU-1580).

Preparation of Starting Compounds 5a–f

Aryl-butenones **5a–f**[73–79] were synthesized from the corresponding aromatic aldehydes and acetone in diluted NaOH solution,[80] and were purified by distillation in reduced pressure or in some cases by crystallization from methanol.

General Method for Preparation of Michael Adducts 6a–f

The corresponding aryl-butenone (10.5 mmol) was dissolved in nitromethane (20 ml, 369.3 mmol) and catalyst **4** (2.1 mmol) was added to the solution. Then, the reaction mixture was stirred for 168 h in room temperature. The solvent was evaporated and the product was isolated by FC on silica gel using ether-pentane (1:1) as eluant.

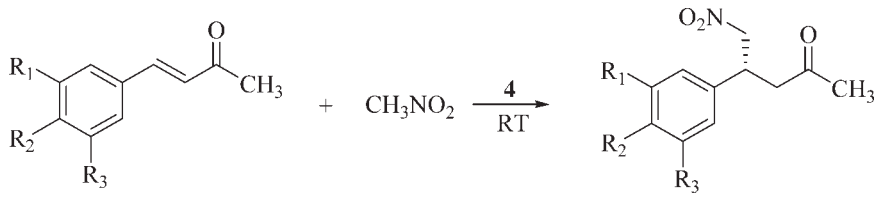

5a-f **6a-f**

Compound	R^1	R^2	R^3
a	CH_3O	H	H
b	CH_3O	CH_3O	H
c	CH_3O	CH_3O	CH_3O
d		$-OCH_2O-$	H
e	CH_3O	HO	H
f	CH_3O	$PHCH_2O$	H

Scheme 2. The enantioselective synthesis of the 4-aryl-5-nitropentan-2-ones.

4-(3-Methoxyphenyl)-5-nitro-pentane-2-one (6a)

Yield: 68%; $[\alpha]_D^{20}$: −1.2° (*c* = 1, $CHCl_3$), 74% ee. The enantiomer excess was determined by HPLC analysis with Chiralcel OD (Daicel Chemical Industries); eluent: hexane:isopropanol = 8:2; flow rate: 1 ml/min; detection: UV 286 nm; temperature: 20°C. Oil. ^{1}H NMR (500 MHz, $CDCl_3$): δ 2.05 (s, 3H, 1-CH_3), 2.83 (d, 2H, 3-CH_2), 3.72 (s, 3H, OCH_3); 3.91 (kv, 1H, 4-CH), 4.50-4.62 (m, 2H, 5-CH_2), 6.67–6.74 (m, 3H, Ar-CH), 7.17 (t, 1H, Ar-CH); ^{13}C-NMR (75 MHz, $CDCl_3$): δ 30.6, 39.3, 46.3, 55.4, 79.6, 113.1, 113.8, 119.7, 130.3, 140.6, 160.2, 205.5; HRMS calcd for $C_{12}H_{15}NO_4$ (M^+) 237.1001, found 237.1004.

4-(3,4-Dimethoxyphenyl)-5-nitro-pentane-2-one (6b)

Yield: 49%; $[\alpha]_D^{20}$: −1.2° (c = 1, $CHCl_3$), 82% ee. The enantiomer excess was determined by HPLC analysis with Chiralcel OD (Daicel Chemical Industries); eluent: hexane:isopropanol = 8:2; flow rate: 1 ml/min; detection: UV 286 nm; temperature: 5°C, mp. 76–78°C, *Reichert* and *Posemann* gave 90–91°C (from methanol) for the pure racemic **6b**.[70,71] ^{1}H NMR (500 MHz, $CDCl_3$): δ 2.05 (s, 3H, 1-CH_3), 2.82 (d, 2H, 3-CH_2), 3.78 (s, 3H, OCH_3), 3.80 (s, 3H, OCH_3), 3.88 (kv, 1H, 4-CH), 4.51–4.59 (m, 2H, 5-CH_2), 6.65-6.75 (m, 3H, Ar-CH); ^{13}C NMR (75 MHz, $CDCl_3$): δ 30.6, 39.0, 46.5, 56.1, 56.2, 79.9, 111.1, 111.7, 119.4, 131.5, 148.8, 149.4, 205.7; HRMS calcd for $C_{13}H_{17}NO_5$ (M^+) 267.1107, found 267.1113.

4-(3,4,5-Trimethoxyphenyl)-5-nitro-pentane-2-one (6c)

Yield: 72%; $[\alpha]_D^{20}$: −1.3° (*c* = 1, $CHCl_3$), 80% ee. The enantiomer excess was determined by HPLC analysis with Chiralcel OD (Daicel Chemical Industries); eluent: hexane:isopropanol = 8:2; flow rate: 1 ml/min; detection: UV 210 nm; temperature: 20°C, mp. 70–72°C. ^{1}H-NMR (500 MHz, $CDCl_3$): δ 2.07 (s, 3H, 1-CH_3), 2.82 (d, 2H, 3-CH_2), 3.74 (s, 3H, OCH_3), 3.77 (s, 6H, 2xOCH_3), 3.87 (kv, 1H, 4-CH), 4.50–4.63 (m, 2H, 5-CH_2), 6.34 (s, 2H, Ar-CH); ^{13}C NMR (75 MHz, $CDCl_3$): δ 30.6, 39.5, 46.5, 56.4, 61.0, 79.6, 104.7, 134.7, 137.8, 153.7, 205.5; HRMS calcd for $C_{14}H_{19}NO_6$ (M^+) 297.1212, found 297.1206.

4-(3,4-Methylenedioxy-phenyl)-5-nitro-pentane-2-one (6d)

Yield: 52%; $[\alpha]_D^{20}$: −2.1° (*c* = 1, $CHCl_3$), 100% ee. The enantiomer excess was determined by HPLC analysis with Chiralcel OD (Daicel Chemical Industries); eluent: hexane:isopropanol = 8:2; flow rate: 1 ml/min; detection: UV 286 nm; temperature: 5°C, mp. 100–102°C, *Walker* gave 96.5–98.5°C (from methanol) for the pure racemic **6d.**[61–69] ^{1}H NMR (500 MHz, $CDCl_3$): δ 2.05 (s, 3H, 1-CH_3), 2.79 (d, 2H, 3-CH_2), 3.85 (kv, 1H, 4-CH), 4.43–4.60 (m, 2H, 5-CH_2), 5.87 (s, 2H, O—CH_2—O), 6.59–6.69 (m, 3H, Ar-CH); ^{13}C NMR (75 MHz, $CDCl_3$): δ 30.6, 39.1, 46.5, 79.9, 101.5, 107.9, 108.9, 120.9, 132.7, 147.4, 148.4, 205.5; HRMS calcd for $C_{12}H_{13}NO_5$ (M^+) 251.0794, found 251.0801.

4-(4-Hidroxy-3-methoxyphenyl)-5-nitro-pentane-2-one (6e)

Yield: 55%; $[\alpha]_D^{20}$: −0.5° (*c* = 1, $CHCl_3$), 67% ee. The enantiomer excess was determined by HPLC analysis with Chiralpak AD (Daicel Chemical Industries); eluent: hexane:isopropanol = 9:1; flow rate: 1 ml/min; detection: UV 224 nm; temperature: 5°C, mp. 66–68°C. ^{1}H NMR (500 MHz, $CDCl_3$): δ 2.13 (s, 3H, 1-CH_3), 2.89 (d, 2H, 3-CH_2), 3.89 (s, 3H, OCH_3), 3.94 (kv, 1H, 4-CH), 4.53–4.69 (m, 2H, 5-CH_2), 5.59 (s, 1H, OH), 6.69-6.88 (m, 3H, Ar-CH); ^{13}C NMR (75 MHz, $CDCl_3$): δ 30.7, 39.1, 46.6, 56.2, 80.0, 110.7, 115.0, 119.8, 130.9, 145.5, 146.9, 205.7; HRMS calcd for $C_{12}H_{15}NO_5$ (M^+) 253.0950, found 253.0955.

4-(4-Benzyloxy-3-methoxyphenyl)-5-nitro-pentane-2-one (6f)

Yield: 55%; $[\alpha]_D^{20}$: +1.5° (*c* = 1, $CHCl_3$), 71% ee. The enantiomer excess was determined by HPLC analysis with Chiralcel OD (Daicel Chemical Industries); eluent: hexane:isopropanol = 8:2; flow rate: 1 ml/min; detection: UV 210 nm; temperature: 30°C, 91–93°C. ^{1}H-NMR (500 MHz, $CDCl_3$): δ 2.03 (s, 3H, 1-CH_3), 2.79 (d, 2H, 3-CH_2), 3.80 (s, 3H, OCH_3), 3.85 (kv, 1H, 4-CH), 4.45-4.60 (m, 2H, 5-CH_2), 5.03 (s, 2H, O—CH_2—Ph), 6.58-6.76 (m, 3H, Ar-CH), 7.18–7.35 (m, 5H, Ar-CH); ^{13}C-NMR (75 MHz, $CDCl_3$): δ 30.5, 38.8, 46.4, 56.2, 71.1, 79.7, 111.6, 114.3, 119.2, 127.3, 127.9, 128.6, 131.9, 137.0, 147.9, 150.0, 205.5; HRMS calcd for $C_{19}H_{21}NO_5$ (M^+) 343.1420, found 343.1427.

Single Crystal X-Ray Diffraction

The crystals of 3,4-methylenedioxy-phenyl-5-nitro-pentan-2-one are colorless platelets. The size of the crystal selected for single crystal X-ray diffraction measurement is 0.40 × 0.35 × 0.10 mm. Formula is $C_{12}H_{13}NO_5$, formula weight is 251.23, F(000) = 528. It crystallizes in the orthorhombic crystal system, space group $P2_12_12_1$. The cell dimensions are a = 5.6021(11) Å, b = 7.7172(13) Å, c = 27.479(6) Å, α = β = γ = 90°, V = 1188.0(4)A^3, Z = 4, D_x = 1.405 mgm^{-3}. A crystal was mounted on a loop in oil. The diffraction measurement was performed at T = 101(1) K. Intensity data were collected on a Rigaku R-Axis Rapid diffractometer (graphite monochromator; Mo-Kα radiation, λ = 0.71073 Å) in the range 3.0 ≤ θ ≤ 27.4°. Cell parameters were determined by least-squares of the setting angles of all collected reflections. A total of 45124 reflections were collected of which 2704 were unique [R(int) = 0.094, R(σ) = 0.0409]; 2576 reflections were >2σ(I). Completeness to 2θ = 0.998. An empirical absorption correction was applied to the data, μ = 0.111 mm^{-1}, the minimum and maximum transmission factors were 0.9571 and 0.9890. The structure was solved by direct methods with SHELXS97.[81] Neutral atomic scattering factors and anomalous scattering factors are taken from International Tables for X-ray Crystallography.[82] Anisotropic full-matrix least-squares refinement with SHELXL97[83,84] on F^2 for all nonhydrogen atoms yielded R1 = 0.0344 and wR2 = 0.0891 for 2576 [I > 2σ(I)], R1 = 0.0364 and wR2 = 0.0906 for all (2704) intensity data (goodness-of-fit = 1.032; the maximum and mean shift/esd 0.000 and 0.000).

TABLE 1. The yield, optical properties and melting point of the substituted phenyl-nitropentanones (6a–f) synthesized by asymmetric Michael addition of nitromethane to 4-aryl-but-3-en-2-ones 5a–f

Compound	R^1	R^2	R^3	Yield[a] (%)	ee[b] (%)	Optical rotation[c]	Mp (°C)
6a	CH_3O	H	H	68	74	−1.2°	– (oil)
6b	CH_3O	CH_3O	H	49	82	−1.2°	76–78
6c	CH_3O	CH_3O	CH_3O	72	80	−1.3°	70–72
6d	—OCH_2O—		H	52	100	−2.1°	100–102
6e	CH_3O	OH	H	55	67	−0.5°	66–68
6f	CH_3O	$PhCH_2O$	H	55	71	+1.5°	91–93

[a]Yields were determined after isolated by FC on silica gel.
[b]Enantiomer excess were determined with chiral HPLC on Chiracel OD.
[c]Conditions: 20°C, solvent: $CHCl_3$, $c = 1$.

The Flack x parameter[87] is −0.7(9), what is poorly reliable because of the lack of atoms with substantial anomalous scattering.

Number of parameters = 164. The maximum and minimum residual electron density in the final difference map was 0.274 and −0.207 e A^{-3}. The weighting scheme applied was

$$w = 1/\left[\sigma^2(F_0^2) + (0.0472P)^2 + 0.2884P\right], \quad \text{where} \quad P = (F_o^2 + 2F_c^2)/3$$

Hydrogen atomic positions were located in difference maps. Hydrogen atoms were included in structure factor calculations but they were not refined. The isotropic displacement parameters of the hydrogen atoms were approximated from the U(eq) value of the atom they were bonded.

Crystallographic data (excluding structure factors) for the above crystal structure have been deposited with the Cambridge Crystallographic Data Centre as supplementary publication number CCDC 642785

RESULTS AND DISCUSSION

The synthesis of six new active 4-aryl-5-nitro-pentan-2-ones (**6a–f**) is reported by asymmetric Michael addition of nitromethane to the appropriate 4-aryl-butenones **5a–f** using Jørgensen's enantioselective organocatalyst **4**. The organocatalyst was carefully chosen based on the reported high enantioselectivity achieved with the unsubstituted phenyl-nitropentanone.

Organocatalyst **4** proved to be highly effective in our experiments: synthesis of all substituted phenyl-nitropentanones **6a–f** gave similar or better ee-ratio than the unsubstituted reactant.

The yield of the syntheses, enantiomer excess, optical rotation and melting point of the substituted phenyl-nitropentanones (**6a–f**) synthesized by asymmetric Michael addition of nitromethane to 4-aryl-but-3-en-2-ones **5a–f** are listed in Table 1. Considering the ee ratio of the products with increasing number of methoxy substituents higher enantioselectivity can be observed. Practically enantiopure product was obtained in case of the 3,4-methylenedioxy substituted derivative (**6d**). Presence of the free phenolic hydroxy or benzyloxy groups yielded lower ee ratio.

The asymmetric Michael addition reactions were carried out in nitromethane as solvent at ambient temperature using 20 mol % of catalyst **4**. The reaction time was 168 h in each case. After evaporation of the nitromethane in reduced pressure, the crude reaction mixture was purified

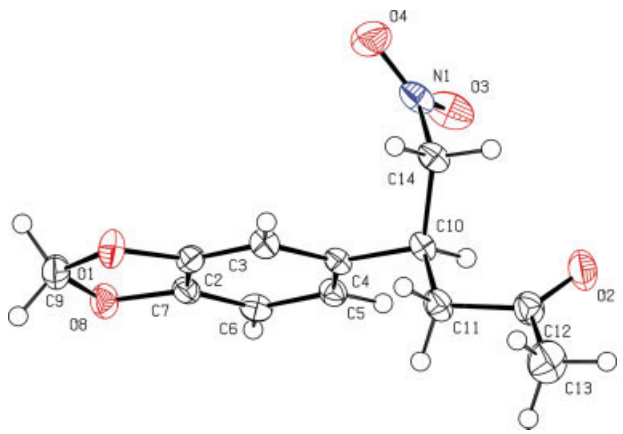

Fig. 1. The molecular structure[85] of **6d**. The displacement parameters are shown on 50% probability level. The chiral center is C10. Heteroatoms are shaded. [Color figure can be viewed in the online issue, which is available at www.interscience.wiley.com.]

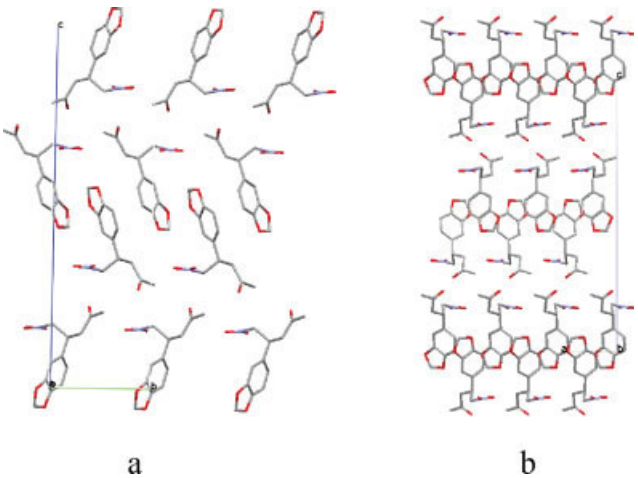

Fig. 2. The packing arrangement[86] in the crystal of **6d**. Hydrogen atoms are omitted for clarity. (**a**), View from the crystallographic axis *a* (**b**), View from the crystallographic axis *b*. [Color figure can be viewed in the online issue, which is available at www.interscience.wiley.com.]

TABLE 2. Hydrogen bonds in the crystal structure

Atoms	D-H	H···A	D···A	D-H···A	Symmetry operation
Intermolecular week H-bonds					
C9 – H9A .. O4	0.990	2.550	3.209(2)	124.00	$1/2 + x, -1/2 - y, -z$
C14 – H14A .. O3	0.990	2.510	3.450(2)	159.00	$1 + x, y, z$
C14 – H14B .. O2	0.990	2.520	3.143(2)	121.00	$-x, -1/2 + y, 1/2 - z$
Weak intramolecular H-bond stabilising the molecular conformation					
C14 – H14B .. O2	0.990	2.460	3.071(2)	119.00	–

by FC on silica gel. The residue was used directly for ee determination by HPLC on Chiracel OD. The products crystallized slowly in most cases. It was used for determination of optical rotation and melting point, and for analytical measurements, NMR and MS spectroscopy. Synthesis of **6d** resulted in practically enantiopure product.

Single crystal X-ray diffraction measurement was performed with 3,4-methylenedioxy-phenyl-5-nitro-pentan-2-one **6d**. There is one molecule in the asymmetric unit of the crystal structure (see Fig. 1).

6d crystallizes in the orthorhombic chiral space group $P2_12_12_1$ (No. 19). The quality of the crystal was good, the measurement was performed at low temperature (101 K), the structure is ordered, it was possible to locate all hydrogen atoms in the difference Fourier maps, and to refine the structure to $R = 0.0344$ for $I > 2\sigma$. The molecules are arranged by alternating layers of the constituents (see Fig. 2), the ring and the alkyl substituent moieties, respectively, along the crystallographic axis *c*, in the crystallographic *ab* plane.

There are no strong intermolecular interactions in the crystal structure owing to the lack of donors, although several potential acceptors are present. There are three weak C—H···O type intermolecular interactions among the molecules (Table 2). One intramolecular weak C—H···O hydrogen bond contributes to the stability of the molecular conformation, its graph set descriptor[87] is S6. There are no attractive π···π interactions, but two C—H···π interactions are found to the aromatic ring: C6-H6···π (2.63 Å, 3.3592(17) Å, 134°) and C9-H9B···π (2.81 Å, 3.4993(18) Å, 127°). The unit cell contains no residual solvent accessible void. The determined (S) absolute configuration[88] by single crystal X-ray diffraction is hardly reliable because of the lack of strong anomalous scattering centers.

CONCLUSION

The imidazolidine-type enantioselective organocatalyst **4** was utilized for synthesizing six new active 4-aryl-5-nitropentan-2-ones. According to the results, the catalyst proved to be very effective: the ee ratios of the products were between 67 and 100%. Single crystal X-ray diffraction was applied to determine the molecular and crystal structure having weak CH···π interactions only.

In summary, the application of the catalyst **4** can be highly utilized towards the synthesis of phenantridine alkaloids.

LITERATURE CITED

1. Rossiter BE, Swingle NM. Asymmetric conjugate addition. Chem Rev 1992;92:771–806.
2. Leonard J, Diez-Barra E, Merino S. Control of asymmetry through conjugate addition reactions. Eur J Org Chem 1998:2051–2061.
3. Tomioka K, Nagaoka Y. Comprehensive asymmetric catalaysis. In: Jacobsen EN, Pfaltz A, Yamamoto H, editors. Berlin: Springer; 1999. vol. 3, p 1105–1120.
4. Yamaguchi M. Comprehensive asymmtric catalaysis. In: Jacobsen EN, Pfaltz A, Yamamoto H, editors. Berlin: Springer; 1999. vol. 3, p 1121–1139.
5. Sibi MP, Manyem S. Enantioselective conjugate additions. Tetrahedron 2000;56:8033–8061.
6. Krause N, Hoffman-Röder A. Recent advances in catalytic enantioselective Michael additions. Synthesis 2001:171–196.
7. Perlmutter P. Conjugate addition reactions in organic synthesis. In: Baldwin JE, Magnus PD, editors. Oxford: Pergamon Press; 1992.
8. Jung ME. Comprehensive organic synthesis. In: Trost BM, editor. Pergamon Press, Oxford; 1991, vol. 4, p 1–67.
9. Tietze LF. Chem Rev Domino reactions in organic synthesis. Chem Rev 1996;96:115–136
10. Bunce RA. Recent advances in the use of tandem reactions for organic-synthesis. Tetrahedron 1995;51:13103–13159.
11. Tietze LF, Beifuss U. Sequential transformations in organic-chemistry–A synthetic strategy with a future. Angew Chem Int Ed Engl 1993; 32:131–163.
12. Posner GH. Multicomponent one-pot annulations forming 3 to 6 bonds. Chem Rev 1986;86:831–844.
13. Ono N. The nitro group in organic synthesis. New York: Wiley-VCH; 2001.
14. Ballini R, Bosica G, Fiorini D, Palmieri A, Petrini M. Conjugate additions of nitroalkanes to electron-poor alkenes: recent results. Chem Rev 2005;105:933–971.
15. Bakó P, Bajor Z, Tőke L. Synthesis of novel chiral crown ethers derived from D-glucose and their application to an enantioselective Michael reaction. J Chem Soc Perkin Trans 1999;1:3651–3655.
16. Bakó P, Kiss T, Tőke L. Chiral azacrown ethers derived from D-glucose as catalysts for enantioselective Michael addition. Tetrahedron Lett 1997;38:7259–7262.
17. Bakó P, Novák T, Ludányi K, Pete B, Tőke L, Keglevich G. D-glucose-based azacrown ethers with a phosphonoalkyl side chain: application as enantioselective phase transfer catalysts. Tetrahedron Asymmetry 1999;10:2373–2380.
18. Bakó P, Szöllősy A, Bombicz P, Tőke L. Asymmetric C-C bond forming reactions by chiral crown catalysts; Darzens condensation and nitroalkane addition to the double bond. Synlett 1997:291–298.
19. Bakó T, Bakó P, Keglevich G, Báthori N, Czugler M, Tatai J, Novák T, Parlagh G, Tőke L. Enantioselective Michael addition of 2-nitropropane to chalcone analogues catalyzed by chiral azacrown ethers based on alpha-D-glucose and D-mannitol. Tetrahedron Asymmetry 2003;14: 1917–1923.
20. Bakó T, Bakó P, Szöllősy A, Czugler M, Keglevich G, Tőke L. Enantioselective Michael reaction of 2-nitropropane with substituted chalcones catalysed by chiral azacrown ethers derived from alpha-D-glucose. Tetrahedron Asymmetry 2002;13:203–209.

21. Funabashi K, Saida Y, Kanai M, Arai T, Sasai H, Shibasaki M. Catalytic asymmetric Michael addition of nitromethane to enones controlled by (R)-LPB. Tetrahedron Lett 1998;39:7557–7558.
22. Corey EJ, Zhang FY. Enantioselective Michael addition of nitromethane to alpha,beta-enones catalyzed by chiral quaternary ammonium salts. A simple synthesis of (*R*)-baclofen. Org Lett 2000;2;4257–4259.
23. Colonna S, Hiemstra H, Wynberg H. Asymmetric induction in base-catalyzed Michael addition of nitromethane to chalcone. J Chem Soc Chem Commun 1978:238–239.
24. Colonna S, Re A, Wynberg H. Asymmetric induction in the Michael reaction by means of chiral phase-transfer catalysts derived from cinchona and ephedra alkaloids. J Chem Soc Perkin Trans 1981;1:547–552.
25. Vakulya B, Varga S, Csámpai A, Soós T. Highly enantioselective conjugate addition of nitromethane to chalcones using bifunctional cinchona organocatalysts. Org Lett 2005;7:1967–1969.
26. Taylor MS, Zalatan DN, Lerchner AM, Jacobsen ENJ. Highly enantioselective conjugate additions to alpha,beta-unsaturated ketones catalyzed by a (Salen)Al complex. Am Chem Soc 2005;127:1313–1317.
27. List ,B.; Yang JW. The organic approach to asymmetric catalysis. Science 2006;313:1584–1586.
28. Berkesel A, Gröger H. Asymmetric organocatalysis. Weinheim, Germany: VCH; 2005.
29. Seayed J, List B. Asymmetric organocatalysis. Org Biomol Chem 2005;3:719–721.
30. Northup AB, MacMillan DWC. Two-step synthesis of carbohydrates by selective aldol reactions. Science 2004;305:1752–1755.
31. Gröger H, Wilken J. The application of L-proline as an enzyme mimic and further new asymmetric syntheses using small organic molecules as chiral catalysts. Angew Chem Int Ed Engl 2001;40:529–532.
32. Lelais G, MacMillan WC. Modern strategies in organic catalysis: the advent and development of iminium activation. Aldrichimica Acta 2006;39:79–87.
33. List B. Proline-catalyzed asymmetric reactions. Tetrahedron 2002;58: 5573–5590.
34. Notz W, Tanaka F, Barbas CF. Enamine-based organocatalysis with proline and diamines: the development of direct catalytic asymmetric Aldol, Mannich, Michael, and Diels-Alder reactions. Acc Chem Res 2004;37:580–593.
35. Enders D, Seki A. Mining sequence space for asymmetric aminocatalysis: N-terminal prolyl-peptides efficiently catalyze enantioselective aldol and Michael reactions. Synlett 2003:1901–1902.
36. Alexakis A, Andrey O. Diamine-catalyzed asymmetric Michael additions of aldehydes and ketones to nitrostyrene. Org Lett 2002;4:3611–3614.
37. Betancort JM, Barbas CF. Catalytic enantioselective direct Michael additions of ketones to alkylidene malonates. Org Lett 2001;42:4441–4444.
38. Pulkkinen J, Aburel PS, Halland N, Jørgensen KA. Highly enantio- and diastereoselective organocatalytic domino Michael-aldol reactions of beta-diketone and beta-ketosulfone nucleophiles with alpha,beta-unsaturated ketones. Adv Synth Catal 2004;346:1077–1080.
39. Yamaguchi M, Shiraishi T, Hiram M. A catalytic enantioselective Michael addition of a simple malonate to prochiral alpha,beta-unsaturated ketones and aldehydes. Angew Chem Int Ed Engl 1993;32: 1170–1178.
40. Yamaguchi M, Shiraishi T, Hiram M. Asymmetric Michael addition of malonate anions to prochiral acceptors catalyzed by L-proline rubidium salt. J Org Chem 1996;61:3520–3530.
41. Yamaguchi M, Shiraishi T, Igarashi Y, Hiram M. Catalytic asymmetric Michael addition of nitroalkane to enone and enal. Tetrahedron Lett 1994;35:8233–8236.
42. Yamaguchi M, Igarashi Y, Reddy RS, Shiraishi T, Hiram M. Asymmetric Michael addition of nitroalkanes to prochiral acceptors catalyzed by proline rubidium salts. Tetrahedron 1997;53:11223–11236.
43. Hanessian S, Pham V. Catalytic asymmetric conjugate addition of nitroalkanes to cycloalkenones. Org Lett 2000;2:2975–2978.
44. Cobb AJA, Shaw DM, Ley SV. 5-Pyrrolidin-2-yltetrazole: a new, catalytic, more soluble alternative to proline in an organocatalytic asymmetric Mannich-type reaction. Synlett 2004;558–560.
45. Cobb A JA, Longbottom DA, Shaw DM, Ley SV. 5-Pyrrolidin-2-yltetrazole as an asymmetric organocatalyst for the addition of ketones to nitro-olefins. Chem Commun 2004:1808–1809.
46. Cobb AJA, Shaw DM, Longbottom DA, Gold JB, Ley SV. Organocatalysis with proline derivatives: improved catalysts for the asymmetric Mannich, nitro-Michael and aldol reactions. Org Biomol Chem 2005; 3:84–96.
47. Kumarn S, Shaw DM, Longbottom DA, Ley SV. A highly selective, organocatalytic route to chiral dihydro-1,2-oxazines. Org Lett 2005;7: 4189–4191.
48. Mitchell CET, Brenner SE, Ley SV. A versatile organocatalyst for the asymmetric conjugate addition of nitroalkanes to enones. Chem Commun 2005:5346–5348.
49. Mitchell CET, Brenner SE, Garcia-Fortanet J, Ley SV. An efficient, asymmetric organocatalyst-mediated conjugate addition of nitroalkanes to unsaturated cyclic and acyclic ketones. Org Biomol Chem 2006;4:2039–2049.
50. Ahrendt KA, Borths CJ, MacMillan DWC. New strategies for organic catalysis: the first highly enantioselective organocatalytic Diels-Alder reaction. J Am Chem Soc 2000;122:4243–4244.
51. Jen WS, Wiener JJM, MacMillan DWC. New strategies for organic catalysis: the first enantioselective organocatalytic 1,3-dipolar cycloaddition. J Am Chem Soc 2000;122:9874–9875.
52. Paras NA, MacMillan DWC. New strategies in organic catalysis: the first enantioselective organocatalytic Friedel-Crafts alkylation. J Am Chem Soc 2001;123:4370–4371.
53. Austin JF, MacMillan DWC. Enantioselective organocatalytic indole alkylations. Design of a new and highly effective chiral amine for iminium catalysis. J Am Chem Soc 2002;124:1172–1173.
54. Paras NA, MacMillan DWC. The enantioselective organocatalytic 1,4-addition of electron-rich benzenes to alpha,beta-unsaturated aldehydes. J Am Chem Soc 2002;124:7894–7895
55. Brown SP, Goodwin NC, MacMillan DWC. The first enantioselective organocatalytic Mukaiyama-Michael reaction: a direct method for the synthesis of enantioenriched gamma-butenolide architecture. J Am Chem Soc 2003;125:1192–1194.
56. Halland N, Hazell RG, Jørgensen KAJ. Organocatalytic asymmetric conjugate addition of nitroalkanes to alpha,beta-unsaturated enones using novel imidazoline catalysts. Org Chem 2002;67:8331–8338.
57. Halland N, Aburel PS, Jørgensen K. A Highly enantioselective organocatalytic conjugate addition of malonates to acyclic alpha,beta-unsaturated enones. Angew Chem Int Ed Engl 2003;42:661–665.
58. Halland N, Hansen T, Jørgensen K. Organocatalytic asymmetric Michael reaction of cyclic 1,3-dicarbonyl compounds and alpha,beta-unsaturated ketones—a highly atom-economic catalytic one-step formation of optically active warfarin anticoagulant. A Angew Chem Int Ed Engl 2003;42:4955–4957.
59. Halland N, Jørgensen KA, Hansen T. Catalytic asymmetric synthesis of warfarin derivatives from hydroxycoumarins and enones. PCT Int Appl 45. pp (2003). Chem Abstr 2003;139:52884.
60. Halland N, Aburel PS, Jørgensen KA. Highly enantio- and diastereoselective organocatalytic asymmetric domino Michael-Aldol reaction of beta-ketoesters and alpha,beta-unsaturated ketones. Angew Chem Int Ed Engl 2004;43:1272–1277.
61. Kohler EP, Drake NL. The catalytic reduction of nitro compounds. II. Gamma-nitro ketonese. J Am Chem Soc 1923;45:2144–2150.
62. Kloetzel MC. Reactions of Nitroparaffins. I. Synthesis and Reduction of Some γ-Nitroketones. J Am Chem Soc 1947;69:2271–2275.
63. Walker GN. Synthesis of 3-Hydroxy-4-nitro-5-arylcyclohexanones by Claisen Condensation and Cyclization Reactions with β-Aryl-γ-nitro Ketones. J Org Chem 1965;30:1416–1421.
64. Irie K, Miyazu K, Watanabe K. Michael additions catalyzed by Nickel(II) or cobalt(II) acetate-2,2'-bipyridine complexes. Chem Lett 1980:353–354.
65. Supuran CT, Popescu A, Ilisiu M, Costandache A, Banciu MD. Carbonic anhydrase inhibitors .36. Inhibition of isozymes I and II with Schiff bases derived from chalkones and aromatic/heterocyclic sulfonamides. Eur J Med Chem Chim Ther 1996;31:439–447.

66. Sar CP, Jeko J, Hideg K. Synthesis of 2-alkenyl-1-pyrrolin-1-oxides and polysubstituted nitrones. Synthesis 2003:1367–1372.
67. Sakthivel K, Notz W, Bui T, Barbas CF. Amino acid catalyzed direct asymmetric aldol reactions: a bioorganic approach to catalytic asymmetric carbon-carbon bond-forming reactions. J Am Chem Soc 2001;123:5260–5267.
68. Alexakis A, Andrey O. Diamine-catalyzed asymmetric Michael additions of aldehydes and ketones to nitrostyrene. Org Lett 2002;4:3611–3614.
69. Kotrusz P, Toma S, Schmaltz H-G, Adler A. Michael additions of aldehydes and ketones to beta-nitrostyrenes in an ionic liquid. Eur J Org Chem 2004:1577–1583.
70. Reichert B, Posemann H. Conversion of 1,3-aminoketones into 1,4-nitroketones. Arch Pharm 1937;275:67–83.
71. Peseke K, Gotze L, Reinke H, Cedeno QA, Suarez JQ, Andreu MG, Castro HV. A synthesis of substituted tetrahydro-2-pyranols. J Prakt Chem Chem Ztg 1997;339:656–659.
72. Huang H, Jacobsen EN. Highly enantioselective direct conjugate addition of ketones to nitroalkenes promoted by a chiral primary amine-thiourea catalyst. J Am Chem Soc 2006;128:7170–7171.
73. Evans DA, Gauchet-Prunet JA, Carreira EM, Charette AB. Synthesis of 1,3-diol synthons from epoxy aromatic precursors. An approach to the construction of polyacetate-derived natural-products. J Org Chem 1991;56:741–750.
74. Katsoulacos P. Synthesis of substituted pyrazolines. Chim Chronika (Athens, Greece) 1966; 31:1–2.
75. Adeva M, Sahagún H, Caballero E, Peláez-Lamamié de Clairac R, Medarde M, Tomé FJ. Open analogues of arcyriaflavin A. Synthesis through Diels-Alder reaction between maleimides and 1-aryl-3-tert-butyldimethylsiloxy-1,3-butadienes. Org Chem 2000;65:3387–3394.
76. Astoin J, Marivain A, Riveson A, Crucix M, Lapotre M, Torrens Y. Central nervous-system agents. New alpha-ethylenic alcohols. Eur J Med Chem 1978;13:41–47.
77. Giswold O, Buelow D, Carlson EH. Synthesis of some α,ω-bis(3,4-dihydroxyphenyl)alkanes. J Am Pharm Assoc 1946;35:188–191.
78. Dickinson R, Heilbron IM, Irving F. The intermolecular condensation of styryl methyl ketones. Part I. J Chem Soc 1927:1888–1897.
79. Drake NL, Allen P. Organic syntheses coll, Vol. I. New York: Wiley; 1932, p 69–71.
80. Drake NL, Allen P. Organic syntheses coll, Vol. I. New York: Wiley; 1932. p 77–78.
81. Sheldrick GM. SHELXS-97 program for crystal structures solution. Göttingen: University of Göttingen; 1997.
82. Wilson AJC, editor. International tables for X-ray crystallography, Vol C. Dordrecht: Kluwer Academic Publishers; 1992. p 500–502, 219–222, 193–199.
83. Sheldrick GM. SHELXL-97 program for the refinement of crystal structures. Göttingen: University of Göttingen; 1997.
84. Barbour LJ. "X-seed—a software tool for supramolecular crystallography." J Supramol Chem 2001;1:189–191.
85. Spek AL. Single-crystal structure validation with the program PLATON. J Appl Cryst 2003;36:7–13.
86. Macrae CF, Edgington PR, McCabe P, Pidcock E, Shields GP, Taylor R, Towler M, van de Streek J. Mercury: visualization and analysis of crystal structures. J Appl Cryst 2006;39:453–457.
87. Grell J, Bernstein J, Tinhofer G. Graph-set analysis of hydrogen-bond patterns: some mathematical concepts. Acta Crystallogr B 2000;56:166–180.
88. Flack HD. On enantiomorph-polarity estimation. Acta Cryst 1983;A39:876–881.

CHIRALITY 20:1127–1133 (2008)

Molecular Dynamics Study on the Conformational Flexibility and Energetics in Aqueous Solution of Methylated β-Cyclodextrins

JAVIER PEREZ-MIRON,[1] CARLOS JAIME,[1]* AND PETKO M. IVANOV[2]

[1]*Departament de Química, Facultat de Ciències, Universitat Autònoma de Barcelona, 08193 Bellaterra, Spain*
[2]*Institute of Organic Chemistry with Centre of Phytochemistry, Bulgarian Academy of Sciences, 1113 Sofia, Bulgaria*

ABSTRACT All possible methylated β-cyclodextrins (CDs) with C7-symmetry have been studied by molecular dynamics simulations, in gas phase and in water solution. Energetic and structural information were obtained from the trajectory analysis. CD flexibility increases with degree of methylation, very likely due to the concomitant reduction of the intramolecular hydrogen bonds. Solvation-free energy was computed for each of the studied CDs using the MM/GBSA method. An analysis of radial distribution functions was used to determine distribution of solvent molecules around the O2, O3, and O6. The number of solvent molecules around these oxygens decreases with an increase in the degree of methylation. The ΔS contribution from solvent thus becomes more positive when the degree of methylation increases and, consequently, the overall ΔG in water diminishes. *Chirality 20:1127–1133, 2008.*

KEY WORDS: cyclodextrins; molecular dynamics; molecular modeling; solvent effects

INTRODUCTION

Cyclodextrins (CDs) are macrocycles formed by five of more α-D-glucopyranose units, linked by α-(1→4)-glucosydic bonds (see Fig. 1a). Native CDs (α-, β-, and γ-CDs) have a doughnut-like shape, with a nonpolar internal cavity and a polar external wall (Fig. 1b). CDs are frequently used as carriers of nonpolar organic substances in polar solvents (mainly water).[1–6] CDs are also commonly used as stationary phases for chiral column chromatography, thanks to their capacity of including organic molecules.

The solubility of CDs in water depends on their size (the solubility of β-CD is 10 times smaller than that of α- and γ-CD) and on their substitution.[7–10] Differences in solubility reflects on concomitant differences in flexibility of the macrorings in solution. Interestingly, the preparation of derivatives improves solubility. Each residue of α-D-glucopyranose has three hydroxyl groups capable of being methylated (see Fig. 1a). There are synthetic procedures to selectively introduce a methyl group at each hydroxyl group (O2, O3, or O6). In this work, our attention is centered on studying the differences in conformational flexibility for the methylated β-CDs in solution. All eight possible methylated β-CDs studied in this work have been or can be synthesized.[11,12]

For the sake of simplicity, each β-CD will be named by a series of three letters representing the functional group at positions 2, 3, and 6, respectively. A hydroxyl will be represented by an H, and a methylated hydroxyl by an M. As an example, the native β-CD will be termed HHH, the permethylated β-CD will be MMM, the monomethylated at O6 will be HHM, the dimethylated at O2 and O3 will be MMH, and so on. It is experimentally known that the solubility of the methylated β-CDs generally increases with the degree of methylation. However, the solubility of the permethylated β-CD, MMM (the heptakis(2,3,6-tri-*O*-methyl)-β-cyclodextrin) is smaller than that for the dimethylated β-CD, MHM (heptakis(2,6-di-*O*-methyl)-β-cyclodextrin). Nevertheless, MMM is still more soluble than HHH.[13–16]

EXPERIMENTAL

Atomic Charge Generation

The eight possible methylated β-CDs require the preparation of eight glucosidic residues. Eight different methylated glucoses (using the O1 and the O4 methylated to simulate the chemical environment of the fragment in a real CD) were manually built using the MacroModel program,[17] and were fully minimized with the AMBER* force field (AMBER* is the MacroModel version of the AMBER force field).[18,19]

A conformational analysis was performed for each of the methylated glucoses to obtain the most representative set of conformations. A Metropolis MonteCarlo method was used, and the rotated bonds were C2—O2, C3—O3, C5—C6, and C6—O6. A total of 1000 structures were generated for each of the glucoses. The most representative set of conformations (formed by as many conformers as necessary to cover more than 80% of the population) were considered. The total number of conformers, the total pop-

Additional Supporting Information may be found in the online version of this article.

Contract grant sponsor: Ministerio de Educación y Ciencia, Spain; Contract grant number: CTQ2006-08256

*Correspondence to: Carlos Jaime, Departament de Química, Facultat de Ciències, Universitat Autònoma de Barcelona, 08193 Bellaterra, Spain.
E-mail: carlos.jaime@uab.cat

Received for publication 20 December 2007; Accepted 29 February 2008
DOI: 10.1002/chir.20571
Published online 27 May 2008 in Wiley InterScience (www.interscience.wiley.com).

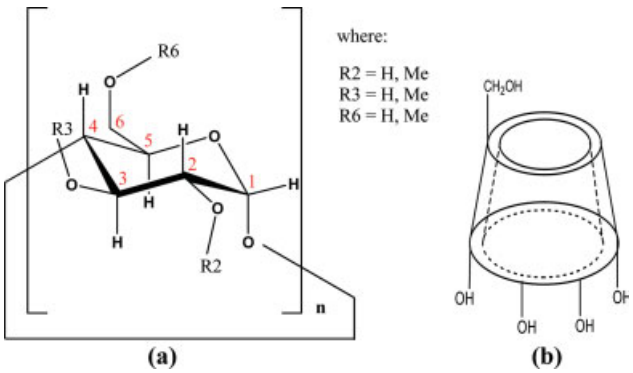

Fig. 1. Schematic representation of a CD. (**a**) Numbering of the atoms of the glucoside unit and positions for methyl group substitutions; (**b**) shape. [Color figure can be viewed in the online issue, which is available at www.interscience.wiley.com.]

ulation covered, the number of conformers in the most representative set, and the population of each of those conformers, are detailed in Table 1. In all cases, the energy difference between the most stable and the last considered conformer is about 3 kJ/mol (0.72 kcal/mol), except for HHH, MHH and MHM, where the difference is about 5–6 kJ/mol (1.19–1.43 kcal/mol). Interestingly, although the number of different conformers is always very similar, the number of conformers considered is two to three times larger than for the other glucoses when O6 is methylated.

The geometry of each of the computed conformers was fully optimized through the Gaussian-98 program (in spite of having a newer version of the Gaussian program, this was the version used, as certain modules of the Amber program only recognize output from the 92, 94, and 98 Gaussian versions),[20] using the STO-3G basis set; electrostatic potential was computed using the 6-31G* basis set with the Merz–Singh–Kollman population analysis (pop = mk).[21,22] All conformers of the representative set for each glucose in Table 5 were used to compute a final set of atomic charges for each glucose residue, using the RESP module.[23]

Computational Details

The AMBER 7.0[24] suite of programs was used with the parm99 parameter set.[25] The use of other more specific parameter sets for carbohydrates, as for example GLYCAM,[26] was not necessary for our purposes due to the fact of that the anomeric carbons in CD's remain in a rigid configuration and cannot epimerize. Additionally, water was the chosen solvent, under the TIP3P model.[27,28] Each CD was immersed in a solvent box with buffer distances of 10.0 Å between the walls of the box and the closest atoms of the solute. Each studied CD was first fully minimized, and the system was then gradually heated from 1 to 298 K over 30 ps, and equilibrated for 70 ps at 298 K, both at constant volume. This procedure was followed by another equilibration for 100 ps at constant pressure. During this process, the density was kept constant around 1.0 g/ml in all cases. Productive runs were then performed using a time step of 1 fs and a length of 900 ps. Periodic boundary conditions were applied in the molecular dynamics simulations with solvent. A cutoff of 8 Å was set for evaluating the nonbonding interactions and 0.00001 Ewald convergence tolerance for the inclusion of long-range electrostatic contributions. The SHAKE algorithm was used to fix the bonds involving hydrogens.

TABLE 1. For each glucose studied, we provide the number of different conformers generated, the number of conformers forming the most representative set, the population covered by this set, and the population for each conformer within the set

Glucose (different conformers)	Conformers considered (population covered)	Population of each considered conformer (%)
HHH (64)	4 (87%)	50, 14, 14, and 9
MHH (57)	4 (85%)	54, 16, 9, and 6
HMH (42)	3 (84%)	49, 20, and 15
HHM (58)	9 (81%)	21, 15, 10, 8, 6, 6, 5, 5, and 4
MMH (49)	3 (83%)	40, 30, and 13
MHM (58)	10 (81%)	23, 17, 10, 7, 6, 5, 4, 4, 3, and 2
HMM (39)	8 (86%)	20, 15, 15, 10, 7, 7, 6, and 6
MMM (44)	8 (86%)	19, 15, 14, 11, 9, 6, 6, and 6

MM/GBSA Analysis

The MM/GBSA method was used to compute the ΔG of a process taking place in solution.[29–32] The equation used for evaluating the energy balance is

$$\Delta G = E_{GAS} + \Delta G_{SOL} - T\Delta S \quad (1)$$

where E_{GAS} is the total energy of the system in the gas phase, and this is obtained from the MD simulation. The ΔG_{SOL} term describes the free energy involved in the process of placing the molecule from gas phase to solution, and is computed as

$$\Delta G_{SOL} = \Delta G_{GB} + \Delta G_{SA} \quad (2)$$

where ΔG_{GB} refers to the electrostatic component of solvation, while ΔG_{SA} is the nonelectrostatic contribution, termed cavitation energy.[33]

Finally, the entropic term, $T\Delta S$, estimates the entropy of the system.

The modules MM-PBSA and NMODE from AMBER 7 package were used to compute the energies given in this analysis.

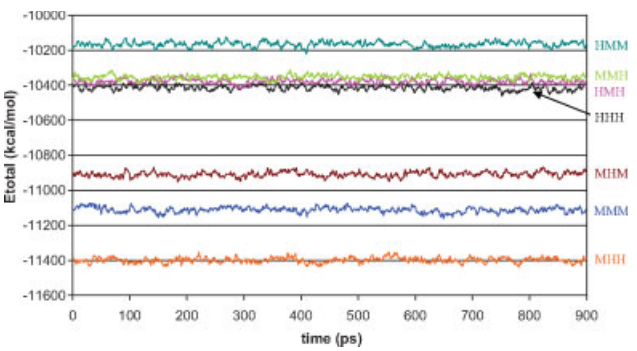

Fig. 2. Variation of total energies in solution (E_{total} in kcal/mol) versus simulation time (ps). [Color figure can be viewed in the online issue, which is available at www.interscience.wiley.com.]

TABLE 2. Difference between the energy of each studied CD in aqueous solution and in the gas phase (ΔE, kcal/mol)

	ΔE_{ELE}	ΔE_{VDW}	ΔE_{INT}	ΔE
HHH	31.4	1.1	−6.8	25.7
MHH	41.4	−8.9	0.6	33.0
HMH	26.7	−2.2	0.6	25.1
HHM	9.6	−0.7	−0.5	8.4
MMH	19.8	3.4	−2.4	20.8
MHM	7.7	1.8	−5.5	4.0
HMM	2.6	0.3	3.3	6.2
MMM	4.5	1.1	−7.4	−1.8

RESULTS AND DISCUSSION

Molecular Dynamics Simulation

All the possible β-CDs with C7-symmetry were built using the glucose residues derived as described in the Experimental section. The CDs were fully minimized with the parm99 Amber force field, and were subjected to MD runs in both gas phase and water solution (see computational details). The computational results indicate that the total energy (E_{total}) does not vary substantially over the simulation time either in the gas phase or in aqueous solution, indicating absence of large conformational variations. Very likely, only movements related to rotations about the C—O and the C5—C6 bonds are produced. Figure 2 shows the energy variations throughout the simulation time for all the studied CDs in water.

Energy Contributions

An energy analysis of the studied CDs was performed using the MM/PBSA methodology.[34–38] Table 2 details the difference between the substrate energy in water and in gas phase. As it could be expected, all the studied CDs have lower steric energies in the gas phase than in water (except for the MMM). This difference in the strain inherent for the molecules decreases with the degree of methylation, indicating that the structure of the CD in water is increasingly similar to the gas-phase geometry.

Average Structures in Water Solution

The methylated CDs are more flexible in water solution than are the native CDs. Certain experiments demonstrate the complete rotation of some of the glucoses around the glycosidic linkages.[39–41] The average structure of the HHH is highly symmetric, with all glucoses in *syn* relative orientation. In contrast, as the degree of methylation increases the macrorings become more flexible, and consecutive glucoses adopt *kink* conformations, in agreement with published theoretical and experimental (NMR and X-ray) studies.[42] Obviously, the present simulations are not long enough in order to arrive at symmetrical average geometries also for the methylated derivatives. The average structure of each studied CD in water solution was computed (see Fig. 3).

Dihedral Angle Analysis

A more precise description of the conformational behavior of the studied CDs was obtained by analyzing the time-dependence of the O5-C1···C4-C5 dihedral angle (see Fig. 4), which indicates the relative position of two glucoses.[43,44] The analysis was carried out on 900 structures taken from the trajectory (one structure per picosecond). Three sets of values were used to define relative conformation: (i) $-60 < w < 60$ (*syn*), (ii) $-120 < w \leq -60$ or $60 \leq$

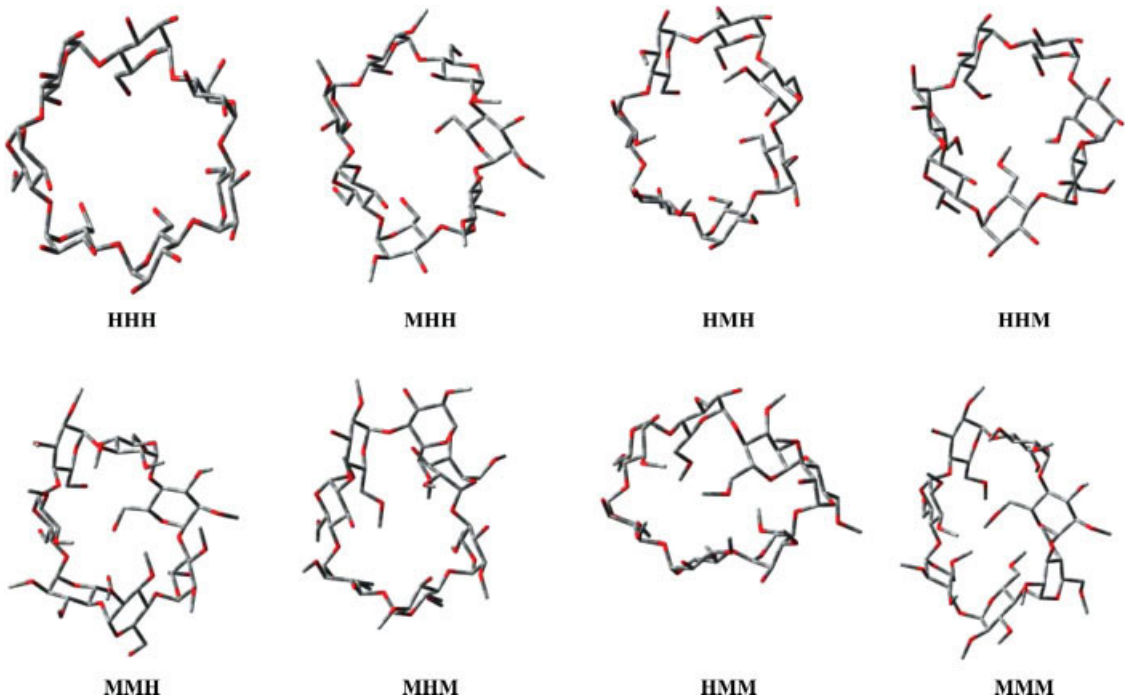

Fig. 3. Average structures in aqueous solution. [Color figure can be viewed in the online issue, which is available at www.interscience.wiley.com.]

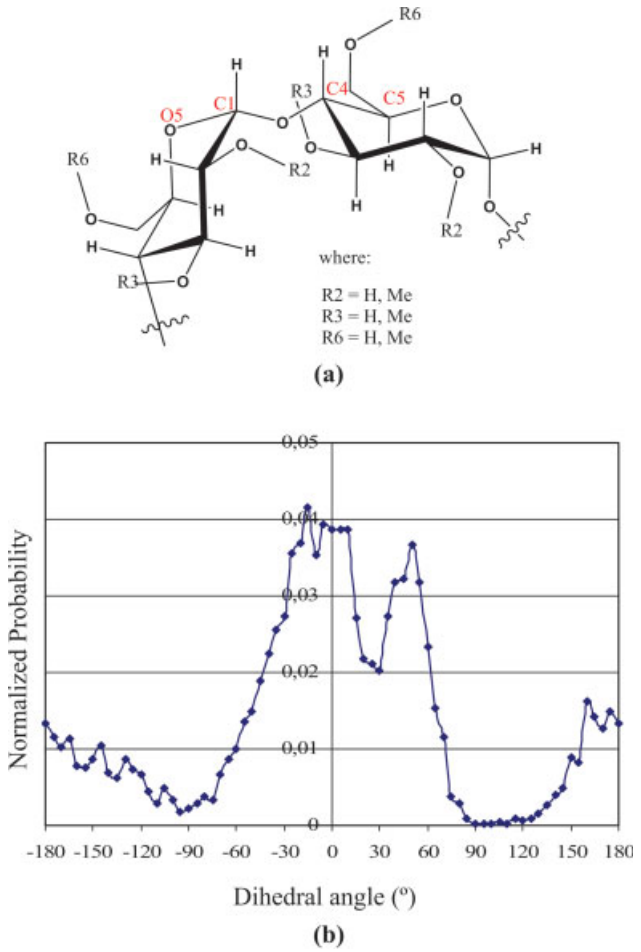

Fig. 4. (**a**) Schematic representation of the O5−C1···C4−C5 dihedral angle; (**b**) Normalized probability for each value of the O5−C1···C4−C5 dihedral angle in the case of HMM as an example. [Color figure can be viewed in the online issue, which is available at www.interscience.wiley.com.]

$w < 120$ (*kink*), and (iii) $120 \leq w \leq -120$ (*anti*). Table 3 contains the number of glucoses in each conformation observed throughout the trajectory for all the CDs studied. It can be observed that all the studied CDs have a majority of glucoses in *syn* conformation, and almost one glucose in *kink* conformation. Although very similar in value, the number of *kink* glucoses seems to be related to the O2 methylation. In contrast, the number of glucoses in *anti* conformation is clearly related to the O6 methylation.

TABLE 3. Number of glucoses in each conformation observed throughout the MD trajectory in all the CDs studied

	Number of glucoses in each conformation		
	syn	*kink*	*anti*
HHH	6.1	0.9	0.0
MHH	5.7	1.3	0.0
HMH	6.3	0.7	0.0
HHM	5.6	0.7	0.7
MMH	5.9	1.1	0.0
MHM	5.9	1.1	0.0
HMM	4.7	0.9	1.4
MMM	5.6	1.4	0.0

Hydrogen Bond Analysis

An analysis of the inter- and intramolecular hydrogen bonds was performed using the ptraj Amber module. This module renders a percentage of occupation for the hydrogen bond analyzed throughout the whole trajectory. The sums of all the occupational percentages for all inter- and intramolecular hydrogen bonds per glucose were used as a measure of facility of hydrogen bond formation. Figure 5 shows the results for all the studied CDs. With increasing the degree of methylation decreases the probability for the formation of hydrogen bonds. When results are compared within CDs with the same degree of methylation, then the smallest number of intermolecular hydrogen bonds present the CDs with O6 methylated. The two degrees of freedom per residue for intramolecular rotations related to hydrogen bonding involving $-CH_2-$O6H groups render more possibilities for intramolecular hydrogen bonding than rotations of the C(2) and C(3) hydroxyl groups.

The HMH is the methylated CD with the largest capability of intramolecular hydrogen bond formation. This result was not expected, as the chain of intramolecular hydrogen bonds[45–47] between the O2 and O3 hydroxyls is disrupted by the methylation of one of those two oxygens. HMH has however a smaller percentage of intermolecular hydrogen bonds thus the O2- and the O3-methylated forms have almost the same total populations of hydrogen bonds. Alternatively, this observation manifests for still not convergent simulation. CDs with a degree of methylation per glucose of two have very similar behavior, MHM and HMM having slightly larger occupational percentages.

Solvation-Free Energy

The solvation-free energies were computed using the MM/GBSA methodology (see below "MM/GBSA analysis" section). Two contributions are estimated (see Table 4)—one from the electrostatic polarization interaction with the solvent and the other from the solvent accessible sur-

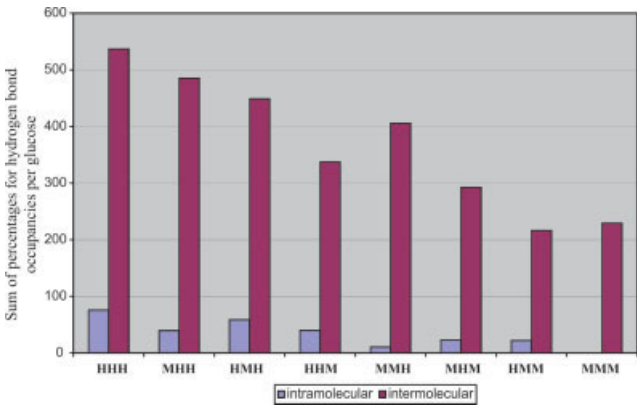

Fig. 5. Graphical representation of the sum of percentages for hydrogen bond occupancies per glucose unit. [Color figure can be viewed in the online issue, which is available at www.interscience.wiley.com.]

TABLE 4. Solvation-free energy components, ΔG_{SA} and ΔG_{GB} (kcal/mol), for each of the studied CDs and energy terms (kcal/mol), E_{GAS} and $T\Delta S$, used to obtain the free energy (ΔG) estimates

	Energy terms			
CD	ΔG_{SA}	ΔG_{GB}	E_{GAS}	$T\Delta S$
HHH	7.7	−80.3	259.8	128.7
MHH	8.7	−73.7	262.1	142.2
HMH	8.2	−56.8	293.0	141.4
HHM	8.2	−34.7	263.1	142.4
MMH	8.9	−46.2	278.5	154.2
MHM	9.2	−27.0	282.4	155.4
HMM	8.7	−20.7	279.9	154.9
MMM	9.3	−20.1	293.2	167.4

face. ΔG_{SOL} increases with the degree of CD methylation (see Fig. 6). The free energy of each CD in aqueous solution was ascertained and the results for each CD are detailed in Table 3 and Figure 6, which show that ΔG increases with the degree of methylation.

Qualitative Evaluation of Entropy

Because of the size of the studied molecules, it is very difficult to adequately estimate the entropy of the solvation process through calculations of the vibrational frequencies of substrate and solvent as a whole. However, a qualitative estimation of its importance has been carried out by computing the radial distribution function (rdf) of the solvent molecules around the substrates, and consequently information about the solvation coordination spheres was obtained. The rdf between three types of oxygens (O2, O3, and O6) of the substrate and the solvent were computed, termed gO2, gO3, and gO6, respectively (the rdf were computed up to 30 Å, and were analyzed at intervals of 0.1 Å).

Figure 7 outlines graphical representation of all rdf curves. Figure 7a details three maxima at radii 2.0, 3.25, and 4.65 Å, corresponding to the first, the second and the third solvation shells around O2, respectively. For HHH and HHM the solvent is highly ordered in the second solvation shell, but for the CDs with O2 methylated (MHH, MMH, MHM and MMM) the solvent is more ordered in the third solvation shell. To summarize, the CDs with methylated O2, show similar behavior; while the first and the second solvation shells favor the solvation-free energy, the third shell disfavors it. Figure 7b shows the rdf curves for the distribution of solvent molecules around O3. Clearly, the behavior of CDs with methylated O3 are different from the other CDs. Qualitatively, HHH, MHH, HHM, and MHM have rdf functions that are very similar for the second solvation spheres, presenting more ordered solvent than HMH, MMH, HMM, and MMM. CDs with methylated O3 behave similarly in the third solvation shell where the solvent is more ordered. In summary, the solvation-free energy of CDs with methylated O3 is favored by water disorder in the first and in the second shells. Two different trends are expressed by the rdf curves of the solvent around O6 (Fig. 7c): that for the HHH, MHH, HMH, and MHH, and that for HHM, MHM, HMM, and MMM (the latter have methylated O6).

The order of solvent molecules in the first and second solvation shells is higher for HHH, MHH, HMH, and MMH, and is very similar in the third shell in all CDs. Thus, solvation of CDs without methylated O6 is entropically disfavored. Table 5 presents a summary of the degree of solvent disorder around O2, O3, and O6 oxygens for the studied CDs. The number of water molecules in the first solvation shell around O6 is always significantly larger than that around O2 and O3, as a direct consequence of being more accessible.

The results show that four classes of CDs exist, depending on the total number of solvent molecules around the substrate: (i) HHH, (ii) MHH, HMH, and HHM, (iii) MMH, MHM, and HMM, and (iv) MMM. The MMM is the CD whose solvation is most entropically favored, as the solvent is more disordered, and in contrast, solvent is highly ordered for HHH. Consequently, as the degree of methylation increases, the solvation is entropically more favored.

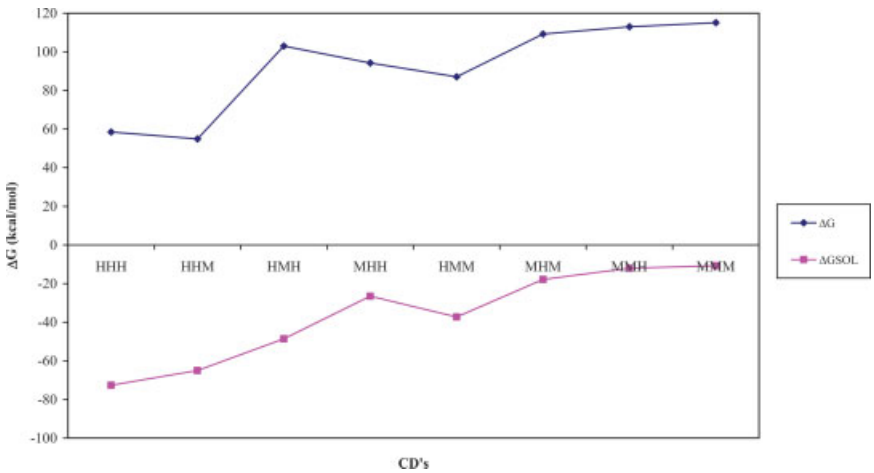

Fig. 6. Graphical representation of (**a**) ΔG_{SOL} and (**b**) ΔG. [Color figure can be viewed in the online issue, which is available at www.interscience.wiley.com.]

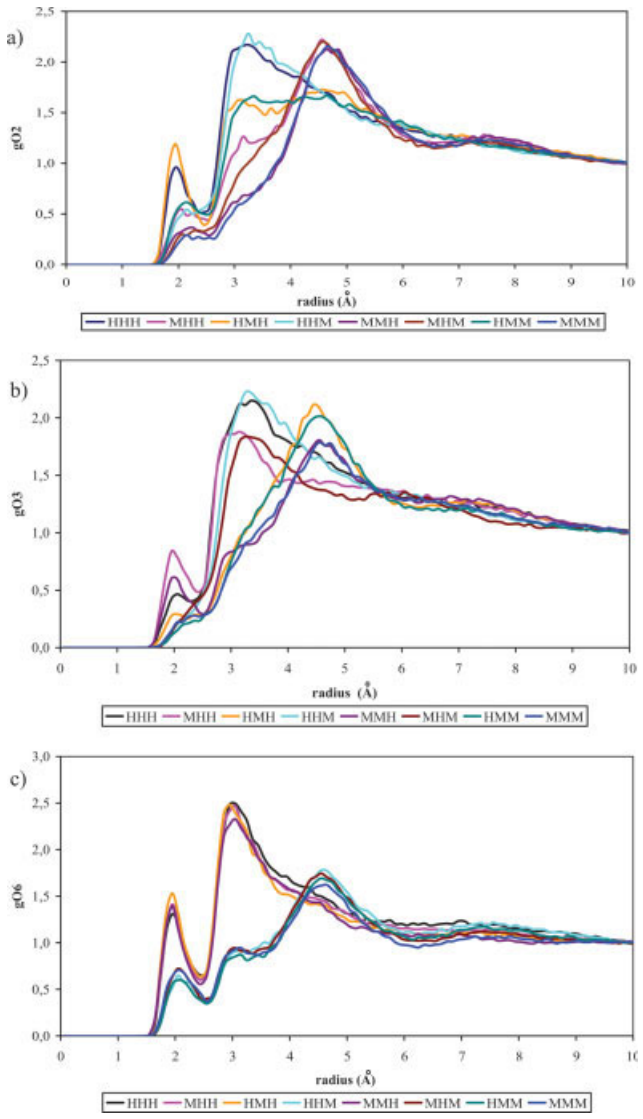

Fig. 7. Radial distribution functions of the solvent molecules around selected types of CD oxygens: (**a**) O2; (**b**) O3; and (**c**) O6. [Color figure can be viewed in the online issue, which is available at www.interscience.wiley.com.]

TABLE 5. Number of solvent molecules around the O2, O3, and O6 oxygens for the studied CDs

	Oxygen								
	O2			O3			O6		
	1st	2nd	3rd	1st	2nd	3rd	1st	2nd	3rd
HHH	2.2	18.4	62.8	2.2	18.4	62.8	2.8	15.4	56.3
MHH	1.0	11.4	55.5	1.7	17.1	51.6	3.0	15.1	54.3
HMH	2.8	14.6	56.4	0.5	7.6	51.9	3.2	18.3	50.8
HHM	0.8	17.5	63.9	0.2	15.7	59.6	0.9	8.1	41.7
MMH	0.6	6.7	48.6	1.2	8.0	45.9	3.1	18.4	53.9
MHM	0.4	8.9	54.4	0.2	14.5	50.3	1.2	7.3	42.9
HMM	1.0	14.0	56.3	0.2	7.3	52.7	1.0	7.6	39.5
MMM	0.3	6.5	49.0	0.2	7.6	45.8	1.3	8.9	40.1

1st, 2nd, and 3rd represent salvation shells.

CONCLUSIONS

The flexibility of the methylated CDs increases with the degree of methylation, because of reduction in the number of intramolecular hydrogen bonds produced by methylation. The solvation energy of the methylated CDs increases with the degree of CD methylation and depends on the entropy of the solvation process. Studies of the rdfs for solvent molecules around selected CD oxygens indicate the importance of water molecules order for the solvation-free energy. The number of water molecules around the substrates diminishes with the degree of methylation, increasing disorder in the system.

ACKNOWLEDGMENTS

This research has been performed, in part, using the CESCA resources.

LITERATURE CITED

1. Dodziuk H. Cyclodextrins and their complexes. Weinheim: Willey-VCH; 2006.
2. Szejtli J. Cyclodextrin technology. Dordrecht: Kluver Academics Publishers; 1988.
3. Brewster ME, Loftsson T. Cyclodextrins as pharmaceutical solubilizers. Adv Drug Deliv Rev 2007;59:645–666.
4. Loftsson T, Jarho P, Masson M, Jaervinen T. Cyclodextrins in drug delivery. Expet Opin Drug Deliv 2005;2:335–351.
5. Chowdary KPR. Cyclodextrins-versatile pharmaceutical excipients. Int J Pharm Excip 2003;70–74.
6. Rao VM, Stella VJ. When can cyclodextrins be considered for solubilization purposes? J Pharm Sci 2003;92:927–932.
7. Naidoo KJ, Chen JY, Jansoon JLM, Widmalm G, Maliniak A. Molecular properties related to the anomalous solubility of β-Cyclodextrin J Phys Chem B 2004;108:4236–4238.
8. Pharr DY, Fu ZS, Thuy K, Hinze WL. Solubilization of cyclodextrins for analytical applications. Anal Chem 1989;61:275–279.
9. Jozwiakowski MJ, Connors KA. Aqueous solubility behavior of three cyclodextrins. Carbohydr Res 1985;143:51–59.
10. Sabadini E, Cosgrove T, Egidio F. Solubility of cyclomalto-oligosaccharides (cyclodextrins) in H_2O and D_2O: a comparative study. Carbohydr Res 2006;341:270–274.
11. Bergeron R, Machida M. Complex formation between mycobacterial polysaccharides or cyclodextrins and palmitoyl coenzyme A. J Biol Chem 1975;250:1223–1230.
12. Khan AR, Forgo P, Stine KJ, D'Souza VT. Methods for selective modifications of cyclodextrins. Chem Rev 1998;98:1977–1996.
13. Nógrádi M. Dimethyl-β-Cyclodextrin. Drug Fut 1984;9:577–578.
14. Szejtli J. Dimethyl-β-cyclodextrin as parenteral drug carrier. J Inclus Phenom 1983;1:135–150.
15. Szejtli J. Highly soluble b-cyclodextrin derivatives. Starch 1984;36: 429–432.
16. Uekama K. Pharmaceutical applications of methylated cyclodextrins. Pharm Int 1985;6:61–65.
17. MacroModel, version 5.0, Schrödinger, New York: LLC; 1995.
18. Weiner SJ, Kollman PA, Case DA, Singh UC, Ghio C, Alagona G, Profeta S, Weiner P. A new force field for molecular mechanical simulation of nucleic acids and proteins. J Am Chem Soc 1984;106:765–784.
19. Weiner SJ, Kollman PA, Nguyen DT, Case DA. An all atom force field for simulations of proteins and nucleic acids. J Comput Chem 1986;7:230–252.
20. Frisch MJ, Trucks GW, Schlegel HB, Scuseria GE, Robb MA, Cheeseman JR, Zakrzewski VG, Montgomery JA Jr, Stratmann RE, Burant JC, Dapprich S, Millam JM, Daniels AD, Kudin KN, Strain MC, Farkas O, Tomasi J, Barone V, Cossi M, Cammi R, Mennucci B, Pomelli C, Adamo C, Clifford S. Ochterski ,J, Petersson GA, Ayala

PY, Cui Q, Morokuma K, Salvador P, Dannenberg JJ, Malick DK, Rabuck AD, Raghavachari K, Foresman JB, Cioslowski J, Ortiz JV, Baboul AG, Stefanov BB, Liu G, Liashenko A, Piskorz P, Komaromi I, Gomperts R, Martin RL, Fox DJ, Keith T, Al-Laham MA, Peng CY, Nanayakkara A, Challacombe M, Gill PMW, Johnson B, Chen W, Wong MW, Andres JL, Gonzalez C, Head-Gordon M, Replogle ES, Pople JA. Gaussian 98 (revision A. 10). Gaussian, Inc., Pittsburgh PA, 2001.

21. Besler BH, Merz KM, Kollman PA. Atomic charges derived from semiempirical methods. J Comp Chem 1990;11:431–439.
22. Singh UC, Kollman PA. An approach to computing electrostatic charges for molecules. J Comp Chem 1984;5:129–145.
23. Case DA, Pearlman DA, Caldwell JW, Cheatham TE III, Wang J, Ross WS, Simmerling C, Darden T, Merz KM, Stanton RV, Cheng A, Vincent JJ, Crowley M, Tsui V, Gohlke H, Radmer R, Duan Y, Pitera J, Massova I, Seibel GL, Singh UC, Weiner P, Kollman PA. Amber 7 User's Manual. California: University of California; 2002.
24. Amber 7, University of California, California, 2002.
25. Wang J, Cieplak P, Kollman PA. How well does a restrained electrostatic potential (RESP) model perform in calculating conformational energies of organic and biological molecules? J Comput Chem 2000;21:1049–1074.
26. Woods RJ, Dwek RA, Edge CJ, Fraser-Reid B. Molecular mechanical and molecular dynamic simulations of glycoproteins and oligosaccharides. 1. GLYCAM_93 parameter development. J Phys Chem 1995;99: 3832–3846.
27. Perez-Miron J. Molecular Modeling with AMBER. Bellaterra: Universitat Autònoma de Barcelona; 2005.
28. Jorgensen WL, Chandrasekhar J, Madura JD, Impey RW, Klein ML. Comparison of simple potential functions for simulating liquid water. J Chem Phys 1983;79:926–935.
29. Weiser J, Shenkin PS, Still WC. Approximate atomic surfaces from linear combinations of pairwise overlaps (LCPO). J Comput Chem 1999;20:217–230.
30. Sitkoff D, Sharp KA, Honig B. J Phys Chem 1994;98:1978–1988.
31. Srinivasan J, Cheatham TE III, Kollman PA, Case DA. Continuum solvent studies of the stability of DNA, RNA, and phosphoramidate-DNA helixes. J Am Chem Soc 1998;120:9401–9409.
32. Kollman PA, Massova I, Reyes C, Kuhn B, Huo S, Chong L, Lee M, Lee T, Duan Y, Wang W, Donini O, Cieplak P, Srinivasan J, Case DA, Cheatham TA III. Calculating structures and free energies of complex molecules: combining molecular mechanics and continuum models. Acc Chem Res 2000;33:889–897.
33. Still WC, Tempczyk A, Hawley RC, Hendrickson TJ. Semianalytical treatment of solvation for molecular mechanics and dynamics. J Am Chem Soc 1990;112:6127–6129.
34. Wang W, Kollman PA. Free energy calculations on dimer stability of the HIV protease using molecular dynamics and a continuum solvent model. J Mol Biol 2000;303:567–582.
35. Reyes C, Kollman PA. Structure and thermodynamics of RNA-protein Binding: using molecular dynamics and free energy analyses to calculate the free energies of binding and conformational change. J Mol Biol 2000;297:1145–1158.
36. Lee MR, Duan Y, Kollman PA. Use of MM-PB/SA in estimating the free energies of proteins: application to native, intermediates, and unfolded villin headpiece. Proteins 2000;39:309–316.
37. Wang J, Morin P, Wang W, Kollman PA. Use of MM-PBSA in reproducing the binding free energies to HIV-1 RT of TIBO derivatives and predicting the binding mode to HIV-1 RT of efavirenz by docking and MM-PBSA. J Am Chem Soc 2001;123:5221–5230.
38. Huo S, Massova I, Kollman PA. Computational alanine scanning of the 1:1 human growth hormone-receptor complex. J Comput Chem 2002;23:15–27.
39. Nishiyabu R, Kano K. Double self-inclusion by rotating glucopyranose units in per-*O*-methylated b-cyclodextrin moieties attached to a porphyrin in aqueous solution. Eur J Org Chem 2004;(24):4985–4988.
40. Impellizzeri G, Pappelardo G, D'Alessandro F, Rizzarelli E, Saviano M, Iacovino R, Benedetti E, Pedone C. Solid state and solution conformation of 6-{4-[*N-tert*-butoxycarbonyl-*N*-(*N*′-ethyl)propanamide]imidazolyl}-6-deoxycyclomaltoheptaose: evidence of self-inclusion of the Boc group within the b-cyclodextrin cavity. Eur J Org Chem 2000;(6):1065–1076.
41. Yamada T, Fukuhara G, Kaneda T. "Molecular magic". Formation of a self-inclusion complex from a dumbbell-shaped permethylated b-cyclodextrin derivative. Chem Lett 2003;32:534–535.
42. Reinhardt R, Richter M, Mager P. Investigation of the conformational behaviour of permethylated cyclodextrins by molecular modelling. Carbohydr Res 1996;291:1–9.
43. Maestre I. Ciclodextrines gegants, ciclodextrines modificades amb grups ancorats: dimers i efecte en sistemes d'interès biològic. Estudis computacionals. Doctoral Thesis. Bellaterra: Universitat Autònoma de Barcelona; 2004.
44. Maestre I, Beà I, Ivanov P, Jaime C. Structural dynamics of some large-ring cyclodextrins. A molecular dynamics study: an analysis of force field performance. Theor Chem Acc 2007;117: 85–97.
45. Koehler JEH, Saenger W, Van Gunsteren WF. The flip-flop hydrogen bonding phenomenon. Molecular dynamics simulation of crystalline b-cyclodextrin. Eur Biophys J 1988;16:153–168.
46. Steiner T, Saenger W, Kearley G, Lechner RE. Dynamics of hydrogen-bonding disorder in b-cyclodextrin undecahydrate. Phys B Condens Matter 1989;156–157:336–338.
47. Steiner T, Mason SA, Saenger WJ. Topography of cyclodextrin inclusion complexes. 27. Disordered guest and water molecules, three-center and flip-flop O—H...O hydrogen bonds in crystalline b-cyclodextrin ethanol octahydrate at T = 295K: a neutron and X-ray diffraction study. J Am Chem Soc 1991;113:5676–5687.

Book Review

A Practical Guide to Magnetic Circular Dichroism Spectroscopy, by W. R. Mason. 240 pp. John Wiley & Sons Inc. 2007. ISBN: 978-0-470-06978-3.

Circular dichroism (CD) spectroscopy is one of the most important techniques for studying chiral molecules. What is much less widely appreciated, however, is that solutions of achiral molecules can also exhibit CD effects when a magnetic field is applied parallel to the axis of light-propagation. This technique is referred to as magnetic circular dichroism (MCD) spectroscopy. CD and MCD analyses provide complementary information, since the physical origin of the two techniques is quite different. Although the MCD technique was first developed in the 1930s, to date, very few textbooks have been published which are readily accessible for experimentalists. W. R. Mason's, "*A Practical Guide to Magnetic Circular Dichroism Spectroscopy*", should help to fill this niche, since it helps the reader to visualize the spectroscopic effects that are accessible through MCD measurements.

This book consists of 9 chapters. Chapter 1 gives a brief introduction into MCD effects and the history of the MCD technique. Chapter 2 describes polarized light in the context of electromagnetic wave equations. Chapter 3 deals with the definition and properties of the MCD terms (symbolized by *A*, *B*, and *C*) and the parameters that describe them and enables the reader to follow the derivation of the complex formulae used to express these MCD terms. Chapter 4 presents a practical guide to MCD spectral measurements, which should prove useful for those who actually plan to measure MCD spectra. The various approaches used to analyze of MCD spectra are described in Chapter 5, including the application of the MCD technique to spin-orbit coupling and vibronic transitions.

The following two chapters contain a number of case studies, which illustrate key points concerning the information that can be derived from MCD spectral data, which should greatly assist to derive key information about the nature of the optically accessible electronic states and the frontier molecular orbitals. The author describes many different experimental systems, including both inorganic and organic molecules. Chapter 6 focuses on systems with diamagnetic ground states, which exhibit *A* and *B* terms, while Chapter 7 describes paramagnetic systems dominated by temperature-dependent *C* terms.

Chapter 8 presents a brief description of the use of MCD spectroscopy to analyze vibrations and rotation-vibrations in the IR and near-IR regions (MVCD), and also explores MCD applications in the X-ray region (XMCD). Several experimental spectra are described to provide examples of the different types of applications. Chapter 9 introduces magnetic linear dichroism (MLD) spectroscopy, which is a magneto-optical technique that is closely related to the MCD technique, which in some situations can provide additional information.

Overall, this book provides an excellent practical guide for using MCD spectroscopy. The author successfully highlights the important features of chiroptical properties that are associated with the presence of a strong magnetic field. Since MCD spectra can be measured in much the same way as CD spectra, simply by inserting a magnet into the sample compartments of commercially available CD spectrometers, this book is highly recommended not only for those scientists who plan to actively study MCD spectroscopy in the near future, but also for scientists who wish to develop a deeper and more complete understanding of the field of optical spectroscopy.

Atsuya Muranaka, Ph.D.
Advanced Elements Chemistry Laboratory
The Institute of Physical and Chemical Research
RIKEN, Wako-shi
Saitama 351-0198, Japan

DOI: 10.1002/chir.20644
Published online 20 June 2008 in Wiley InterScience (www.interscience.wiley.com).